



UNIVERSITY OF CENTRAL FLORIDA

**EEL 4914 – Senior Design II, Fall 2021**  
**SASSPR:**  
**Semi-Automated Sensor for Surface Plasmon**  
**Resonance**

Group 2

Robert Ballentine, Photonics Engineering

Robin Howell, Photonics Engineering

James Henderson, Computer Engineering

# Table of Contents

<b>Project description</b>	<b>1</b>
<b>1.A Defined Project</b>	<b>1</b>
<b>1.B Motivation</b>	<b>2</b>
<b>1.C Project Goals and Objectives</b>	<b>2</b>
<b>Requirements</b>	<b>3</b>
<b>2.A Features</b>	<b>3</b>
<b>2.A.1 Basic Features</b>	<b>4</b>
<b>2.A.2 Advanced Features</b>	<b>5</b>
<b>2.A.3 Stretch Features</b>	<b>6</b>
<b>2.B List of Requirement Specifications</b>	<b>6</b>
<b>2.C Table of Specifications</b>	<b>7</b>
<b>2.D House of Quality</b>	<b>8</b>
<b>Device Illustration</b>	<b>11</b>
<b>Block Diagrams</b>	<b>11</b>
<b>Project Research</b>	<b>13</b>
<b>5.A Existing Products</b>	<b>14</b>
<b>5.A.1 Smartphone Based SPR Sensor using Multimode Optical Fiber</b>	<b>14</b>
<b>5.A.2 Smartphone Based SPR Sensor using an External LED</b>	<b>15</b>
<b>5.A.3 Prism-coupled Method for SPR Sensors</b>	<b>16</b>
<b>5.B Optical Fiber for Wave Propagation</b>	<b>17</b>
<b>5.C Light Sources</b>	<b>18</b>
<b>5.C.1 LED as a Light Source</b>	<b>18</b>
<b>5.C.2 Laser Diode as a Light Source</b>	<b>19</b>
5.C.2.1 Determining the Wavelength of the Laser Diode	20
<b>5.D Physical Optics</b>	<b>21</b>
<b>5.D.2 Right-Angle N-BK7 Glass Prism</b>	<b>22</b>
4.D.3 Motorized Rotation Stage and DC Servo Motor Controller	22
<b>5.E CMOS Sensor and Microcontroller for SPR Detection</b>	<b>23</b>
<b>5.F SPR Sensor Surface</b>	<b>24</b>
5.F.1 Thickness of Gold Film for Sensor Surface	24
<b>5.G SPR Sample Preparation</b>	<b>26</b>
<b>5.H SPR Sensor Accuracy</b>	<b>27</b>
<b>5.I Power Delivery</b>	<b>28</b>
<b>5.J 3D-Printed Housing and Mounts</b>	<b>29</b>
<b>5.K Software Solutions</b>	<b>29</b>

<b>5.L Different SPR Monitoring Methods</b>	<b>30</b>
<b>5.L.1 Angular Scanning</b>	<b>30</b>
<b>5.L.2 Wavelength Modulation</b>	<b>31</b>
<b>5.L.3 Intensity Modulation</b>	<b>32</b>
<b>Constraints and Standards</b>	<b>33</b>
<b>6.A Constraints</b>	<b>33</b>
<b>6.A.1 Financial</b>	<b>34</b>
<b>6.A.2 Environmental</b>	<b>34</b>
<b>6.A.3 Social</b>	<b>35</b>
<b>6.A.4 Political</b>	<b>35</b>
<b>6.A.5 Ethical</b>	<b>35</b>
<b>6.A.6 Health and Safety</b>	<b>35</b>
<b>6.A.7 Manufacturability</b>	<b>36</b>
<b>6.A.8 Software Compatibility</b>	<b>36</b>
<b>6.A.9 Sustainability</b>	<b>36</b>
<b>6.A.10 Covid and the Global Semiconductor Shortage</b>	<b>37</b>
<b>6.A.11 Time Constraints</b>	<b>37</b>
<b>6.A.12 Storing and Handling of SPR Chips</b>	<b>38</b>
<b>6.B Standards</b>	<b>41</b>
<b>6.B.1 Laser Safety</b>	<b>41</b>
<b>6.B.3 Communication Standards</b>	<b>44</b>
<b>6.B.4 Software Standards</b>	<b>44</b>
<b>6.B.7 Chemical Laboratory Safety in Academic Institutions</b>	<b>46</b>
<b>6.B.7.1 Personal Protective Equipment (PPE)</b>	<b>46</b>
<b>6.B.7.2 Maintaining an Organized Environment</b>	<b>47</b>
<b>6.B.7.3 Labeling Chemicals</b>	<b>48</b>
<b>6.B.7.4 Cleaning Glassware and Disposal of Chemicals</b>	<b>48</b>
<b>6.B.7.5 Safety Procedures for Using Electrical Equipment</b>	<b>50</b>
<b>6.B.7.6 Refrigerating Chemical or Biological Samples</b>	<b>50</b>
<b>6.B.10 NASA-STD-8739.3</b>	<b>50</b>
<b>Project Hardware Design Details</b>	<b>51</b>
<b>7.A Design Calculations</b>	<b>51</b>
<b>7.A.1 Snell's Law Calculations for Total Internal Reflection</b>	<b>51</b>
<b>7.A.2 Surface Plasmon Dispersion for Different Wavelengths</b>	<b>53</b>
<b>7.B Initial Designs and Related Diagrams</b>	<b>59</b>
<b>7.B.1 Initial Design Idea – Smartphone Based SPR Sensor</b>	<b>60</b>
<b>7.B.1.1 Light Source Design</b>	<b>61</b>
<b>7.B.1.2 SPR Detector Design</b>	<b>62</b>

<b>Project Testing and Prototype Construction</b>	<b>62</b>
<b>8.A Hardware Testing</b>	<b>63</b>
<b>8.A.1 Microcontroller and Power Supply Testing</b>	<b>63</b>
<b>8.A.2 3D Printed Housing / Mounts</b>	<b>69</b>
<b>8.A.3 Laser Diode Testing</b>	<b>73</b>
<b>8.A.4 Simulating the Surface Plasmon Resonance Curve</b>	<b>76</b>
<b>8.B Software Testing</b>	<b>78</b>
<b>8.C Prototype Construction</b>	<b>80</b>
8.C.1 Initial Prototype for Senior Design I	80
<b>8.C.1.1 Determining the Polarization of our Incident Light</b>	<b>85</b>
8.C.1.2 Investigating the Properties of our SPR Chip	93
<b>8.C.2 Final Prototype for Senior Design II</b>	<b>94</b>
<b>Bill of Materials</b>	<b>102</b>
<b>Project Milestones</b>	<b>103</b>
<b>Conclusion</b>	<b>104</b>
<b>Appendix A – Permissions</b>	<b>1</b>
<b>Appendix B – References</b>	<b>8</b>



## List of Tables

<b>Table 1.</b> Table of Specifications for Optical, Electrical, Computer, and Biological Components	7
<b>Table 2.</b> House of Quality Diagram.	9
<b>Table 3.</b> Comparison of Laser Diodes to Purchase.	20
<b>Table 4.</b> Considered Choices for Wavelength Filters for the SPR Sensor.	23
<b>Table 5.</b> Scratch-dig specifications and some of their applications for practical use.	43
<b>Table 6.</b> Real and Imaginary Part of the Dielectric Function of 50 nm Gold	56
<b>Table 7.</b> Real and Imaginary Parts of Complex Wave Vector for Differing Wavelengths	57
<b>Table 8.</b> Length of Intensity Decay of Surface Plasmons for Different Wavelengths	58
<b>Table 9.</b> Phase Velocity of Surface Plasmons for Differing Wavelengths	58
<b>Table 10.</b> Experimentation to Determine Polarization of the Laser Diode.	75
<b>Table 11.</b> ESP32-CAM Capture vs Clock Frequency	79
<b>Table 12.</b> Experimentation for Determining Polarization Axis for SPR Effect: Right-Angle Prism without SPR Chip Attached.	88
<b>Table 13.</b> Experimentation for Determining Polarization Axis for SPR Effect: Right-Angle Prism with SPR Chip Attached.	88
<b>Table 14.</b> Experimentation to Measure Output Power with Polarizing Beam Splitter.	93
<b>Table 15.</b> Experiment for Surface Plasmon Excitation using 635 nm Laser Diode	98
<b>Table 16.</b> Project Financing Table.	102
<b>Table 17.</b> Project Milestones Table.	103

## List of Equations

<b>Equation 1.</b> Conversion of Energy relating to Reflection, Transmission, and Absorption.	25
<b>Equation 2.</b> Formula for Critical Angle.	51
<b>Equation 3.</b> Transverse and Longitudinal EM Field for Surface Plasmon Oscillations.	55
<b>Equation 4.</b> Retraded Dispersion Relation for the Plane Surface of a Semi-infinite Metal.	55
<b>Equation 5.</b> Dielectric Function of Metal-air Interface. Transverse components of SP vectors.	55
<b>Equation 6.</b> Complex Wave vector at Metal-air Interface	56
<b>Equation 7.</b> Real part of the Complex Wave Vector	56
<b>Equation 8.</b> Imaginary part of the Complex Wave Vector	56
<b>Equation 9.</b> Length of Intensity Decay of Surface Plasmons	57
<b>Equation 10.</b> Phase Velocity of Surface Plasmons	58

## List of Figures

<b>Figure 1.</b> Illustration of SPR Sensor device	11
<b>Figure 2.</b> Block Diagram of Optics (top) and Computer (bottom) Hardware Interactions.	12
<b>Figure 3.</b> Use Diagram of Application.	13
<b>Figure 4.</b> Instrumentation of the smartphone based SPR imaging biosensor.	14
<b>Figure 5.</b> SPR Imaging Platform with a Smartphone.	16
<b>Figure 6.</b> Angle-resolved SPR for smartphone application.	17
<b>Figure 7.</b> Reflection on Silver Film with Differing Thicknesses	25
<b>Figure 8.</b> Comparison of Smartphone Based SPR Sensor vs. Commercial SPR Sensor.	28
<b>Figure 9.</b> Reflectance Spectra for Angular Scanning.	31
<b>Figure 10.</b> Reflectance Spectra for Wavelength Modulation	32
<b>Figure 11.</b> Reflection Intensity Curve for Intensity Modulation.	33
<b>Figure 12.</b> Surface Plasmon Resonance Sensor Chip Manufacturer Label	38
<b>Figure 13.</b> Reflection Intensity Curve for Intensity Modulation.	35
<b>Figure 14.</b> Technical Grade Distilled Water	39
<b>Figure 15.</b> Image of Gold Coated SPR Chip.	40
<b>Figure 16.</b> Scratch-dig table from the MIL-PRF-13830B.	43
<b>Figure 17.</b> Simulation Parameters to Simulate Total Internal Reflection using WinSpall.	52
<b>Figure 18.</b> Simulation of Reflectivity Curve for Total Internal Reflection using WinSpall.	53
<b>Figure 19.</b> Simulation of Reflectivity Curve for Differing Wavelengths using WinSpall.	54
<b>Figure 20.</b> Initial Divide and Conquer Block Diagram.	59
<b>Figure 21.</b> First Illustration of the SPR Sensor Prototype.	60
<b>Figure 22.</b> Microcontroller Testing with L805 Voltage Regulator and 9V Battery.	64
<b>Figure 23.</b> Microcontroller Testing with LM2596 Switching Regulator and 7.4v LiPo.	65
<b>Figure 24.</b> Capture Test with Microcontroller.	66
<b>Figure 25.</b> Async Webserver Test with Microcontroller.	66
<b>Figure 26.</b> Drain Current and Voltage Saturation Graph.	67
<b>Figure 27.</b> Final Schematic for Power Design.	68
<b>Figure 28.</b> Battery Powered System Test.	68
<b>Figure 29.</b> AC-DC Adaptor Powered System Test	69
<b>Figure 30.</b> First iteration of ESP32-CAM housing using a 9v battery.	70
<b>Figure 31.</b> First test using housing.	71
<b>Figure 32.</b> Semi-final variation of ESP32-CAM mount.	72
<b>Figure 33.</b> Prototype mount of laser diode.	72
<b>Figure 34.</b> Output Power of Laser Diode from LaserLands.	74
<b>Figure 35.</b> Output Power of 635 nm Laser Diode Module	75
<b>Figure 36.</b> Simulation Parameters for the Resonance Curve of Gold Film using WinSpall.	77
<b>Figure 37.</b> Simulation of Resonance Curve of Gold Film using WinSpall.	77
<b>Figure 38.</b> Simulation of Resonance Curve of Gold Film 632.8 nm Wavelength with WinSpall.	80
<b>Figure 39.</b> Experimental set up that displays an angle smaller than the critical angle.	81
<b>Figure 40.</b> 532 nm Experiment Displaying Angle at TIR.	81
<b>Figure 41.</b> Initial Prototype of Optical Setup.	83
<b>Figure 42.</b> Attaching the SPR chip to the Right-Angle Prism.	84
<b>Figure 43.</b> Mounted Linear Polarizer for Optical Demonstration.	85
<b>Figure 44.</b> SPR Chip Attached to 40 mm Right-Angle Prism.	87
<b>Figure 45.</b> Polarizing Beam Splitter for Transmitting P-polarized Light.	89
<b>Figure 46.</b> Measured Output Power before Polarizing Beam Splitter.	90

<b>Figure 47.</b> Measured Output Power of P-Polarized Light.	91
<b>Figure 48.</b> Measured Output Power of S-Polarized Light.	92
<b>Figure 49.</b> Schematic Diagram of SASSPR Version 2.	95
<b>Figure 50.</b> Experimental Setup for Final Prototype.	96
<b>Figure 51.</b> SPR Chip Attached to Prism using Index Matching Gel.	97
<b>Figure 52.</b> SPR Curve Simulation vs. Experimental for Reflectance	99
<b>Figure 53.</b> Final Schematic Design for SASSPR	100
<b>Figure 54.</b> SASSPR Software Displaying Experimental Curve in Air	100
<b>Figure 55.</b> SASSPR Software Displaying Experimental Curve with Distilled Water	101

# 1. Project description

## 1.A Defined Project

Surface plasmon resonance, or SPR for short, is an optical effect that can measure the binding of molecules in real time without labels. The SPR sensor is a biological sensor used to measure the kinetics and affinity of the interactions within the sample. These interactions can be seen through dips in spectral intensity as a light source interacts with a dielectric film layered with the analyte.

The goal of this device is to create a more affordable and compact sensor for commercial use that is controlled using a software application. This will be done using an optical set up that detects the surface plasmon interactions through changes in the light source's intensity. This change in intensity will be detected using an external CMOS sensor camera that will be controlled using a microcontroller unit. The captured images from the camera will be transmitted via Wi-Fi to a compatible device where the detectable information will be extrapolated and displayed through a self-developed android application. The application will display various characteristics and information pertaining to the processed information from the sensor. A 635 nm focused laser diode will be the light source of choice for this experiment. The beam will undergo slight modifications before the light propagates through the prism and interacts with the SPR sensor chip attached to the prism's uppermost face. Before the beam interacts with the prism, it will pass through a filter ensuring the correct polarization of the light is transmitted. This means that the light's electric field is polarized to be parallel to the plane of incidence, otherwise known as p-polarized light. This will lessen the amount of light traveling at different angles, reducing the divergence within the initial region of the system. Linear polarized light is an asset for this project because linear polarized light operates under the constraint of a single dimensional vector plane for propagation. This light will be directed onto a right-angle prism. For surface plasmon resonance to occur, light needs to penetrate the surface the SPR chip is attached to at an angle greater than the critical angle of the glass prism's face. It was calculated that a simple angle such as  $90^\circ$  allows for surface plasmons to be detected through detection of evanescent waves. This angle will be produced by mounting the right-angle prism onto a motorized rotation stage that is controlled using the Kinesis software provided by Thorlabs. The motorized rotation stage allows for the user to control with high precision the angle of the prism to ensure proper phase-matching between the incident light wave and the wave of the surface plasmons can take place. The prism of choice is a right-angle flint (N-BK7) prism that lacks coating. The lack of coating is important to note as the risk of not attuning the light with filters before arriving at the interface would result in the targeted data being contaminated with unwanted information generated within the diode. After the excitation occurs, the light will be guided directly onto the CMOS sensor. The CMOS sensor will capture one image every 0.5 seconds. After the images are captured, the CMOS sensor will transmit the images via Wi-Fi to the compatible device. Once the images are transmitted, the application will process the images to determine the

changes in intensity during the SPR sensing process and convert the data into user-friendly graphs that inform when surface plasmon excitation began, ended, or did not occur.

This document describes the design process of the SPR sensor. The report begins with a device description and the motivation behind choosing the sensor, as well as the initial goals and objectives. The requirements and specifications of the device follow. A research section will be included to describe the process of choosing different optical components including a comparison between different technology compatible with the device. The research section will also describe the benefits of each component in the system. Following the research, a section describing the standards and constraints of the device will be introduced. The following section will be dedicated towards describing the hardware and software design of the device, including the process of 3D printing components and housing. The document will then include information on the administrative aspect of the project. This includes a timetable for the paper and the development of the device and financing. The end of the report will include a conclusion, references, and an appendix if necessary.

## **1.B Motivation**

There are various questions that exist that can be solved from the SPR detection method. Such questions include: Are pesticides lingering on produce? Is there contamination in a body of water? Does my food contain traces of salmonella? As mass production of perishables becomes more and more processed, these are important things to be aware of before consumption. Yet the challenge for many SPR sensors are their price and portability. Commercial SPR sensors can cost thousands of dollars and are not well designed for many remote and low-income locations. The need for low-cost yet high quality devices is crucial for the democratization of medical services. Therefore, we propose to develop a compact SPR sensor that can be attached to a compatible device to provide rapid, on-site detection while significantly reducing the manufacturing cost of the SPR sensor itself.

## **1.C Project Goals and Objectives**

The proposed idea for this project is to create a portable, accurate, and low-cost SPR sensor that can be easily controlled using various devices. For this idea to come to fruition, the main goals and objectives must be defined to provide direction in the development of our product. The four main goals for our portable SPR sensor are as follows:

1. Cost
2. Compact in size
3. Consumer Friendly
4. Repeatable results

The first goal of the device is to build a product that is at a more affordable price range compared to commercial SPR sensors in the market today. The average price of a commercial SPR sensor is \$40,000 which limits the use of this technology to only those with large budgets. Our device would allow for lower-income or remote locations that may not have the necessary expenses to be able to build or use our SPR sensor to understand molecular interactions of antibodies or other substances.

The second goal is to allow our device to be as compact as possible for easy use. To do this, the dimensions of our device will be no greater than 8 inches in width, 16 inches in length, and 12 inches in height. This ensures our system is easy to relocate and not constrained by its dimensions.

The third goal is to create a device that is simple and easy to use for a consumer. This goal will be achieved in multiple ways. First, our design will use a prism as the SPR sensing location in order to keep the optical components separate from the solution to be tested so the sensor can easily be replaced and cleaned by the consumer. Second, the software application to control the camera, microcontroller, and graphical representation of SPR occurring will be accessible for Windows, Android, Linux, iOS, and MacOS devices. This will allow our final product to be compatible with various devices, allowing the consumer to control the detector and visualize their data from multiple platforms.

The fourth goal is to develop an SPR sensor that can have easily repeatable results each experiment. To do this, the prism will be mounted onto the motorized rotation stage at the proper angle and position so that the critical angle will remain constant each experiment. As well, the sensor location where the SPR chip and liquid solutions will be added are easy to maintain and replace for each experiment. Doing this will minimize any changes to each experiment, ensuring that the angle where SPR occurs remains relatively the same in each experiment if using 50 nm gold film SPR chips, as our device has been intended for.

## **2. Requirements**

### **2.A Features**

During the initial planning of any design, it is necessary to decide on the main features of the project one hopes to accomplish. These features provide a detailed explanation of the main functions of the final product and how they aid in accomplishing the goals set by the entire team. The features are separated into three sections: basic features, advanced features, and stretch features. Basic features are the set attributes we will accomplish for our project at the end of Senior Design II. These features will be detailed in their explanations to properly express the final design ideas from each team member. Advanced features are ideas for upgrading our project that would enhance the

functionality of our product but may not be possible to accomplish given the allotted time. Stretch features are ideas to take our project to the next level if it were to become a marketable product. It would place our device at the same level as commercial SPR sensors but would require even more time to accomplish. The following sections will describe the three features and the benefits they bring to our final idea.

## **2.A.1 Basic Features**

The basic features of our project will describe each optical, electrical, and computer component required for our final design. This project is primarily optical, with some systems and electrical engineering to create a fully functional SPR sensor. A 635 nm laser diode module, mounted in a kinematic mount for precise alignment, will be externally powered using a wall plug. An external CMOS sensor camera will be connected to the microcontroller unit and will be used as the detector for our SPR sensor, which can be battery powered or connected via wall plug. Throughout the experiment, the camera will capture one image every 0.5 seconds at a 1600 x 1200-pixel resolution. This will provide us with the necessary data to determine when surface plasmon excitation takes place. A battery-powered power supply unit can be used as a power source for our CMOS sensor camera and microcontroller. The power supply will consist of one 9V Alkaline battery. The light from the laser diode will be manipulated by a polarizing beamsplitter. The polarizing beamsplitter is crucial to create surface plasmon excitation, as it allows only light that is linearly polarized parallel to the plane of incidence to interact with our SPR sensor. The p-polarized light is then directed to a pinhole iris which is used to control the shape and diameter of our beam before it interacts with the surface plasmons on the gold film. The light is then directed onto a right-angle prism which is mounted onto a motorized rotation stage. This is where the surface plasmon detection occurs. By rotating our motorized rotation stage to angles greater than the critical angle of the prism, we can create the phenomenon called total internal reflection as the beam hits the right-angle prism. At a certain angle after the critical angle, phase-matching can occur between the incident wave of our light and that of the surface plasmons. This coupling of the light using the prism creates a perfect situation where surface plasmon excitation can occur as most of the energy from our incident light will be transferred to the surface plasmons at the metal/dielectric interface on our SPR chip. This leads to a decrease in intensity of our received light onto the CMOS camera. The decrease in intensity of our received light indicates that surface plasmon excitation occurred.

For our experiment, once surface plasmon excitation is found with our device with air as our dielectric material interacting with the gold film on the prism, distilled water will then be added to the 3D printed sensor chamber where the prism is mounted. Distilled water was chosen as the testing liquid due to it having a higher refractive index than air, where air has a refractive index of 1 and distilled water has a refractive index of 1.324. This allows us to observe a shift in the surface plasmon resonance angle as we change our dielectric medium in contact with the gold film from a low refractive index to a high

refractive index. Our device utilizes intensity modulation to detect changes in the surface plasmon resonance angle, where the angle of incidence remains fixed and an increase in light intensity is observed by the detector when the angle for surface plasmon resonance changes. Distilled water was also chosen because of its common use in laboratory settings. This is due to the distillation process removing the electrical charge from the atoms and molecules in the water which ensures accurate final laboratory results. Thus it ensures our experimental data is as accurate as possible for determining changes to the resonance curve when changing the refractive index of the dielectric medium.

A software application was developed to analyze the captured images from the external CMOS sensor camera and control the camera settings. The application will control the camera to capture one image every 0.5 seconds of the reflected light from the SPR sensor while surface plasmon excitation is occurring. A custom-programmed application will be used to map the relative intensity profile of the received images and display them in a graphical form, providing the user with the change in relative intensity over time. The application will be able to analyze the increase or decrease in relative intensity and provide the user with information on what time interval surface plasmon excitation begins, ends, and if it did not occur at all. The application will also allow the user to see the numerical values of the intensity changes observed, as well as the execution interval and average runtime for the system. The user will also be able to log the experiment and view it for later use. This would easily allow the user to visualize past experiments for comparison. The final software application was designed for compatibility with Windows, Linux, iOS, and MacOS to provide a more versatile product. However, due to Thorlabs containing a closed source software for its motorized rotation stage, a Windows computer is required to control the motorized rotation stage if the user would rather use the Kinesis software from Thorlabs to control the motorized rotation stage instead of the K-Cube DC Servo Motor Controller, also provided by Thorlabs.

## **2.A.2 Advanced Features**

An advanced feature we would like to implement into our final design is a flow cell that would be attached to our SPR sensing location. A flow cell is a tube designed for liquid samples to continuously flow through using a pump. A pump is attached to two small holes on the flow cell and pushes the liquid sample through at a certain flow rate. This is beneficial for samples that can be damaged by light sources or for samples that are changing their concentration. Many SPR sensors that we have researched contain flow cells to allow for a constant flow of the sample across the SPR sensing location, which aids in the molecular binding process. One such example was in a 2015 smartphone based SPR sensor created in China [1], which used optical fiber as its SPR sensing location and placed the flow cell around the exposed core of the fiber that contained the gold film functionalized with immobilized Protein A. Another example is a smartphone based SPR sensor created in Turkey in 2016 [2], which used a flow cell to pump mouse



IgG antibodies onto a SPR sensor chip designed using a Blu-ray disk coated with silver and gold nanoparticles. Both examples utilized a flow cell in their final design due to the constant flow rate of the analyte solution allowing for more molecular binding to occur on the SPR sensing location. A flow cell is a very practical addition to an SPR sensor as it allows for a more accurate reading of the analyte solution to occur due to the constant movement of the solution across the SPR sensor itself.

### **2.A.3 Stretch Features**

A stretch feature for our design would be to upgrade the pump connected to the flow cell to automatically pump our phosphate-buffered saline solution or bovine immunoglobulin G solution into the flow cell and drain it once SPR detection is complete. The idea is very similar to commercial SPR sensors, which contain plastic bottles on the outside of the SPR sensing device where the buffer and analyte solutions can be added by the user. These bottles are attached to the sensing location of the SPR device with tubes that, when the pump is activated, will transfer their solution into the sensing location at a constant flow rate. A third bottle would be used to transfer the waste solution that is no longer needed after SPR detection is complete.

### **2.B List of Requirement Specifications**

The following requirement specifications for a successful SPR sensor are as follows:

- Power consumption must be under 10 watts.
- The wavelength of our laser must be greater than 600 nm, ensuring minimum broadening of SPR angular dependence.
- The software application will collect the intensity profile of images captured and process the data into graphs showing the SPR angle when surface plasmon excitation occurs within the specified time.
- Camera must be able to capture one image every 0.5 seconds.
- Transmission range will be around 10 meters.
- Simple, consumer-friendly graphical user interface for software application.
- The motorized rotation stage provides high precision to create excitation of the surface plasmons. High precision relates to 25 arcsec achievable incremental motion and 0.1% percentage accuracy.
- Application to observe SPR will be compatible with Windows, Android, Linux, iOS, and Mac OS.

## 2.C Table of Specifications

Table 1 below illustrates the specifications for the main optical, computer, electrical, and biological components that will be used in our SPR sensor.

Item	Specifications
Right-Angle Prism	<b>Material:</b> N-BK7 (K9) glass <b>Surface Flatness:</b> $\lambda/8$ <b>Surface Quality:</b> 40-20 <b>Dimensions:</b> 20x20x20 mm <b>Coating:</b> none
Motorized Rotation Stage	<b>Units:</b> Imperial <b>Range:</b> 360° continuous <b>Platform Size:</b> 2.56" <b>Bidirectional Repeatability:</b> +/- 0.1° <b>Backlash:</b> +/- 0.3° <b>Achievable Incremental Motion (min):</b> 25 arcsec <b>Horizontal On-Axis Load Capacity:</b> 1.5 kg <b>Percentage Accuracy:</b> 0.1%
DC Servo Motor Controller for Motorized Rotation Stage	<b>Nominal Voltage:</b> 6 V <b>Nominal Speed:</b> 1050 rpm <b>Nominal Current:</b> 0.156 A <b>Rotor Inertia:</b> 0.298gcm <sup>2</sup>
Polarizing Beam Splitter	<b>Beamsplitter Material:</b> N-SF1 <b>AR Coating Range:</b> 420-680 nm <b>Surface Quality:</b> 40-20 <b>Surface Flatness:</b> < $\lambda/4$ at 633 nm <b>Extinction Ratio:</b> Tp:Ts > 1000:1 <b>Transmission Efficiency:</b> Tp > 90% <b>Reflection Efficiency:</b> Rs > 99.5%
Laser Diode Module	<b>Laser Safety Class:</b> 3R <b>Center Wavelength:</b> 635 nm <b>Output Power:</b> 1.2 mW <b>Beam Divergence:</b> 0.6 mradian <b>Dot Diameter:</b> 2.9 mm <b>Operating Voltage:</b> 4.9V-5.2V DC
Pinhole Iris	<b>Aperture:</b> 1-25 mm in diameter <b>Number of Leaves:</b> 14 <b>O.D./Thickness:</b> 43.7 mm / 6.6 mm
Microcontroller and CMOS Sensor	<b>Resolution:</b> 1600x1200 pixels <b>Module Development Board:</b> ESP32-CAM <b>Microcontroller Chip:</b> ESP32 <b>Camera Module:</b> OV2640 <b>Camera Lens Diameter:</b> 5 mm <b>Energy Efficiency:</b> 5 mA LPM <b>Extra Features:</b> Wi-Fi enabled, compliant with Wi-Fi 802.11b/g/n/e/i and Bluetooth 4.2 standards
SPR Sensor Chip	<b>Dimensions:</b> 20x20x1 mm <b>Functionalized Chemical Group:</b> none
Distilled Water (Technical Grade)	<b>Amount:</b> 64 oz. <b>Refractive Index:</b> 1.324

**Table 1.** Table of Specifications for Optical, Electrical, Computer, and Biological Components

## 2.D House of Quality

A House of Quality diagram provides a guide for communicating both the marketing and engineering requirements for a project. It allows one to easily visualize what is considered a crucial parameter based on the particular need for the project and how it could work for or against the needs of the marketing or engineering team. It is difficult to describe what a customer means by quality, with each product and consumer different from the other. Many times this leads to producing items that are costly and missing key functions that were not noticed during the initial planning. This is why diagrams such as House of Quality are so important: they provide a map for planning the cheapest yet most efficient product possible. A good House of Quality ensures that each component chosen for the product is meeting both the marketing and engineering goals agreed to by each party. The following table below shows a crossover between engineering requirements and marketing requirements for our SPR sensor and how each requirement correlates with one another.

			Engineering Requirements				
			1. Transmission Range	2. Detector Response Time	3. Power Draw	4. Data Storage Space	5. Cost
			+	+	-	+	-
Marketing Requirements	1. Transmission Range	+	↑↑	↓↓	↓	○	↓
	2. Moderate Power Consumption	-	○	○	↑	↓	↑
	3. SPR Experiment Repeatability	+	○	↑↑	↑	↑↑	↓↓
	4. Simple GUI	+	○	○	○	↓	↑↑
	5. Cost	-	↑	↑↑	↓	↓↓	↑↑
Target			~10 m	0.5 s	< 10 W	~256 MB	\$600

*Table 2. House of Quality Diagram.*

Legend:

- ↑↑ Strong Positive Correlation
- ↑ Positive Correlation
- ○ No Correlation
- ↓↓ Strong Negative Correlation
- ↓ Negative Correlation

Table 2 illustrates the House of Quality designed for our portable SPR sensor. The House of Quality allows for us to easily visualize the necessary requirements from both a marketing and engineering standpoint to ensure our device is as successful as possible. Marketing requirements explain what is essential for our SPR sensor to achieve success from a marketing standpoint, while the engineering requirements illustrate what is essential for success from an engineering standpoint. Transmission

Range for both marketing and engineering describe how far the wireless device can be positioned and still communicate with our SPR sensor using Wi-Fi. Allowing for the device to have a large transmission range is beneficial for both marketing the device to consumers and for allowing the device to work reliably from an engineering perspective. Moderate Power Consumption in the marketing requirements correlates with Power Draw for engineering requirements, as both should be low to ensure we have a long battery life for our SPR sensor. Other similar requirements include Cost which should be low for both marketing and engineering to provide users with an affordable device when compared to commercial SPR sensors.

Some requirements have a negative correlation with one another, as can be seen with SPR Experiment Repeatability in marketing requirements and Cost in engineering requirements. As is to be expected, a higher accuracy and repeatability of our SPR sensor would allow our product a competitive edge when competing with more expensive SPR sensors on the market today. However, to obtain higher accuracy, many components such as the motorized rotation stage, laser, prism, and CMOS sensor would need to be of a higher quality in order to achieve the precision accuracy many commercial SPR sensors can achieve. It then becomes a trade-off when designing the device on how accurate our final product can be while still maintaining a low budget. These negative correlations should be carefully considered when designing our product in order to find the right balance between both the management and engineering requirements.

### 3. Device Illustration

This section provides an illustration of an ideal device for our surface plasmon resonance sensor, as can be seen in Figure 2 below. This image provides a visual representation of the final product with all the included components.

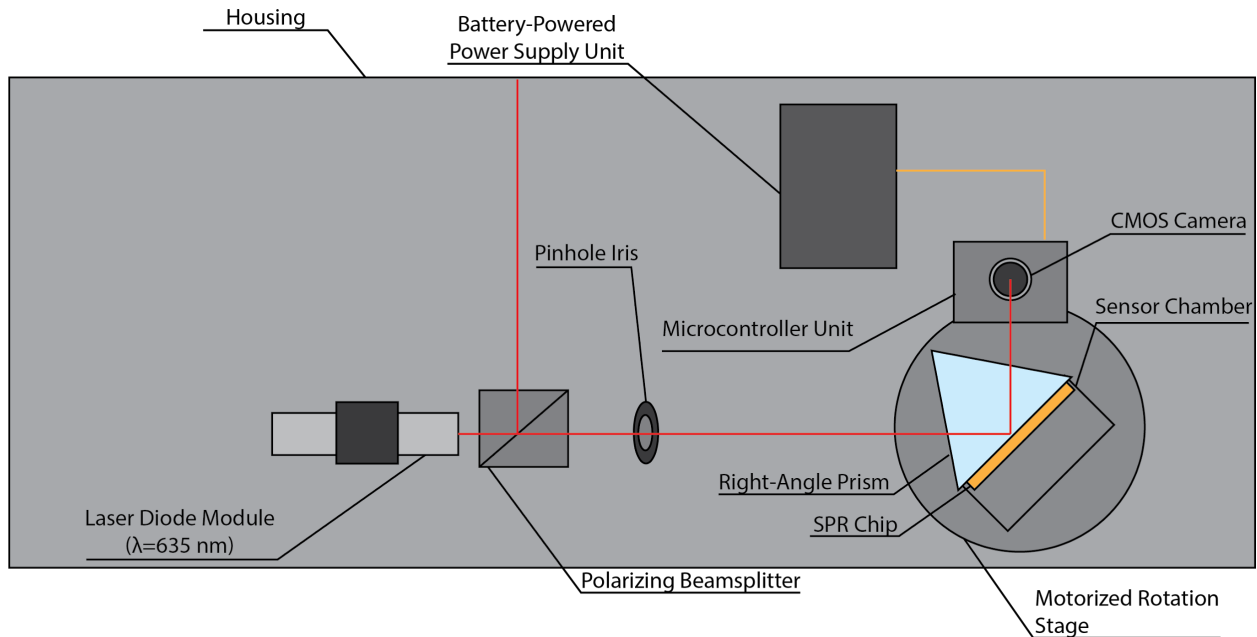


*Figure 1. Illustration of SPR Sensor device*

### 4. Block Diagrams

Our final design will consist of optical components, computer hardware components, and software components to ensure we have a fully functional SPR sensor. To accurately represent each piece in our design, three block diagrams were created to illustrate the various components and how they all work cohesively together. Figure 3 shows the optical design for our SPR sensor and how the final output from our CMOS sensor will connect to the computer hardware components that will deliver the captured images to the software application. Each block is color coded to illustrate how the responsibilities of each device have been divided among the group members. A separate section in the bottom left illustrates other components such as the power supply and 3D printed case which will be a part of our final product but are not directly linked to any one component in the block diagram. Figure 4 explains in more detail the software application we will design and its various functions available to the user when operating the SPR sensor. This provides one with a simple illustration detailing how our software application will ask the user for information and how it will be delivered.

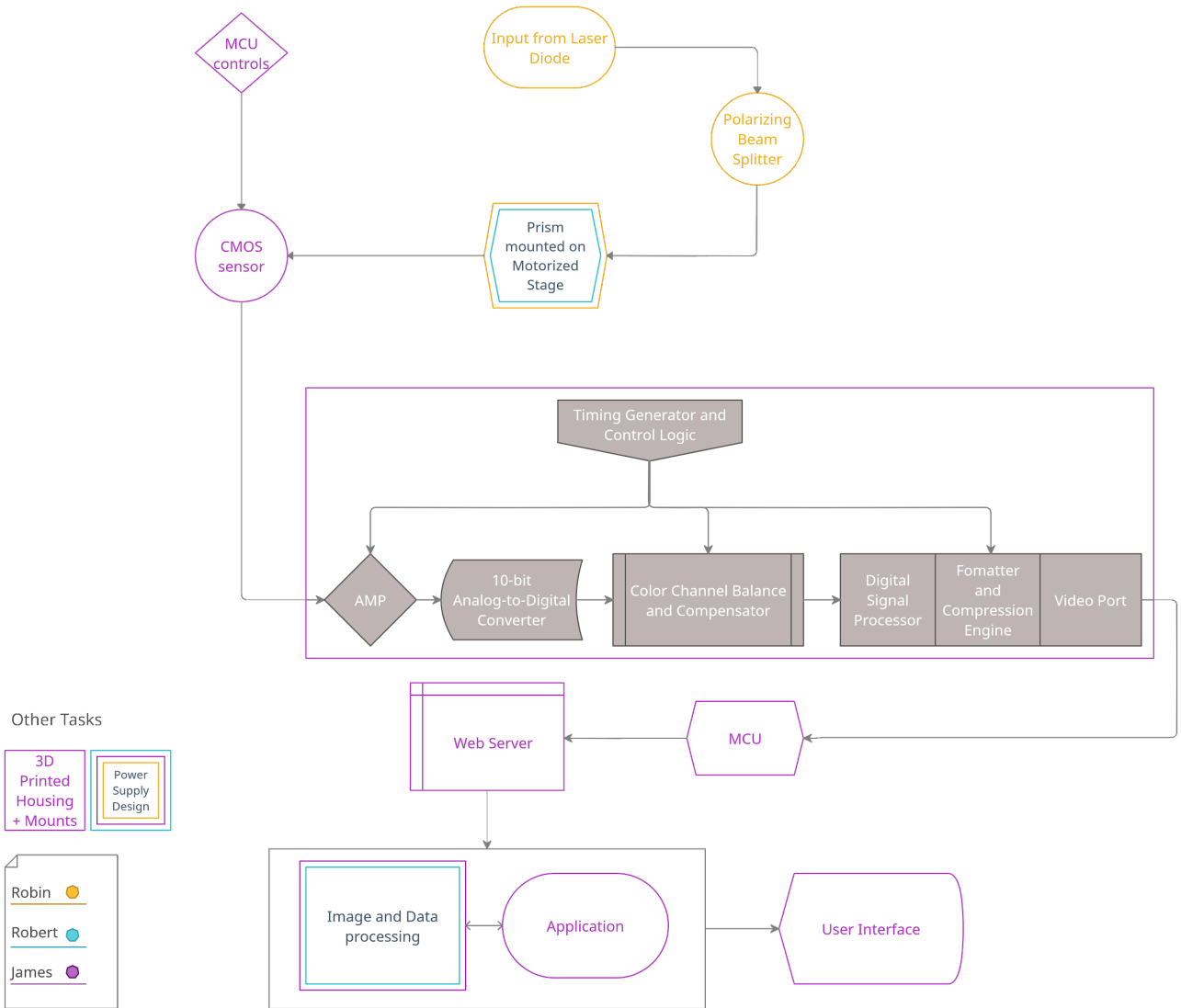


**Figure 2. Block Diagram of Optics (top) and Computer (bottom) Hardware Interactions.**

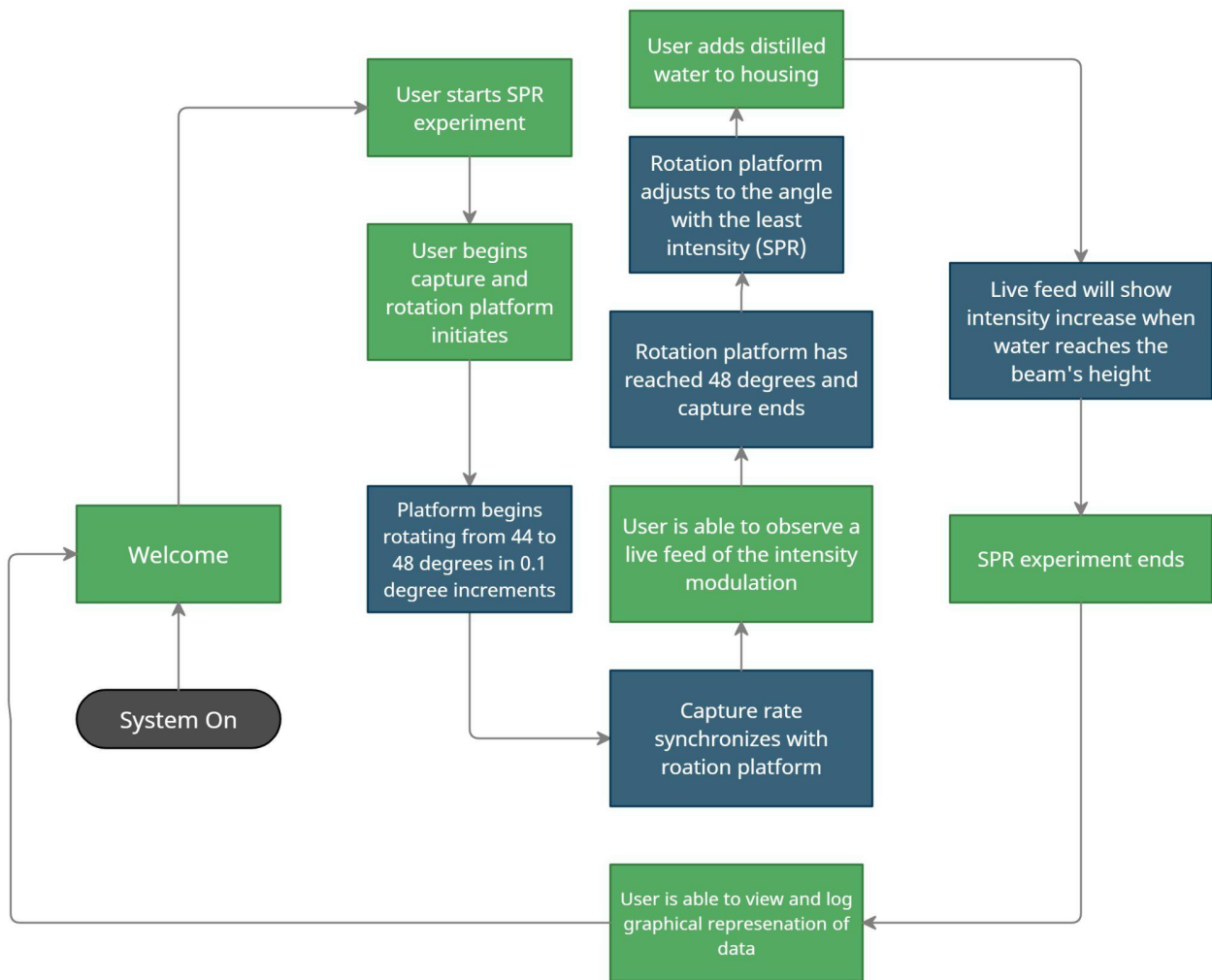


Figure 3. Use Diagram of Application.

## 5. Project Research

In this section, we discuss the decision-making process that occurred in the amalgamation of the surface plasmon resonance sensor. We discuss various technologies and design ideas used by previous SPR sensors and the benefits and concerns their approach has on the final product. Through our research of various mobile SPR sensors, we were able to design a product that meets our needs for the completion of the project. Additionally, we discuss improvements we've made on past design ideas that will ensure our final product is more efficient and consumer friendly.



## 5.A Existing Products

The following sections will describe various existing products we have researched that are similar to our final design. The purpose of this research was to gain a better understanding of the challenges designing a low-cost SPR sensor can bring and the multiple methods past designers have used to overcome these challenges. From our research, we were able to decide on which of these methods would be the most beneficial for our particular goals and constraints while also improving upon their original designs.

### 5.A.1 Smartphone Based SPR Sensor using Multimode Optical Fiber

In the early days of our project, our design for a low-cost surface plasmon resonance sensor centered around utilizing a smartphone device as the controller, light source, and detector for the SPR sensor itself. In doing so, much of the cost would be mitigated and allow us to spend more money on other aspects of our product. One study conducted in China in 2015 gave us our initial ideas on how a smartphone can be used to detect molecular binding [1]. In this study, a smartphone based SPR sensor was developed using intensity modulation to monitor the light intensity of the LED source during molecular binding. In their device, the flashlight LED of the smartphone device was used as the light source for the SPR sensor. A schematic of their final design as well as an image of the finished product can be seen in Figure 5.

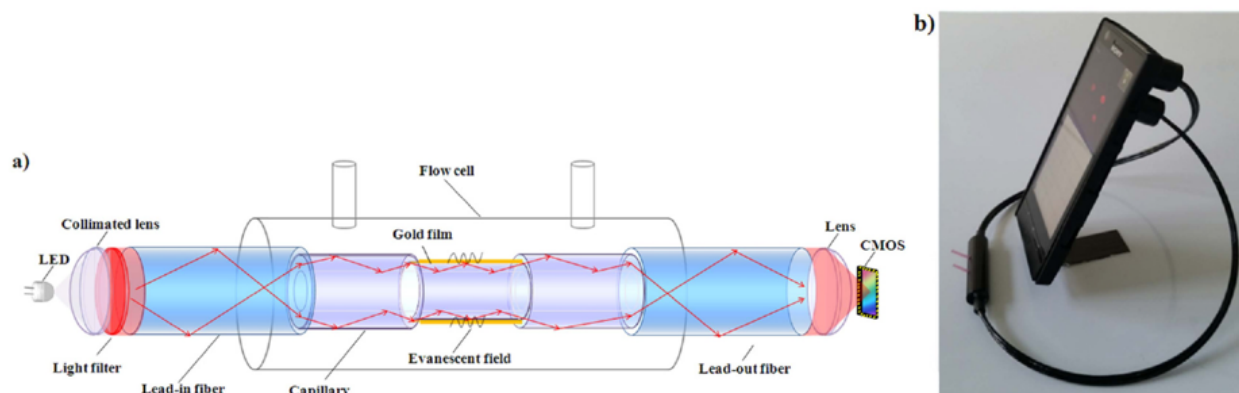


**Figure 4.** Instrumentation of the smartphone based SPR imaging biosensor.

(a) Schematic of the smartphone based SPR sensor, (b) Image of final SPR sensor installed on Android smartphone. The above work is licensed under a Creative Commons Attribution 4.0 International License and is free for public redistribution.

A collimating lens was placed after the LED on the smartphone camera to collimate the incoming light into the multimode optical fiber. For intensity modulation, the light source needed to be of one central wavelength. The white light of a flashlight LED is made of multiple wavelengths which need to be filtered out before travelling through the optical fiber. Therefore, a bandpass filter with a central wavelength of 590 nm was placed after the collimating lens. The optical fiber was used as the sensor location for the SPR device by exposing the core of the fiber and coating the exposed core with gold nanoparticles. The gold nanoparticles were functionalized with Protein A, the ligand used in the experiment, and a flow cell encased the entire section where the core of the fiber was exposed. The camera of the smartphone device was used as a detector, which would capture one image every 0.5 seconds to measure the variation in intensity seen during molecular binding. The final device proved to be able to detect concentrations of bovine immunoglobulin G as low as 47.4 nanomolar. While this was not as sensitive a detection level as commercial SPR sensors, which with the same analyte and ligand were able to detect concentrations as low as 15.7 nanomolar, the device does have the advantages of being much more portable and lower cost compared to a commercial SPR sensor.

### **5.A.2 Smartphone Based SPR Sensor using an External LED**

It was apparent from our research that many smartphone based SPR sensors would use the LED flashlight on the smartphone itself as the light source for the excitation to occur. But after careful consideration, we decided that having the light source be separate from the smartphone device would be much more beneficial to our final design. A separate light source from the device would allow us to manipulate the optical path to fit our needs, as opposed to constraining ourselves to have the light from the smartphone be redirected back onto the camera of the smartphone. One example of using an external LED as their light source was a study done in Turkey in 2016 [2]. In this experiment, a green LED with a central wavelength of 520 nm was used as the light source and was directed towards the SPR sensing location using multimode optical fiber and a beam splitter plate. A schematic of the final device and two images of the finished product can be seen below in Figure 6.

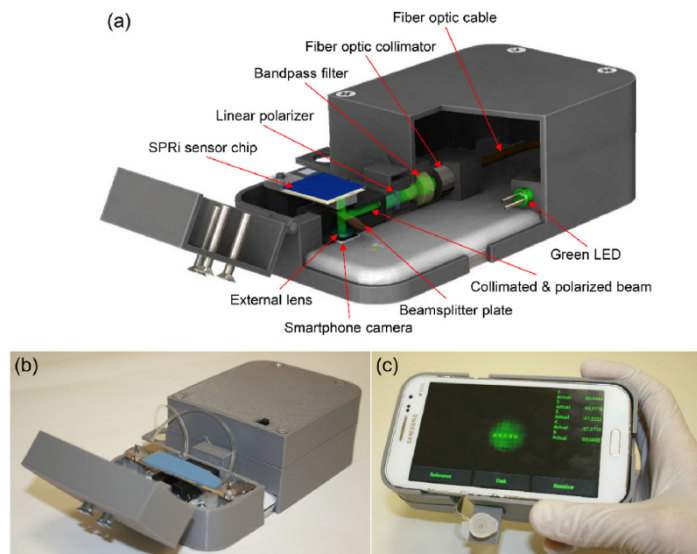


**Figure 5. SPR Imaging Platform with a Smartphone.**  
 (a) Schematic illustration, (b) Image of final product, (c) Image of application for monitoring.  
 Reprinted with permission from Copyright Clearance Center's RightsLink service.

The optical fiber would direct the emitted light from the LED towards a bandpass filter and a linear polarizer to ensure the incident light was correctly polarized and had a central wavelength of 520 nm for intensity modulation. After this, the light was directed onto the sensing location of the SPR sensor. The SPR sensing location used a lab made SPR chip which used a Blue ray disk coated with gold and silver nanoparticles and functionalized with RAM IgG antibodies that were immobilized onto its surface. A beam splitter was placed in the optical path to direct half of the light onto the Blue ray disk SPR chip and the other half onto the camera of the smartphone device. The light directed onto the SPR chip would experience surface plasmon excitation which would cause a dip in its intensity. The reflective surface of the Blue ray disk would allow the light to then be redirected into the beam splitter and into the camera of the smartphone device where it could record a video of the intensity changes seen by the SPR sensor during the experimentation.

### 5.A.3 Prism-coupled Method for SPR Sensors

The two products mentioned previously both used multimode optical fiber for wave propagation of their incident light. The purpose of this was to ensure their final product was more compact compared to commercial SPR sensors. However, the traditional method of a prism based SPR sensor commonly used for commercial devices is a much simpler setup that provides a high level of sensitivity to the device. To accomplish this, a method called angle-resolved SPR detection is used where molecular binding is measured based on the changes in the resonance angle observed when the refractive

index of the sample material changes. Figure 7 below illustrates a device using angle-resolved SPR that can be attached to a smartphone device [3].

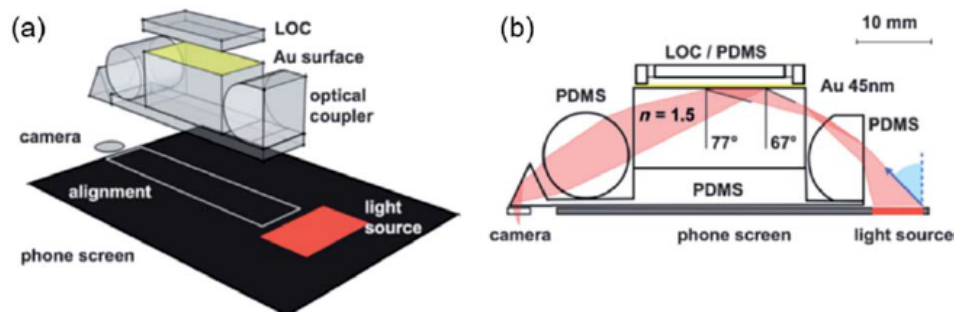


**Figure 6.** Angle-resolved SPR for smartphone application.  
 (a) 3D schematic of disposable device, (b) 2D schematic of experimental light path. Reprinted with permission from Copyright Clearance Center's RightsLink service.

Although this device does not use a prism in its optical path, it uses the idea of angle-resolved SPR detection and the light is manipulated using the refractive index of the various materials used. For this device, a disposable component was assembled to be placed on the front camera of a smartphone for molecular binding detection. The light source used was the screen of the cell phone itself instead of the LED flashlight as has been previously used. The disposable component was made of PDMS and epoxy, which has a particular refractive index that allowed the light to be redirected onto the gold coated surface where the SPR sensing would take place. This device provided us with ideas on how one can use 3D printed components or other materials such as prisms to direct your incident light in a way where one could observe angle-resolved SPR detection. It also showed us how we could design an optical path that is compact for our final product without the need for optical fiber.

## 5.B Optical Fiber for Wave Propagation

To avoid the traditional method of a prism based SPR sensor for surface plasmon excitation, many mobile SPR sensors utilized multimode or single mode optical fiber as the optical coupling element for wave propagation [1]. This method allows for a more compact and simple optical system for the incident light to be directed onto the SPR sensing region. However, the SPR sensor is installed directly onto the optical fiber by depositing a metal layer onto an exposed portion of the fiber core. An SPR sensor contains a disposable component where the molecular binding takes place. After a certain number of experiments, the optical fiber would require replacement and the metal layer deposited once again. A more consumer-friendly approach would be to avoid requiring any optical realignment for reuse of the product. Our final product will

utilize a prism-based system where the phenomenon of total internal reflection enables surface plasmon excitation, thus removing the complication of disrupting the optical path whenever SPR sensor replacement is required. The prism-based system will be discussed more in detail in section 3.D.4 below.

## **5.C Light Sources**

Semiconductor devices are the most important discoveries for modern technology. Semiconductors are an essential component in electronic devices, allowing the positive advancement of society. In SPR sensing surface plasmon resonance detection only occurs at certain spots along the noble metal thin film attached to the prism. As the light propagates through the prism, it will contact the film at the angle of total internal reflection, causing some of the light to be absorbed into the film, minimizing the light intensity. When the wave vector of the incident light, or momentum of photons matches the wavelength of the surface plasmons, the electrons resonate. This is the reason for the technique's name. This section will discuss two variations of a semiconductor technology, a light emitting diode and a laser diode.

### **5.C.1 LED as a Light Source**

Past SPR sensors that utilized LEDs as a light source include a smartphone based SPR sensor developed in Turkey in 2016 [2]. In this experiment, a green LED with central wavelength at 520 nm was coupled to a multimode fiber which was directed onto a bandpass filter with a central wavelength of 520 nm and full width half maximum wavelength of 10 nm. A polarizer was placed afterwards to only allow transverse magnetically polarized light into the system, where it was then directed onto an SPR sensor chip created with a Blu-ray disk coated with silver and gold nanoparticles. A multimode fiber was chosen to direct the light to capture as much of the LED light as possible, but even using optical fiber leads to some loss of light from the widespread use of the LED itself. Using an LED as the SPR sensor's light source is beneficial because LEDs are affordable and easy to install into a circuit board. A simple circuit would be enough to make the device operational. A monochromatic LED is important to use to prevent any inconsistency regarding the dip in intensity. This means that a specific wavelength of light must be chosen in place of a modern commercial white LED.

LEDs typically have a turn on voltage of 0.7 volts and are operated using a DC power source. The LED consumes the current from the power source to produce light. The power of LEDs can be plotted with respect to the input current to determine the threshold current of the LED. Due to the cost of a pre- collimated LED light source, an unmounted LED would be ideal for the development of a lower cost system.

An LED is not the chosen light source for this device because the photons generated from spontaneous emission do not have a fixed direction. The lack of direction would result in a loss of optical power as the light must be focused in a specific direction to enter the optical system, however an LED can be focused using a collimating lens. A collimating lens induces uniformity on the light before the gold film within the SPR sensor chip absorbs the light to indicate biological interactions within the sample. A lens placed directly in front of the CMOS sensor would be necessary to focus the light into the sensor to analyze and display the transmitted data.

### **5.C.2 Laser Diode as a Light Source**

A laser diode module can be used as the light source for SPR sensing. This device requires a collimated beam to interact with the thin film of metal for uniform data collection so using a laser diode can be seen as a more optimal light source than an LED as an LED requires a bit more optical manipulation to utilize the style of light desired. A few options for diodes will be analyzed in this section.

The first laser diode in question is a 635-nanometer diode pumped solid state laser from the vendor Thorlabs. This laser diode emits an output power of 1.2 mW, which makes it a Class 3R laser. This laser has a beam divergence of 0.6 milliradians and a axis deviation of 5 milliradians. Another important characteristic necessary for the device is laser module size. The dimensions of this module are 11.0 mm by 58.0 mm. This module is small enough to fit within the 3D printed casing without occupying a great amount of space, and large enough for adjusting in accordance with what is necessary for the finished product. A heatsink is directly installed into the laser diode to direct heat flow away from the diode. The heatsink moves any heat generated from the laser diode away to prevent damage. If this were not installed directly into the module, it would be placed into the circuit board that is going to power the diode. Another important characteristic about this diode module is that it has a fixed focus. This removes the importance of using a collimating or a focusing lens as the laser beam will be focused uniformly as it travels through the system. The power stability of the diode is 8 hours on 1 minute off. This means that the module can operate continuously for 8 hours before it begins operating intermittently. The module will begin operating as normal after being powered off for an estimated one minute. This makes it a decent choice for imaging as the device will require the laser to operate consecutively in ten to twenty minute intervals to collect images of the light's intensity. Finally, the laser diode module is mounted into a kinematic mirror mount with two adjusters for the X and Y axis. This ensures our laser is properly aligned before beginning any experiments, which is crucial to ensure phase-matching will occur between the incident wave of our light and the wave of our surface plasmons on the gold film.

Another laser diode that was considered is a 532-nanometer fixed focus diode pumped solid state laser from Thorlabs. This class 2 laser diode module has an output power of 0.9 milliwatts and has a wavelength tolerance of 1 nanometer. The beam diameter is 3.5

millimeters and a beam divergence of 0.5 milliradians. The minimal divergence from this laser diode makes it appealing. The operating voltage for this diode is 4.9V to 5.2 V, the same as our 635 nm laser described above. Information on the chosen 635 nm wavelength over that of the 532 nm is discussed in Section 5.C.2.1 later in this document.

Table 3 below displays similarities between the two diodes that assisted in deciding which was more desirable for the device.

Diode Vendor	Pricing (USD)	Wavelength (nm)	Divergence (milliradian )	Power (milliwatt)	Operating Voltage (V)
Thorlabs	97.37	635	0.6	1.2	4.9-5.2
Thorlabs	160.15	532	0.5	0.9	4.9-5.2

*Table 3. Comparison of Laser Diodes to Purchase.*

The diode that was purchased was the one from Thorlabs with a wavelength of 635 nm. This laser diode is the best choice for the device taking the wavelength of each diode into consideration.

### 5.C.2.1 Determining the Wavelength of the Laser Diode

Calculations that aided in determining the wavelength of our laser diode are discussed further in section 7.A.2.

From the calculations of the length of intensity decay along the direction of propagation and the phase velocity of the surface plasmons for both a 532 nm wavelength laser and a 635 nm wavelength laser, the correct wavelength for our device was chosen. Light slows down when coupled to a plasmon [10], but it can be concluded from our calculations that the phase velocity is slower for shorter wavelengths when compared to longer wavelengths. The decrease in phase velocity, alongside the strong damping observed by shorter wavelengths, leads to a noticeable broadening of the resonance curve. The broadening informs us how quickly over a distance the modes lose their amplitude [10]. As the plasmon propagates over many wavefronts, the angle of the light source must be exact so phase matching can occur between the phase fronts of the incident beam and those of the plasmons. For longer wavelengths, the precise angle for phase matching to occur is only required over a short distance, as can be seen by the narrower dip of the resonance curve. However, shorter wavelengths require that the angle of the incident beam allow for phase matching to occur over a longer distance of wavefronts. A slight tilt of the angle would lead to the system being out of phase and coupling to the plasmons will not occur [10]. Due to this, the longer wavelength 635 nanometer light source was a preferred choice for our surface plasmon resonance sensor.

## 5.D Physical Optics

The following below will be a detailed description of the physical optics that were chosen to align the laser beam into the CMOS sensor. The beam will pass through a polarizing beamsplitter. The polarizing beamsplitter has an extinction ratio of 1000:1, ensuring that only p-polarized light is transmitted while reflecting s-polarized light away from our optical setup. A pinhole iris is placed after the polarizing beamsplitter to control the shape and diameter of the beam. iris, the beam is directed into a right-angle prism mounted in a 3D printed chamber for the liquid to be later added, which is all mounted onto a motorized rotation stage. A bare gold SPR chip is placed onto one side of the right-angle prism where it can interact with the light so that phase-matching can occur at the proper angle between the wave of our incident light and that of the surface plasmons. After interacting with the gold SPR chip, propagating light reflects off at a 90-degree angle after leaving the prism to direct the light into the CMOS sensor. Below we will discuss the importance of our polarizing beamsplitter, motorized rotation stage, and right-angle prism and why each component was specifically chosen for our final product.

### 5.D.1 Polarizing Beamsplitter

Surface plasmon excitation occurs when incident light at a certain angle stimulates electrons at the interface between metal and a dielectric material. This surface plasmon polariton, which is a combined excitation of surface plasmons and photons, is an electromagnetic wave that propagates in the parallel direction to the dielectric material. The surface plasmon polariton cannot be excited simply by unpolarized incident light, but instead requires the incident light to be polarized parallel to the dielectric material so the two waves can combine. To manipulate the incident light to become polarized, a linear polarizer can be used to polarize the light parallel to the plane of incidence. This will allow for surface plasmon excitation to occur when the polarized incident light interacts with the surface plasmon polariton wave. For ease and to ensure only p-polarized light is interacting with our optical setup, a polarizing beam splitter was used to ensure that the amount of S polarized light that travels through the system is limited by the polarization being split. The beam splitter is designed to allow S polarized light to exit perpendicular to the system. To do this, two right-angle prisms are cemented together to create a cube shape. All faces of the cube have broadband anti reflective coating to minimize losses due to reflection. A dielectric coating is placed along the diagonal interface between the two right-angle prisms. This coating reflected s-polarized light while transmitting only p-polarized light. This would ensure that the light contacting the gold film is linear P polarized light. The polarizing beamsplitter was crucial for ensuring that our device properly contains the correct polarization of our incident light so phase-matching between the wave of the surface plasmons and that of our light can occur.



## 5.D.2 Right-Angle N-BK7 Glass Prism

The most widely used design for SPR sensing is through the Kretschmann geometry for total internal reflection. This configuration uses an incident wave, polarized parallel to the plane of incidence, and directs it onto a prism at an angle larger than the calculated critical angle. This creates the phenomenon of total internal reflection, where all the light is reflected off the prism and none is transmitted through the glass material. SPR sensors take advantage of this phenomenon by depositing a noble metal layer onto the side of the prism where the light is reflected off. By doing so, the majority of the light is no longer reflected but instead will travel through the metal layer and excite the surface plasmon polariton wave located between the metal and dielectric layers. To ensure total internal reflection occurs, the glass material of the prism must be chosen carefully. The most common material for optical experiments is N-BK7 due to the purity of its raw ingredients used in the manufacturing process. This allows for a smooth transition and low absorption of the light entering the material, which leads to a refractive index of around 1.5. Utilizing Snell's Law, one can determine the critical angle of N-BK7 glass in air which is calculated to be 41.8 degrees. Total internal reflection only occurs when the incident angle of light is larger than the critical angle when travelling from a medium of high refractive index to a medium of low refractive index. Therefore, if our incident light is angled at 45 degrees, total internal reflection will occur inside our prism. To ensure our reflected light is directed at a 90 degrees angle, a right-angle prism was chosen. This allows for the light to easily be directed onto our CMOS sensor camera for detection of the surface plasmon excitation to occur. Another crucial component to consider in a prism is its surface quality and surface flatness. Surface quality is how many imperfections on the surface of the optical component, such as bubbles, fractures in the glass, and any defects in the coating. A scratch-dig surface quality of 40-20 is recommended for powerful lasers and imaging systems to ensure the light scattering is reduced to a minimum. Surface flatness is a measure of the flatness of your optical surface, usually measured in fractions of a reference wavelength. This is tested by placing the flat, polished surface of the optical component next to a reference surface. A monochromatic light source is directed through the optical component and dark and light bands, known as interference fringes, can be visualized on the reference surface. The amount of curvature seen in the spacing between the fringes is indicative of the surface flatness, with straight lines indicating a high surface flatness. The prism chosen for our SPR sensor contains a surface flatness of  $\lambda/8$ , which is a relatively high standard for general laboratory use. For our purposes, a surface flatness of  $\lambda/8$  is an acceptable range since our SPR sensor does not require a very precise surface flatness to create surface plasmon excitation.

## 4.D.3 Motorized Rotation Stage and DC Servo Motor Controller

A motorized rotation stage is a critical component to the observation of surface plasmons. Motorizing the rotation platform allows the prism to be rotated remotely and more precisely than traditional means. This stage has a mountable 2.56' center platform

that will have the 3D printed chamber attached to the center with the prism at the very center to prevent any lateral deviation from occurring as the stage rotates. This will allow for a reduction in light deviation on the sensor lens as the only movement occurring will be rotational. Some of the stage specifications include a full 360-degree continuous rotation range, a maximum rotation velocity of 25 degrees per second, a calculated resolution of 2 arcseconds, and a percentage accuracy of 0.1%. The rotation stage comes with a K-Cube Brushed DC servo motor controller used to adjust the angles, home the rotation stage to ensure that the angle displayed on the LCD screen is mechanically synchronized with the platform, and manually adjust the angles to the 0.001st degree. The DC servo motor requires a nominal voltage of 6 V, a nominal current of 0.156 A, nominal speed of 1050 rpm, and rotor inertia of 0.298gcm<sup>2</sup>. The DC servo motor will be powered by a wall outlet. The rotation stage also came with access to the Kinesis software to control the rotation stage virtually, with more customization than the DC Servo Motor. Extra customization features include options such as velocity and acceleration adjustments. Unfortunately, due to the closed source nature of the Kinesis software the rotation stage will be controlled primarily through the Kinesis software instead of being controlled remotely from the intensity monitoring software developed for this device.

## **5.E CMOS Sensor and Microcontroller for SPR Detection**

The initial design of our project was to utilize the CMOS camera of a smartphone as the detector for the SPR sensing system. Upon further investigation, we concluded that our project would benefit from removing the smartphone from the optical path altogether. To increase the compatibility of the SPR device, a decision was made to remove the 3D printed smartphone mount that would otherwise position the rear-camera lens for proper lining with the laser. This way the smartphone running the software can be free to move within the transmission range of the microcontroller. This also provides the added benefit of our SPR sensor becoming adaptable to various types of smartphones regardless of its camera's location. However, this provided a new challenge where we had to provide a standalone image sensor to record the data from the laser and upload the images to a webserver for the application to retrieve and process. When choosing a camera module, specifications like capture rate, array size, power consumption, sensor size, and output format were the most important for the accuracy of the processed data. The ESP32 was the first microcontroller that stood out for its low power mode efficiency, low price point, reliability, and wireless features such as Bluetooth low-energy (BLE) and Wi-Fi. Until 2018, ESP32 could not support a parallel camera interface but with the addition of pseudo static RAM (Random Access Memory), this became possible and enhanced the microcontrollers functionality for IoT applications and even artificial intelligence.

With the microcontroller unit selected and because of its newly redesigned parallel camera interface support, there are a lot of varying options for a CMOS sensor.

OmniVision, a leading CMOS image sensor manufacturer, has 30 years of experience in the industry and has become very popular for its system on chip CMOS image sensors. During the inception of our project, we wanted to use a smartphone's internal CMOS image sensor but as said before, we scrapped that idea for the sake of compatibility and an easier user experience. The iPhone 5 uses the OV2C3B unit which was the main source of influence to find the manufacturer and incorporate their image sensors into our SPR device. Our priority requirement for an imaging sensor would be fast processing and reaction time and one that makes use of the digital video port, a parallel source synchronization camera interface with 8-bit data signals. This interface specifically is very friendly with low-end ARM microprocessors such as the ESP32. In contrast, a similar functionality would only exist on high-end MIPI processors. The OV2640 camera module was first on the list and for many reasons. What influenced our decision the most was the JPEG encoder onboard the camera module, it off-loads the processing power in order to reduce the memory footprint on the microcontroller. For a comparison, the max resolution for this camera module is 1600 x 1200 pixels. A typical raw format in RGB656 would be just over 3.5 MB of memory space but with JPEG compression, it would only occupy 150 KB: almost x25 compression ratio.

## **5.F SPR Sensor Surface**

Surface plasmon resonance can be successfully monitored on multiple different types of substrates under the condition of a dielectric film coated on a surface of the substrate. It is a requirement to have the dielectric material be in contact with a noble metal, such as gold or silver, to create surface plasmon excitation. The noble metal will capture the light being reflected off its surface at a certain angle, termed the resonance angle, and excite the mobile electrons that oscillate on the surface of said metal. The wave created by the mobile electrons will combine with the wave of the incident light and create a dip in intensity observed by the SPR detector.

After careful consideration, the noble metal chosen for our SPR sensor was gold. This is due to the oxidation of silver which can lead to complications when reusing the SPR sensor surface for multiple experiments. It was also decided to purchase an SPR sensor chip for our experiment instead of creating our own, due to the time consuming and delicate process of depositing the noble metal evenly onto the sensing location and immobilizing the ligand to be used in our experiment. If the noble metal is not evenly distributed, it can lead to incorrect data and an inconsistent location of our resonance angle.

### **5.F.1 Thickness of Gold Film for Sensor Surface**

Our project focuses around the excitation of the surface plasmons at the gold-dielectric interface. Commonly, the metal film is deposited on one side of a very thin glass slide where the glass surface is pressed against the prism. The thickness of the film itself is a crucial component to consider for excitation of the surface plasmons to occur. Figure 3

illustrates the reflectivity of various thicknesses of silver film at a constant wavelength using attenuated total internal reflection. Although this example is utilizing silver instead of gold, it nevertheless informs us of the varying reflection observed at different thicknesses. Equation 1 below represents the conservation of energy for reflection, transmission, and absorption of our light for surface plasmons.

$$R + A + T = 1$$

**Equation 1.** Conservation of Energy in relation to Reflection, Transmission, and Absorption of Light for SP.

In the above equation, reflection is represented by R, absorption is represented by A, and transmission is represented by T. Energy conservation requires that the sum of reflection, transmission, and absorption equal to 1 [11]. The incident light wave is partially reflected at the interface. It partially transverse the metal film as an exponentially decaying wave. At half the interface, it induces excitation which in turn radiates light back into the metal film [11]. Figure 7 below illustrates the reflection observed on silver film at varying thicknesses measured using attenuated total internal reflection. For thicknesses smaller than 490 Å, the back scattered field increases. Since it is in antiphase with the incoming light wave, the two destructively interfere which reduces R. Since transmission, T, equals 0, and at the minimum thickness, d(min), R = 0, A subsequently becomes 1. This leads to all of the energy being absorbed into the metal film and can be noted by the reflection observed at 290 Å film thickness. For thicknesses larger than 490 Å, the back scattered field disappears so that R approaches close to the value unity, 1. Thus, absorption in the metal film is not greatly observed which leads to a small and narrow dip in reflection as can be seen for the film thickness 890 Å.

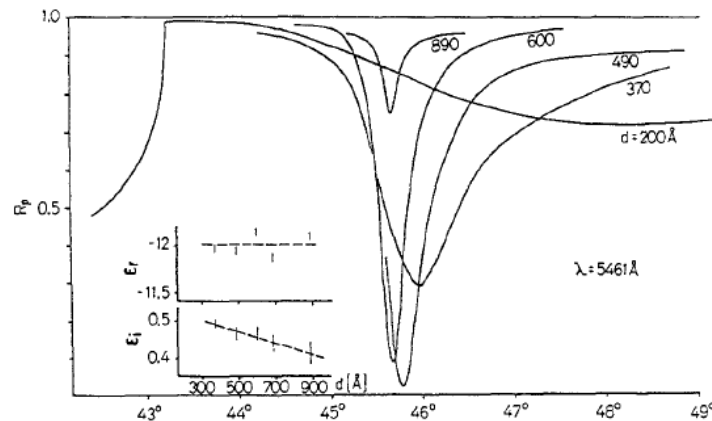


**Figure 7.** Reflection observed on silver film at varying thicknesses measured using attenuated total internal reflection. Permission given by citation [11].

Therefore, it can be concluded that for proper excitation of the surface plasmons to occur, the metal should have a film thickness of about 490 Å, or 49 nm. Manufactured glass slides with the proper film thickness deposited are available for consumer

purchase, commonly known as surface plasmon resonance (SPR) sensor chips. The chips purchased for this experiment are from the company Sofchip, which provided 20 x 20 mm bare gold chips with a film thickness of 50 nm. The chips were chosen due to the ease of use for the experiment, allowing us to avoid depositing 50 nm in diameter gold nanoparticles onto a microscope slide ourselves which could have led to an uneven surface and potential errors in our final calculations. It should be noted, however, that the SPR chips cannot be reused indefinitely and wear and tear was observed on each chip after multiple uses in experiments, especially when submerged in the liquid solution. Therefore, our device contains a parameter where constant purchase of gold SPR chips is required in order to use the device. This parameter cannot be avoided, as it is a feature of all surface plasmon resonance sensors.

## **5.G SPR Sample Preparation**

To obtain measurements that will be used in our experiments to determine the levels of accuracy our SPR sensor can detect, distilled water was used as our test sample. While preparing the samples, care in cleaning the sensing location as well as ensuring the samples avoid contamination was required. Below is a list of the procedures followed for measurement and preparation of our samples:

1. Obtain technical grade distilled water for use as liquid sample for determination of SPR sensor accuracy.
2. Ensure hands are covered with powder-free nitrile disposable gloves to avoid oils from skin affecting optical components.
3. Clean and sterilize table surface and place pre-packaged container with bare gold SPR chips, the index matching gel, a clean syringe and needle for the index matching gel, a sterilized 10 mL syringe, a sterilized glass measuring cup, kimtech wipes for cleaning optics, and isopropyl alcohol of 70% or greater.
4. Clean 3D printed sensor chamber using isopropyl alcohol.
5. Clean surface of right-angle prism using isopropyl alcohol.
6. Ensure the surface of the right-angle prism and 3D printed sensor chamber are dry before continuation of procedures.
7. Remove the bare gold SPR chip from its pre-packaged container using sterilized tweezers to avoid damage to the sensor surface.
8. Using a sterilized 1 mL syringe provided with the index matching gel, gently squeeze a small amount of the index matching gel onto the glass side of the bare gold SPR chip. Extreme care must be taken to avoid touching the index matching gel or one's hands to the gold side of the SPR chip.
9. Gently place the glass side of the SPR chip in contact with the side of the right-angle prism facing the 3D printed sensor chamber. Press firmly on the edges of the SPR chip to create a close seal between the right-angle prism and

the SPR chip to ensure the wave of the incident light can properly interact with the wave of the surface plasmons during the experiment.

10. Pour 50 mL of the distilled water into a sterilized glass measuring cup.
11. Slowly pour the distilled water from the glass measuring cup into the 3D printed sensor chamber.
12. To remove the distilled water from the 3D printed sensor chamber once the experiment is complete, use a sterilized 10 mL syringe to carefully remove the water and discard in a waste container.

After each experiment, the housed device is covered to avoid the 3D printed sensor chamber containing the mounted right-angle prism from contamination by dust or other particles when not in use.

## **5.H SPR Sensor Accuracy**

An SPR sensor utilizes the phenomenon of surface plasmon excitation created when incident light is directed onto a noble metal to determine when molecular binding occurs in an analyte and ligand. Every SPR sensor has a certain level of accuracy for determining when surface plasmon excitation occurs. This accuracy or sensitivity is determined by the quality of optical and electrical components used in the SPR device as well as the quality of the manufactured SPR chip being used as the disposable portion of the sensor. For our device, a set goal for the accuracy level of our SPR must be determined to guide us in deciding how efficient our product will be. To decide this accuracy level, several previously designed SPR sensors were researched to gain an educated idea on what is feasible to accomplish with our design. One such design was a smartphone based SPR sensor created in China in 2015 [1]. The smartphone based SPR sensor used multimode optical fiber for wave propagation of its incident light onto the SPR sensing location. The cladding of the fiber was cleaved to expose the core and gold nanoparticles were brushed onto its surface. Protein A was then functionalized onto the gold surface to create the SPR sensing location. A flow cell was then placed around the exposed core to create a chamber for the testing solution to remain during experimentation. The analyte and ligand used in their experiment was bovine immunoglobulin G and Protein A respectively. From our research, we gained a clear comparison of the limits of detection for a cheaper, smartphone based SPR sensor when compared with a commercially designed one. Figure 11 below illustrates the results for both the commercial and smartphone based SPR sensors.

	Commercial SPR instrument(Biosuplar 6)	Smart phone SPR biosensor
Resolution	$2.7 \times 10^{-5}$ RIU	$7.4 \times 10^{-5}$ RIU
Limit of detection	15.7 nM	47.4 nM
Cost	220,000¥	240¥
Size (without computer/smart phone)	20 cm × 9 cm × 8 cm	12 cm × 6 cm × 2 cm
Weight (without computer/smart phone)	2.5 kg	40 g
Computer/smart phone and operating system requirements	PC, Windows 98/2000 or Windows XP	Smart phone, Android

**Figure 8.** Comparison of Smartphone Based SPR Sensor vs. Commercial SPR Sensor. The above work is licensed under a Creative Commons Attribution 4.0 International License and is free for public redistribution.

For our experiment, we designed an SPR sensor that can monitor changes in the intensity of our reflected light at minimum every 0.5 degree as our prism is rotated using our motorized rotation stage. Due to the high precision provided by our chosen motorized rotation stage, we are able to achieve 25 arcsec incremental motion with 0.1% accuracy, making us accurately determine at what angle surface plasmon excitation occurs during each experiment.

## 5.1 Power Delivery

During the inception of our SPR device, we planned to use the internal camera of an Android smartphone to capture the information and process it. Now we have redesigned the device to use an exclusive camera mounted inside our SPR device. To control this camera module, we would use a low-power microcontroller unit. The ESP32-CAM was a perfect choice for its wi-fi and Bluetooth low-energy functionality as well as its compact size. The ESP32-CAM has two different powering methods, a 3.3v and a 5v input. The 5v method was selected to ensure reliability and a stable clock rate. The maximum current draw of the ESP32-CAM is 1200 mA but with our limited use and proper programming we expect our maximum current draw to be 500 mA. When prototyping the ESP32, it was observed that the device can draw 500 mA for startup before settling to a lower and more consistent current.

Before changes were made to our SPR design, we had the smartphone mounted to the side of the device to use its camera as the primary CMOS image sensor. The touch screen display would still be usable, but this caused compatibility issues and could disturb the experiment if the device was moved too much. Our current design is to use an internal camera module inside the device with a microcontroller wirelessly feeding the captured data to a compatible computer or smartphone. Since our focus is no longer on the smartphone mount, we had to forgo the use of a smartphone battery to power the SPR device. Our current design is utilizing one 9v Alkaline by Energizer. A linear regulator was used to drop the voltage from around 9v to a steady 5v with the use of two electrolytic capacitors. Although this was successful at properly supplying our microcontroller with enough power, the L7805 linear regulator is very inefficient, and we

observed in our prototype that almost two thirds of the total energy released by our single 9v battery was released into the form of heat. After researching alternative methods, our next decision was to invest in an integrated switch or buck converter. If properly designed, we can increase our efficiency up to 95 percent without a negative effect on the microcontroller performance. Even in the worst case of drawing 500mA for an hour, we expect a single 9v Alkaline battery to satisfy the requirements of the microcontroller.

Further research will be done on the chemical makeup of batteries to narrow down the most appropriate choice for our microcontroller. In order to avoid disturbances of the internal electronics and unnecessary waste, our next focus would be on rechargeable batteries. This will influence our decision on the battery's chemical makeup and the number of cells we use in the device. We will use a USB connection port for charging input.

## **5.J 3D-Printed Housing and Mounts**

The Surface Plasmon Resonance device will use several specially designed 3D printed housing and mounts for convenience, reusability, and minimal monitoring to ensure a perfectly performed experiment.

Polylactic acid is a popular thermoplastic used with fused deposition modeling (FDM) printers. It's cheap, abundant, and derived from fermented plant starch, usually from corn. This thermoplastic has been chosen for its high tensile strength of 7,200 psi, biodegradable nature, and appropriate thermal resistance. The glass transition phase starts at 60 degrees Celsius; this phase is described by the thermoplastic's ability to deform and lose structural tension. The thermoplastic that will be used for our housing is a compound of polylactic acid to account for a better ability to dampen vibrations; because the compound varies between manufacturers, we can only use the pure form of polylactic acid as a baseline for measurements.

## **5.K Software Solutions**

The ESP32-CAM will be controlled by a get request through HTTP, we need an application to perform these requests in a timely manner. Our engineer requirement has the capture frequency at 0.5 seconds between captures. This is achievable with the chosen hardware with plenty of room for energy optimizations. The next responsibility for our software solution is to then process the captured data and create visual representations for the user to read and analyze. Processing the captured data at the same time as capturing the data does not need to be processed at the same time but it will greatly shorten the time between the start of the experiment and the moment the data can be readable from a visualization. Most modern hardware such as smartphones and laptops should be more than enough to do both tasks simultaneously, but no testing has been done on cheaper smartphones or weaker computers yet.



As stated previously, the main task for the software solution is to process the data gathered by the image sensor. When the processing happens has not been fully decided upon but the decision has little impact on the concept behind the processing. The expected behavior of the surface plasmon resonance phenomenon can be measured through the form of intensity modulation. To the CMOS sensor, the intensity can be described as 'brightness' when looking at the captured data. The data capture can be simplified by capturing only monochromatic images and interpreting perfect black as a value of 0 and perfect white as a value of 255 in reference to brightness. The caveat of our software solution is as follows, what decides the brightness of an image. There are three possible approaches that seem to give the best results for our situation: average brightness of the pixels, a histogram of brightness distribution amongst the pixels, or the root mean square value for all pixels. Each method can produce a different value, but one method may be better than the rest for our use case. Our first elimination was the average brightness of the total pixels, we expect interference noise and artifacts to be present on each captured image and that will distort the accuracy of our data. Root mean square can process undesirable information in the image, but the value would be more generalized and should prove to be more accurate for our needs. The histogram approach seems more desirable since we'll be able to ignore the values of some pixels that could be interpreted as noise or artifacts, but all three methods could still be sufficient during testing.

Once the image data has been captured and the software has finished processing all needed data, the user should be able to read the visualizations on screen and discern if excitation has occurred. Our sub-goal is to allow the user to know if excitation is occurring or not during the experiment, but this is not a requirement. The user should be able to explore past experiments and export the data as needed. The software will have complete control over the microcontroller and therefore the entire device.

## **5.L Different SPR Monitoring Methods**

There are three classified forms of monitoring surface plasmon excitation: angular, wavelength, and intensity modulation. There is no perfect one, as each different form is based on the particular light being measured or the molecular binding that will be observed. In the following sections, we will discuss the three different modulations that are common in a commercial surface plasmon resonance sensor and the pros and cons of each.

### **5.L.1 Angular Scanning**

The most common modulation method used in commercial surface plasmon resonance sensors is angular scanning. In this method, a monochromatic light source is directed at different incident angles to the noble metal on the prism [4]. As excitation of the surface plasmons is created, the detector will observe a dip in the intensity of the reflected light where the resonance angle is located. Figure 12 below illustrates the reflection spectra

for an angular scanning method where two incident angles were measured and their respective dips in intensities were observed.

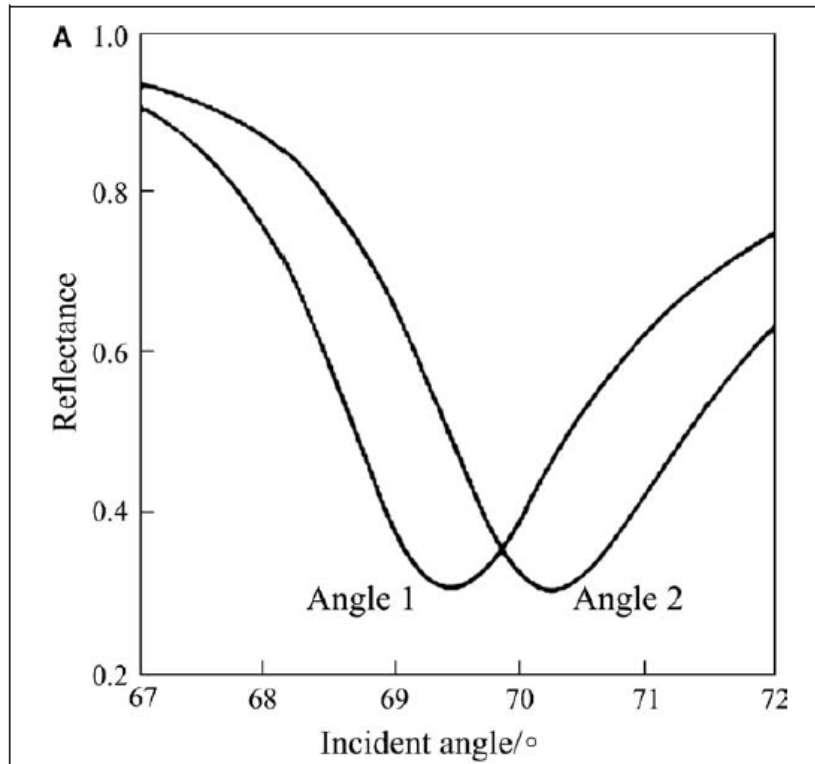


**Figure 12.** Reflectance Spectra for Angular Scanning.  
Permission for figure given from citation [5].

This method is most widely used due to its high resolution and wide range of refractive index measurements as it scans a range of various incident angles to show the changes created by molecular binding. However, this setup can be costly due to the mechanical components required to allow the incident angle of your light source to change throughout the experiment. It also creates a more complicated optical setup as well, as you must consider the change of the incident angle also having an effect on the reflected light path. Many surface plasmon resonance sensors that utilize angular scanning use the Kretschmann configuration, which involves a light source directed at a prism to use total internal reflection as a method to excite the surface plasmons on the noble metal surface. This monitoring method therefore can be very useful but does greatly increase the cost and difficulty of the final surface plasmon resonance sensor.

### 5.L.2 Wavelength Modulation

Another method to monitor surface plasmon excitation is with wavelength modulation. In wavelength modulation, the incident angle of the light source is fixed during the experimentation. However, unlike angular scanning, the light source is not monochromatic but has a spectrum of wavelengths. This is commonly done using a

white light source and measuring the red, green, and blue wavelengths of the reflected light. When surface plasmon excitation is created, the intensity of the reflected light is at a minimum at the resonance wavelength [5]. Figure 13 below illustrates the reflectance spectra for wavelength modulation.

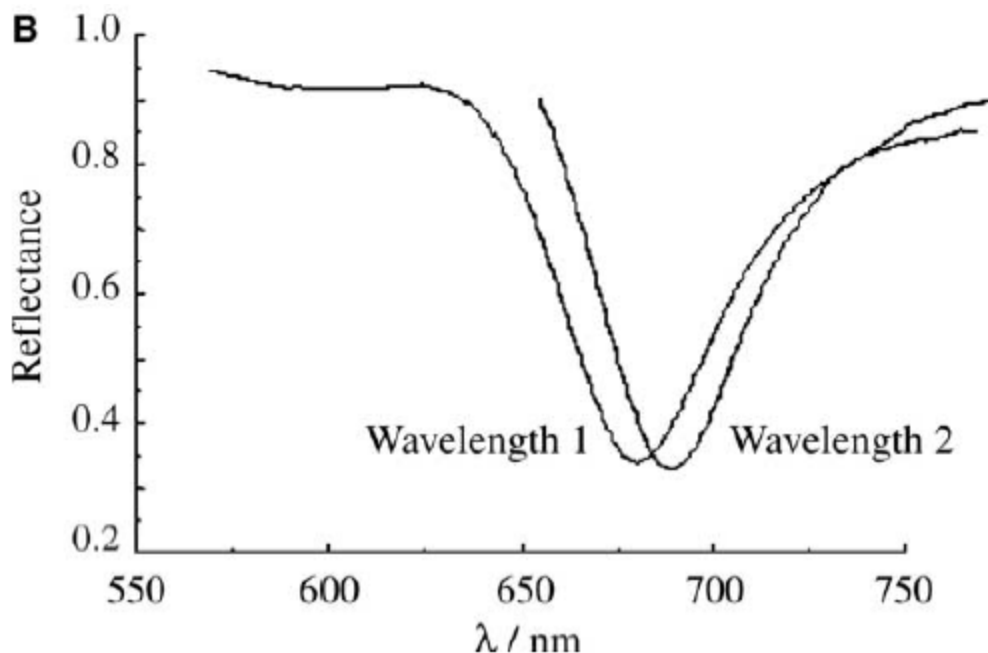


**Figure 10.** Reflectance Spectra for Wavelength Modulation.  
Permission for figure given from citation [5].

The interaction of the molecules being observed can be monitored by measuring the shift of the resonance wavelength over time. This method is easy to miniaturize and is commonly used for low-cost surface plasmon resonance sensors that use a smartphone's white LED as the incident light source and optical fiber for wave propagation.

### 5.L.3 Intensity Modulation

The third method used for monitoring surface plasmon excitation is called intensity modulation. In intensity modulation, a monochromatic light source is fixed at a specific incident angle and the detector measures the intensity changes of the reflected light. Intensity modulation allows for a simple and low-cost setup for surface plasmon resonance sensors, but at the cost of the overall sensitivity of the device. Figure 14 below illustrates the reflective intensity curve created using different extinction refractive indexes with a 632.8 nm wavelength laser fixed at an incident angle of 74 degrees. As can be seen, the dip in intensity observed is much shallower compared to the one observed with wavelength modulation and angular scanning illustrated in prior sections.

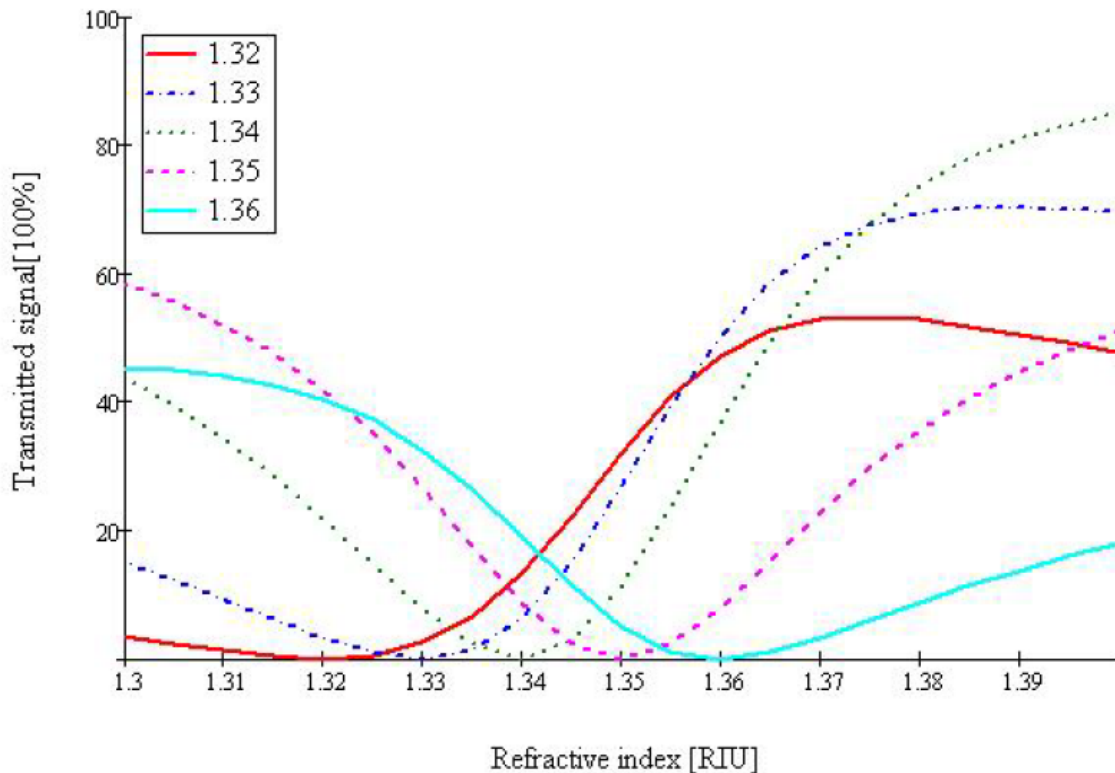


**Figure 11.** Reflection Intensity Curve for Intensity Modulation.  
 Permission for figure given from citation [6].

However, research has been done to combine intensity modulation with changes in the polarization state of the incident light to allow for more complex and higher sensitivity of molecular binding to be monitored [6].

## 6. Constraints and Standards

A key aspect in project development is production under certain conditions. The constraints listed below will discuss the areas of development that are limited to specific criteria. These constraints can have a negative impact on the design process depending on government issued regulations such as ITAR. The standards of optical components and computation of images, such as data processing will be noted in this section. Basic laser safety will be introduced as well.

### 6.A Constraints

For every product design, there are a level of constraints that must be considered which can limit the final project. Common constraints such as financial and software are the first that come to mind, but a professional engineer should consider the more abstract

constraints such as ethical and environmental to ensure their product is safe and sustainable for long term use. In this section, we will discuss the various constraints specific to our product and our plans to ensure our final design is in compliance with each one.

### **6.A.1 Financial**

Financial constraints stem from the limitations of college students. This project is not funded or sponsored by a third party, leaving the financial decisions and spending up to the developers. This allows for freedom of choice when applied to catalog browsing for the desired equipment but can be very costly. To keep the pricing to a minimum, some of the basic components will be purchased online through a third-party website for vendors, Ebay. The basic components purchased from Ebay will not be the highest quality but will function as intended and allow more lucrative spending on the more important components.

The financial goal for this sensor is a \$600 investment ceiling. Commercial SPR sensors have a cost estimate of \$40,000. Because of the financial disparity, this device will not provide as high of a sensitivity for surface plasmon detection as can be achieved using a commercial SPR sensor. This device can be seen as a more affordable option if mass manufacturing for consumerism is pursued. The total cost is anticipated to be within a 10% window of the \$600 investment goal. This is a result of the SPR sensor chip package being priced at half of the investment goal. Luckily the manufacturer the sensor chip is being purchased from has the most cost-effective sensor chip. This allows for the device to be less expensive, as other sensor chips on the market are priced around \$700.

In addition to the financial constraints above, CREOL at UCF purchased some of the equipment used in this device, preventing the progression of mobilizing our device. This is due to a policy that states the equipment purchased by CREOL is the property of the college and must be returned in the original state once the semester is complete. This means that the equipment cannot be altered in any way to fit the needs of the device to complete the desired goals and restricted this device to only being operable on an optical breadboard.

### **6.A.2 Environmental**

The components will be housed inside of a 3D printed casing made from thermoplastic polyurethane. TPU longer lasting plastic that is more eco-friendly than other commercial plastics. Using this type of plastic for the device housing does not result in any sort of constraints, as it benefits the longevity of the project, and the environment as polyurethane can be broken down using microorganisms without emitting toxicity.

### **6.A.3 Social**

Social constraints are limitations set upon a device's development that stem from the influence of social behaviors. Upon further inspection, a mobile surface plasmon resonance sensor has miniscule societal constraints that will prevent or limit development of such a device. The constraints that do exist pertain to government regulations on light sources.

### **6.A.4 Political**

Political constraints are limitations set upon development that stem from local to federal political climates that influence policies. Upon further inspection, there are no political constraints that are applicable to the surface plasmon resonance sensor being developed. However, political constraints can be applied towards regulation and importation of optical components from trade restricted regions.

### **6.A.5 Ethical**

Ethical constraints are limitations set upon development that involve and potentially intrude on user privacy, and safety. Ethical constraints do not apply to the sensor's anatomy but can potentially apply to app development. This can be resolved by asking the user to consent to any sort of involvement of privacy, such as accessing the mobile device's photo reel to read pre-recorded data if needed.

### **6.A.6 Health and Safety**

The light source used in the device is classified as a 3R laser source and has a power output of 1.2 milliwatts. The beam generated is bright and can potentially damage the eye's rods, cones, or retinas if proper eye safety is not taken into consideration during construction and operation. The specifics of the safety concern will be discussed in greater detail further down in the document.

SPR sensors detect molecular binding that occurs in specimens such as antibodies, proteins, bacteria, and other biological substances. Therefore, it is important that proper health and safety precautions are taken when using certain substances that can be harmful to humans or other living organisms. The substance used with our SPR sensor was distilled water. This substance is not harmful to humans, making them ideal for testing our SPR sensor in a safe environment. However, our SPR sensor could be upgraded and used to detect other substances such as pesticides or bacteria which could pose a health risk to those in close contact with them for an extended period of time.

## **6.A.7 Manufacturability**

Constraints on manufacturing limit the device's design that can hinder the device's mass production capabilities. One constraint can be found with the external camera's ability to transfer the captured images to the software application in a timely manner. Our external camera will capture an image every 0.5 seconds which could result in 1,200 captured images at 1080-pixel resolution if the device operates for 10 minutes, which is an average range of time for many SPR sensors to gather an accurate representation of molecular interactions. The camera, microcontroller unit, and Wi-Fi components would therefore need to be powerful enough to store and transfer this information in a timely manner. This constraint would cause the cost to increase and could affect the manufacturability of the final product.

## **6.A.8 Software Compatibility**

In the technology age, it is important to consider the constraint software can have on the versatility of your product. A successful product should attempt to be compatible with multiple operating systems to reach a larger audience. Our software application to control the SPR sensor will attempt to be compatible with Windows, Linux, Android, iOS, and MacOS. This will be done by using a cross platform Python framework that would be compatible with the inputs of different devices such as multi-touch, Windows Pen, and the MacOS touchpad.

## **6.A.9 Sustainability**

When designing a product, it is essential to consider the longevity of the system after its initial completion. Sustainability requires one to consider the lifespan of the device and how reliable its results will be after prolonged use. A professional engineer should always consider sustainability when choosing components and any design decisions throughout the building process.

One sustainability constraint for our product will be measuring the concentration of the analyte solution to test with the SPR sensor. While our experiment tested 50 mL of distilled water in our sensing chamber, any future tests involving biological samples would most likely be measured in micrograms. Measuring to the microgram scale requires precision grade scales that may not be available to every customer wishing to use our product. Scales that measure to the milligram scale are much more affordable to most, with many in the price range of \$16-20. Therefore, this puts a strain on the sustainability of our final product as it requires the user to obtain microgram or milligram scales to properly measure any biological samples they wish to use.

Another constraint for our product is ensuring the chamber for SPR sensing is sealed properly to avoid any leakage. The solutions we will measure in the SPR sensing chamber will be in a liquid form when interacting with the SPR chip, which makes it a

hazard to our sensitive electrical and optical components inside the 3D printed case. To avoid leakage, we sealed the base of our right-angle prism with hot glue, which is made from ethylene vinyl acetate, amorphous poly alpha olefin, and polyamides. Hot glue as a sealant is safe to use on glass and plastic materials, making it a safe choice to interact with our glass prism and the plastic of our 3D printed case. However, the longevity of the sealant itself is something to consider for our final product. After a certain amount of time, the sealant may need to be reapplied to avoid any liquid from entering the rest of the device.

## **6.A.10 Covid and the Global Semiconductor Shortage**

The global shortage of semiconductors was very influential on our decisions with electronic components. With our time constraints, there was only so much that can be done when one of the key components that was planned from the beginning has a production lead time over three months. In some extreme cases, these lead times can range from a few weeks to a couple years. Alterations to the overall design had to be made when there are no alternative components to be purchased without risking other portions of the project. Forethought had to be taken seriously when purchasing a component that could be damaged or dead-on-arrival. A prime example would be our camera module, the OV2640. This is a camera module manufactured by OmniVision that was released in 2005 but discontinued in 2009. This sensor was targeted to the mobile phone industry, so the production volume has been so large that they are still popular in IoT camera applications to this day. Texas Instruments is a very trusted manufacturer of semiconductor devices and creates a lot of ease with their intuitive catalog organizing and WEBENCH Power Designer for development purposes. They are no exception when it comes to this global shortage. When searching for a proper switching regulator for direct current, it was easier to find something out of stock without a solid estimated time for resupply than it was to find something with a lead time that worked with our time constraints. Thankfully they have such a large supply of their integrated circuits that we were able to find components that we could work with.

## **6.A.11 Time Constraints**

Time constraints are one of the main challenges for our design. With only two semesters to research, build, test, and finalize our device, many of our advanced and stretch features we would hope to accomplish will have to be discarded. We also must consider that one of our two semesters is during Summer, which is only twelve weeks as opposed to fifteen weeks during Spring and Fall semesters. During this time, each of us has obligations that take away time we could otherwise dedicate to our design, which can pose a serious threat to our final project. If we were given more time to dedicate to our final project, there are various advanced and stretch features which were previously mentioned we would like to accomplish that would perfect the accuracy, response time, and longevity of our SPR sensor. The detailed explanation for our advanced and stretch features can be found in the section titled 2.A Features above.



## 6.A.12 Storing and Handling of SPR Chips

To test the accuracy of an SPR sensor, a bare gold SPR chip was used. The SPR chip used was manufactured with 50 nm gold particles evenly distributed over a 1 mm thin square glass surface. Per the manufacturer's instructions, the gold SPR chips are sensitive to temperature changes. Therefore, the SPR chips were stored at 4 degrees Celsius when not in use, as can be seen on the manufacturer label for the SPR chip shown in Figure 15 below.



**Figure 13.** Surface Plasmon Resonance Sensor Chip Manufacturer Label.

Our liquid solution used, distilled water, also had to be properly stored when not in use. Technical grade distilled water is not suitable for drinking and therefore should be properly labeled and stored to avoid accidental contamination or spillage. Once an experiment was complete, the used distilled water was placed in a waste container which was properly disposed of. The container in which the distilled water originated from is stored away from any locations where food or drinks for human consumption are also stored, and the proper safety labels are displayed to ensure no accidental contamination occurs. Figure 14 below shows the container used for the distilled water with the correct labeling to avoid contamination.



**Figure 14.** Technical Grade Distilled Water, 64 oz.

Another constraint is in handling the SPR chips used in our experiment. The SPR chip is extremely sensitive, especially on the side that contains the gold film. As can be seen in the figure above, the manufacturing label warns of avoiding contamination to the functionalized side which contains the gold film. To avoid any contamination, the surface of the chip must avoid contact with any surfaces not being used for testing. The surface of the chip is 20 mm by 20 mm, which makes the task of avoiding contamination much more difficult due to its small size. Figure 16 is an image of the bare gold SPR chips used in the experiments.

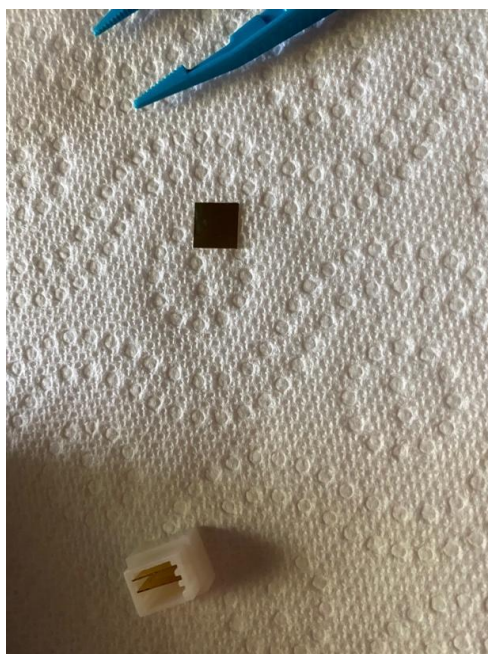


**Figure 15.** Image of Gold Coated SPR Chip.

As can be seen in the figure above, the SPR chips are very small. This will require us to wear gloves to avoid damaging the chip with oils from our skin, as well as using precision instruments such as tweezers that have been sterilized with alcohol and air dried before use. Extreme caution must be taken when transferring the SPR chip from its package onto the base of the right-angle prism to avoid damaging or contaminating the surface of the chip. We will also be required to fix the SPR chip onto the base of the prism with index matching gel, which will also be a constraint to consider as this can become difficult to perform without damaging the surface of the chip. The glue must be placed in a way that ensures the chip remains fixed on the prism during experiments while also not interfering with the surface. When performing the experiment, measures must be taken to ensure nothing bumps or disturbs the surface of the SPR chip when attached to the prism. A chamber was created to protect the SPR sensing location, as well as provide a dark environment to ensure the only light interacting with the sensing location is the light emitted from the laser diode. But when cleaning or transferring different solutions into the chamber, the risk of contamination is once again present. This constraint is one of the most important to consider during our entire design process, as contamination of our SPR chip can not only be a costly error but also a damaging one to our final results. Similar care must be taken when handling the liquid solution, the distilled water. For our experiments, the distilled water must be transferred from the packaged container into a sterilized measuring cup to properly pour into the sensing chamber. When we begin our experiments, care must be taken when transferring the solution from one container to another. Proper equipment such as sterilized syringes should be used to avoid any contamination of our substances. Clean and sterilized glassware, such as beakers, should be used when transferring the materials and properly handled to avoid contamination from the environment. As well, proper procedures for handling chemicals in a laboratory setting must be followed to ensure the safety of those involved in the experiment. Although our substances are not toxic or otherwise irritable to the skin, they are still liquid solutions found in laboratory settings that should be treated with care, nonetheless.

## **6.B Standards**

Standards are a necessary requirement for every industry, providing safe and reliable methods for designing and manufacturing industry components. A set of standards ensures common appliances such as light fixtures or computer hardware can work together even across different industries. Without them, many components we rely on would not work cohesively and could pose a health and safety risk in some instances.

Each industry has its own set of standards that manufacturers follow to allow for easy communication between the consumer and creator. Some standards may involve safety guidelines and procedures that are universal in certain industries. These guidelines must be understood and followed to ensure we minimize and safety hazards that could be present in our work environment. It is good practice as engineering students to learn about the various set of standards in our respective fields and how to design products

following these guidelines. Below we will discuss various standards that are relevant to our project and how we plan to follow these standards throughout our design process.

## **6.B.1 Laser Safety**

Lasers can be classified into multiple distinct categories for safety purposes based on their emission characteristics. Most lasers are required by the law to classify lasers using the IEC 60825-1 and 60601-2-22 standard. The five categories are listed below.

- Class I: The output power is less than 0.39 milliwatts. This laser is not capable of producing dangerous levels of light.
- Class II: Has a visible beam that has a power of less than 1 milliwatt. Only applicable to visible light lasers.
- Class IIIa: The output power ranges from 1 to 4.99 milliwatts. Generally safe but recommended to view with proper eye equipment.
- Class IIIb: The output power ranges from 5 milliwatts to 499.99 milliwatts. The beam is hazardous if directly viewed without proper viewing equipment.
- Class IV: Output power of 500 milliwatts or greater. Beam can cause irreparable damage even if indirectly viewed.

The laser in this device is classified as a 3R laser. The output power of the device's laser diode is 1.2 milliwatts. While operating the laser, proper eyewear must be worn to prevent eye injury. Eye protection will not be necessary once the laser diode is mounted within the casing.

The eye protection necessary for operating this type of classification will assist in filtering out 635 nanometer wavelength light to prevent any devastating damage to the eyes.

## **6.B.2 Surface Quality of Optical Components**

The surface quality of optics is important because it is an evaluation of faults on the surface of the optics. One of the standard classifications for surface quality is known as the scratch-dig metric. The United States Military Performance Specification MIL-PRF-13830B documentation, as seen in Figure 11, describes and classifies the surface quality of optics using the scratch-dig metric. The document states that all optical elements, components and systems must comply with the scratch-dig metric for military use.

A scratch, as defined by section 3.5.2.1 of the document is a mark on the surface of the optics. The surface marks can be ranked on their brightness using these arbitrary numbers: 10, 20, 40, 60 or 80. The assigned value increases as the brightness of the scratches increases. The values for classification are arbitrary because the number is not an exact measurement but are a subjective comparison between component and

calibration. The maximum permissible scratch size is one fourth of the optical component's diameter. If a maximum permissible scratch size is on the surface, the sum of the scratch numbers multiplied by the ratio of their length with respect to the diameter must be below one half of the maximum scratch number. When there is no maximum sized scratch, the sum multiplied by the ratio must stay below the maximum permitted scratch number. Scratches on optical coatings that do not interfere with the surface of the glass must also abide by these guidelines.

A dig, unlike a scratch, is a measurable value. A dig, as classified in section 3.5.3.1 of the document, is the diameter of defects allowed, specified in units of 1/100mm. The maximum dig size permissible is one per each 20mm of diameter, or a fraction of that optical surface. Any digs with a diameter size of less than 2.5 microns are negligible. If the optical material has a bubble within the surface it is classified as a dig. The maximum size of surface bubbles allowed is one per 20mm of light travel, under the impression that this is placing arbitrary normal reference points on the optical axis. For example, if a BK7 prism, such as the one in this device, was arranged so that the light penetrates the hypotenuse to transmit through the glass, bubbles within the glass are only permissible for every inch of travel inside of the prism. If nonsymmetrical shaped digs occur on the surface of the optic, then the diameter will be accounted for as the average of the maximum length and width on the surface. In the case of bubbles, irregular shapes will be considered as one half of the sum of the maximum length and width. Figure 17 illustrates the scratch-dig for optical devices and their various optics specifications. This figure informed us on the proper scratch-dig that would be required for our optical setup. Table 5 below shows the scratch-dig specifications and their application for practical use from the company Newport Optics.

Focal planes and near focal planes			Central zone 1/2 diameter of surface		Outer Zone	
Beam diameter (mm)	Magnifying power	Focal length (mm)	Scratch	Dig	Scratch	Dig
Over 5.....	.....	.....	80	50	80	50
4-5.....	.....	.....	60	40	60	40
3.2-4.....	.....	.....	60	30	60	40
2.5-3.2.....	.....	.....	40	20	60	40
2.1-2.5.....	.....	.....	40	15	60	30
1.6-2.1.....	.....	.....	30	10	40	20
1.0-1.6.....	.....	.....	20	5	40	15
0.6-1.0.....	.....	.....	15	3	30	10
0.4-0.6.....	.....	.....	10	2	20	5
0.2-0.4.....	.....	.....	10	1	15	3
0.2.....	20-10	12.5-25	10	1	15	3
0.4.....	10-5	25-50	10	2	20	5
0.6.....	5-3.3	50-75	15	3	30	10
1.0.....	3.3-2	75-125	20	5	40	15
1.6.....	2-1	125-250	30	10	40	20

**Figure 16.** Scratch-dig table from the MIL-PRF-13830B.

*This figure is approved for public release from the AMSC N/A FSC 6650, and distribution is unlimited.*

Scratch-Dig	Quality	Applications
60-40	Low	Commercial use
40-20	Standard	Imaging and low power lasers
20-10	High	Laser mirrors and high-power lasers
10-5	Highest	High energy applications

**Table 5.** *Scratch-dig specifications and some of their applications for practical use. This table was created using the citation [7].*

The scratch-dig metric is important in optical manufacturing because it forces manufacturers to construct their optical components fit within certain specifications for sales. The benefits of following the scratch-dig metric when it comes to component shopping is being able to determine which specification is more appropriate for the system being built. The scratch-dig metric helps determine the amount of internal scatter since the tighter the specification, the lower the scatter. For example, if a system does not have a need for reducing scatter or the scatter is negligible, a 60-40 scratch-dig specification is optimal. If the system needs minimal scatter due to the amount of precision needed, such as a laser system or an imaging system, a 20-10 or 40-20 scratch-dig specification is best. The prism in this device has a 40-20 scratch-dig specification making it a good choice because the device will be recording images of the laser after the beam contacts the SPR sensor chip. Table 3 above describes some applications based on the scratch-dig specification of the optics.

### 6.B.3 Communication Standards

The Surface Plasmon Resonance device will utilize the wireless capabilities of our chosen microcontroller unit to expand compatibility amongst all devices that can function with the following IEEE wireless communication standards.

#### 6.B.3.1 IEEE 802.11

The IEEE 802.11 is part of the IEEE standards for local area network technical standards [8]. The wireless local area network standard is used for implementing communication between the microcontroller unit and the computational device used for processing the data retrieved from the CMOS image sensor. The IEEE standard describes the compatible wireless communication bands of 2.4 GHz and 5 GHz that will be used by the system on chip Wi-Fi module.

#### 6.B.3.2 IEEE 802.15.1

The IEEE 802.15.1 covers wireless personal area networks such as Bluetooth and is intended to expand the functionality of the SPR device with multiple forms of wireless communication [8]. Although Bluetooth is not the primary wireless communication

standard, the option of use for Bluetooth Low Energy mode which operates at a frequency of 2.4 GHz can greatly expand the device's battery life without compromising performance.

## **6.B.4 Software Standards**

The Surface Plasmon Resonance device relies entirely on the collection of data during experimentation and the software must follow strict standards set by recognized organizations to ensure reliability in our experiments. If we cannot be confident in our software due to bugs or unintended features, then we cannot be confident in the accuracy of our processed data. These standards are applied to the communication features, electronic connections controlled by the software, and the source code itself.

### **6.B.4.1 Agile Development Method**

The Agile Development Methodology is based on iterative development by communicating with the targeted user or customer, developing in phases while adapting to changes in the design requirements. This method will ensure the software to be useful for prototyping without being fully completed, creating a greater ease when reassessing the design to satisfy the requirements more precisely. Since the software is made up of multiple functions and has a final goal of interpreting data visually for an enhanced user experience, a lot of the functionality of the software can be completed without the reliance on other features. By utilizing this method, our team will be able to communicate more thoroughly with a schedule that's made to ease adaptability.

### **6.B.4.2 Android Developers Core App Quality**

The Android Developer's Core App Quality is a set of guidelines used to help ensure the quality of the application [8]. They are very commonly used in the community to set a standard for the user experience and to avoid unintended features. These guidelines work like a checklist which covers a large variety of topics such as visual design and navigation, notifications, pop ups, privacy and permissions and even performance on varying devices.

### **6.B.4.4 IEEE 830.1998**

The IEEE 830.1998 is part of the IEEE standards for recommended practices for software development. The standard is a rubric for assessment of software requirements and is intended to be used as a scoring guide [8]. This standard will have direct influences on our development environment and how the software will behave on both mobile devices and personal computers. Since the SPR device is intended for commercial use for the industry and possible everyday consumers, then it is very important these standards are utilized to ensure proper uniform scaling and a streamlined development process.

## **6.B.5 Battery Standards**

IEEE 1625-2008, a standard on rechargeable batteries for multi-cell mobile computing devices. The established criteria are intended to be used for design analysis for quality, reliability of the battery system, and qualifications of the battery itself. It provides methods for quantifying the operational performance of the batteries and their control systems. The battery technologies covered in this standard are limited to lithium-ion polymers. This does include the battery's electrical and mechanical construction such as the system, pack, cell level charge and discharge controls as well as the battery status communications. The follow topics are the focus of this standard: qualification process, manufacturing process control, energy capacity and demand management, levels of management and control in the battery systems, packaging technologies, and finally the considerations for end-user notification for the battery's status [8].

## **6.B.6 Microcontroller Standards**

IEEE 1118.1-1990 is part of the IEEE standards for microcontroller system serial control buses. A serial control bus for inter device as well as intrasite interconnection of microcontrollers is described. The bus, which is defined for microcontrollers and devices with limited reprogrammability, provides a multidrop bit-serial communication protocol that will allow the interconnection of disturbed independently manufactured devices. The protocol is optimized for instrumentation, disturbed data acquisition systems, control devices, and test and measurement. Specifications for a common architecture, generic bus services, system wagement, data link, and several physical media are provided [8].

## **6.B.7 Chemical Laboratory Safety in Academic Institutions**

Whenever chemicals or biological samples are used in a laboratory setting, certain standards must be followed to ensure the safety of everyone involved. It is crucial that the standards decided upon remain the same in every laboratory setting to ensure that everyone understands the hazards and safety procedures required when handling toxic or otherwise dangerous materials. The American Chemical Society for Lab Safety has devised a set of standards and procedures that can be adapted to various environments, from academic to professional settings. The purpose of these guidelines is to promote safe, ethical, responsible, and sustainable practices that are accessible through educational training provided by the society to all academic and professional laboratories [9]. The 8<sup>th</sup> edition of the American Chemical Society Safety in Academic Chemistry Laboratories will provide us with guidance on the best practices to perform when handling the various biological samples we will use in testing the accuracy of our surface plasmon resonance sensor. Below are certain sections from the text that are applicable to us throughout the design process of our project to ensure our laboratory settings are as safe as possible for those present in the laboratory environment.



### 6.B.7.1 Personal Protective Equipment (PPE)

Personal protective equipment is one of the fundamental ways to protect yourself when in a laboratory setting. It is used to avoid exposure to hazardous materials you may encounter when working on an experiment in the laboratory. PPE can include items such as gloves, eyewear, and lab coats that protect sensitive areas of your body from exposure to chemicals that may be used during an experiment [9]. For our experiment, PPE such as eyewear should be worn when interacting with the biological samples as they are being mixed and added to the surface plasmon resonance sensor sensing chamber. This is to avoid any of the liquid chemicals being used from entering the eyes in the event of any splashes or spills. The types of chemicals being used determine the type of protective eyewear that should be used. For our experiment, since we will not be using any toxic or hazardous chemicals, regular goggles that cover both the front and side of our face are appropriate for protection. Gloves are also appropriate for our experiment, as it protects the wearers hands from interacting with the liquid materials. It also protects the various samples being tested from the oils on our skin, such as the SPR chip which can be damaged if in contact with our skin. The length of the gloves and the type of material they are made of is another factor to consider when choosing the correct gloves for your experiment. For our experiment, disposable gloves made of latex are acceptable for our purposes, although any members of the group who are allergic to latex should avoid using gloves of this material and instead use ones made of neoprene or butyl rubber that are acceptable as well for our purposes. The length of the gloves can be up to our wrists for this experiment, as we will not be dealing with any substances that can cause burning or irritation to the skin when in contact. In circumstances where one uses chemicals that have negative effects on exposed skin, gloves that cover the entire arm or at least the forearm should be used. As we will be using disposable latex gloves, proper safety procedures dictate that the gloves should not be reused to avoid any contamination from chemicals that may have interacted with the gloves in the previous experiment without notice.

Other forms of PPE include what is appropriate to wear when in a laboratory environment. Loose-fitting clothing such as long sleeves should be avoided as it can be a hazard to any open flames or toxic chemicals that may be present in the laboratory [9]. The material the clothing is made of should also be considered if you will be dealing with open flames or chemicals in a liquid form. The most appropriate clothing to wear is materials made of cotton or other natural fibers which can be less dangerous in case of fires compared to polyester materials that can cause serious burns when melted. Other clothing one should consider is the type of shoes to wear in a laboratory. Closed toed shoes are always recommended even for the least hazardous experiments to avoid not just chemicals from interacting with exposed skin but any glassware or other lab equipment that could break and cause damage to exposed skin. In our experiment, we will not be using flames or chemicals that can damage clothing when exposed to certain materials. However, clothing such as closed toed shoes should be always worn in the laboratory to protect the wearer from lab equipment that could be broken in an accident during the lab, such as beakers or other glassware we will use to transfer our samples.

It also protects us from any other chemicals that may be present in the lab from previous or current experiments without our knowledge.

### **6.B.7.2 Maintaining an Organized Environment**

When in the laboratory, it is essential to maintain an organized environment that is free of obstructions and other obstacles. This is to minimize any tripping hazards from the floor and any spilling hazards from a cluttered workbench [9]. This also ensures that in case of an emergency, the walkways are free and easily accessible so that everyone can safely evacuate the lab in a timely manner. Part of maintenance includes cleaning the floor and tables of any spills that may have occurred during the experiment as soon as possible. Not only can these become tripping hazards, but they can also lead to dangerous chemical or biological interactions if they interact with substances on the floor or workbench that were not properly cleaned by a previous group performing an experiment. Should any glassware break during an experiment, proper cleaning and glass disposal procedures should be taken to avoid any injury. Glass should never be disposed of in a regular trash can, but instead should be placed in a separate receptacle designated for broken glass. Each laboratory contains specific procedures for disposal of glass or chemical and biological substances and should be followed to ensure the safety of everyone that enters the lab. During our experiment, all the procedures involved in maintaining a clean and organized laboratory environment should be followed at all times to ensure everyone that enters the lab during or after our experiment is safe.

### **6.B.7.3 Labeling Chemicals**

During an experiment involving chemicals, various vials or beakers may be used to store any samples used or created. These samples can become a danger in the laboratory environment if not properly and clearly labeled with what type of substance was used. Without proper labels, substances could be wrongly mixed in a dangerous or sometimes deadly manner. Labeling chemicals is one of the most important procedures to follow when in a lab setting and should be handled with care during each experiment. Labels used in laboratory settings fall into two categories: manufacturer and secondary [9]. Manufacturer labels are ones that are found on the container of the substance to be used that was sold by a manufacturer. These labels are not to be damaged, covered, or changed in any way until the container is verified to be empty, due to the wording and information on the label being essential for understanding any interactions that substance could have with other chemicals found in the laboratory. In some circumstances, empty containers that once contained chemicals are reused for other experiments. Before any container can be reused, the label on the verified empty container should be removed completely and the container should be thoroughly cleaned and allowed to air dry. This ensures that no chemical to be placed in the reused container can interact with past chemicals. Under no circumstances should a marker be used to write over an existing manufacturer label and no container should be more than

one label present. The second category is secondary labels. These are temporary labels used during an experiment on substances that were mixed or created in a laboratory environment. At a minimum, the secondary label for temporary storage of a chemical substance should contain the name of the chemical or chemicals being used, the name of the person who filled the container, the date it was filled, and the hazards for the chemical. Should the container be used for long term storage, the label should follow the standards of the Globally Harmonized System of Classification and Labelling of Chemicals (GHS) [9]. Our experiment will include using technical grade distilled water as our liquid solution. This will require us to ensure that any containers containing the distilled water have the proper labeling to avoid accidental consumption, as technical grade distilled water is not intended for consumption under any circumstances. The containers our chemicals arrive in will contain manufacturer labels that must remain undamaged and clearly legible throughout our entire experiment to avoid any cross-contamination from occurring in and outside of the laboratory setting.

#### **6.B.7.4 Cleaning Glassware and Disposal of Chemicals**

Once an experiment is complete, disposal of the substances used must be considered. Proper handling of chemical waste is an important part of incident prevention, leading to very strict rules that must be followed for disposing of chemicals [9]. When disposing of chemical waste, different containers should be used for disposal of different classes of chemicals. This is to avoid any cross-contamination from occurring accidentally, which could result in adverse reactions that may cause fire or other serious damage. The containers used for disposing waste should follow the labelling procedures described above to avoid any confusion as to which container should be used when cleaning. In some circumstances, reactions created in experiments can be neutralized to help reduce waste handling. When disposing of chemicals, the following guidelines should be followed [9]:

- When disposing of chemicals, each class of waste chemical should be placed in its specific disposal container that is properly labeled. The label should be read carefully before disposal and the cap replaced securely on the container after disposal.
- Never pour chemicals into a sink or down a drain unless instructed to by an instructor or lab assistant certified in laboratory safety guidelines. This is to avoid chemicals from entering the sanitary sewer system which could cause adverse effects.
- Materials contaminated with chemicals, such as paper towels used to clean spills during the experiment, should be disposed of in special containers marked for this use.
- Broken glass should be placed in disposable containers specially marked for glassware. If the glassware contained chemicals used during the experiment, a separate waste container should be used to properly dispose of the contaminated glassware. Should any hazardous materials be exposed from

broken glassware, such as mercury, the on-duty lab instructor should be notified immediately and proper cleanup procedures for hazardous materials should be followed.

Once chemicals are disposed of in their proper waste containers, they are now subject to hazardous waste regulations regulated by the local state government and the federal Environmental Protection Agency (EPA) [9].

After all chemicals are properly disposed of, the glassware and other laboratory equipment used should be properly cleaned. Dirty glassware should be cleaned using hot water with environmentally acceptable cleaning agents in a laboratory sink. Chemical splash goggles should be worn while cleaning laboratory glassware to avoid any chemicals from splashing into your eyes. Care should be taken while cleaning, such as not forcing a brush into the glassware or using a high-velocity stream of water, as this can cause the glassware to break and create a hazardous environment. Should the glassware break, use a pair of cut-resistant gloves, tweezers, or tongs to remove the broken pieces of glass from the sink [9].

For our experiment, both the procedures mentioned for disposal of chemicals and cleaning of glassware must be followed. We will be experimenting with distilled water and should follow any proper guidelines described by the Florida Department of Environmental Protection, the federal Environmental Protection Agency, and the University of Central Florida Environmental Health and Safety department. Our liquid samples will be transported in glassware, such as glass measuring cups, that must be properly cleaned and stored once the experiment is completed.

### **6.B.7.5 Safety Procedures for Using Electrical Equipment**

In many chemistry laboratory settings, electrical equipment may be used for equipment used for measurements, Bunsen burners, and other necessary equipment for the completion of an experiment. It is therefore crucial to ensure that all electrical equipment is in good and working condition to avoid using anything that could pose a fire hazard. Before beginning an experiment, all insulation on the electrical cord for each equipment must be inspected to ensure no wires are exposed [9]. If any liquids are being used during the experiment, all liquids should be placed far enough away from any wall outlets or other live electrical wires that could pose a safety hazard. Our experiment will include chemicals in a liquid form that will be close to multiple electrical components, namely laser diodes, microcontrollers, and other various electrical components. Care should be taken to avoid any spillage of our liquid samples that could cause damage not only to ourselves but to our electrical components as well.

### **6.B.7.6 Refrigerating Chemical or Biological Samples**

Some substances used in chemical laboratories require low-temperature storage when not in use. These substances will normally contain a required temperature on their specific manufacturer label to ensure the longevity of the product. Any chemicals or other substances that require refrigeration should be properly labeled in a fridge designated for chemical or biological storage. Some substances may be flammable and should be stored in fridges rated for storage of flammable materials [9]. Food and beverages should not be stored in the same refrigerator that chemical or biological samples are stored to avoid accidental consumption. Our experiment contains some substances that require refrigeration, such as our SPR chip and therefore must be stored in a refrigerator at 4 degrees Celsius. Proper care and labeling of our biological material must be taken to avoid any accidental consumption or cross-contamination from occurring.

### **6.B.10 NASA-STD-8739.3**

NASA's technical standards on soldered electrical connections does not represent formal requirements but acts as guidance to use when preparing or evaluating process procedures for the manufacture of mission critical hardware [8]. Although the focus of these standards is for space flight and ground support equipment, the same practices can be followed when soldering electrical connections and to ensure a less susceptible product due to rough handling as well as implementing safety methods.

## **7. Project Hardware Design Details**

The hardware components of our design relate to the physical parts that will aid us in manipulating the light in our system, measuring the final output of our sensor, providing power to the entire system, and housing the entire setup. The following sections will discuss how these components evolved since our initial design idea and how we decided on our present project design based on research and testing.

### **7.A Design Calculations**

The purpose of design calculations is to determine relevant values to our optical subsystems. These calculations were performed using relevant equations and software that simulates optical results to aid us in determining the best components and specifications for our project.

#### **7.A.1 Snell's Law Calculations for Total Internal Reflection**

In our surface plasmon resonance sensor, the core optical phenomenon observed is total internal reflection created using a right-angle prism and a 635-nanometer

wavelength laser diode. As we know, total internal reflection only occurs when light travels from a medium of high refractive index to a medium of low refractive index. These refractive indices, as well as the incident angle, play a key role in the critical angle which determines when we will experience total internal reflection. Using Snell's Law, we can determine the relationship between the directions our light will travel in these two mediums. Equation 3 below is Snell's Law rearranged to determine the critical angle our light will travel.

$$\theta_2 = \sin^{-1}\left(\frac{n_1}{n_2} \sin \theta_1\right)$$

**Equation 2.** Formula for Critical Angle.

The standard material used for glass in optics is N-BK7 due to its high purity and is why it was chosen as our material for the right-angle prism. Using the equation above, our first index of refraction is the N-BK7 glass which has a standard refractive index of 1.52 with a 532-nanometer wavelength, and the second index of refraction is air which has a value of 1. When light is incident on a medium with a lower refractive index, the ray is directed away from the normal, so the exit angle is greater than the incident angle. The exit angle approaches 90 degrees for some critical angle value, where incident angles greater than the critical angle create total internal reflection. Using the values given above, it can be determined that the critical angle of the prism is 41.81 degrees.

From our calculations, total internal reflection should be observed when the incident angle of our light is greater than the critical angle. To better determine when we should see total internal reflection occurring, the software called WinSpall was used to simulate the reflectivity curve created using a 635-nanometer wavelength laser and a N-BK7 right-angle prism. WinSpall was developed to simulate surface plasmon resonance curves based on the Fresnel formalism. It allows one to add various layers that the rays will travel through, specifying their real and imaginary parts of the dielectric constants, to output a theoretical reflection curve at each angle. In our experiment to determine total internal reflection, there are only two layers the light will travel through: the right-angle prism and air. For the prism layer, the real part of the dielectric constant is 2.29 which corresponds to a refractive index of 1.5. The imaginary part is zero because there is no absorption of our light from the glass prism. For the second layer, air, the real part of the dielectric constant is 1 which corresponds to a refractive index of 1. The imaginary part is zero as well because there is no absorption of our light when in air. The parameters used to simulate the reflectivity curve for total internal reflection using WinSpall can be seen below in Figure 18.

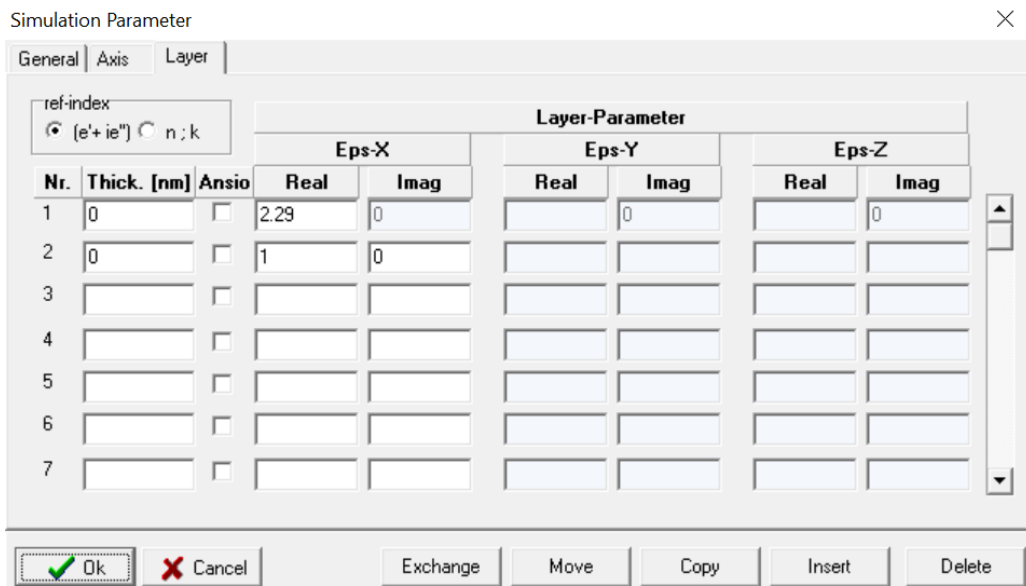


**Figure 17.** Simulation Parameters to Simulate Total Internal Reflection using WinSpall.

With our parameters in place, a simulation of the reflectivity curve we should observe was created. The simulated reflectivity curve can be seen below in Figure 19.

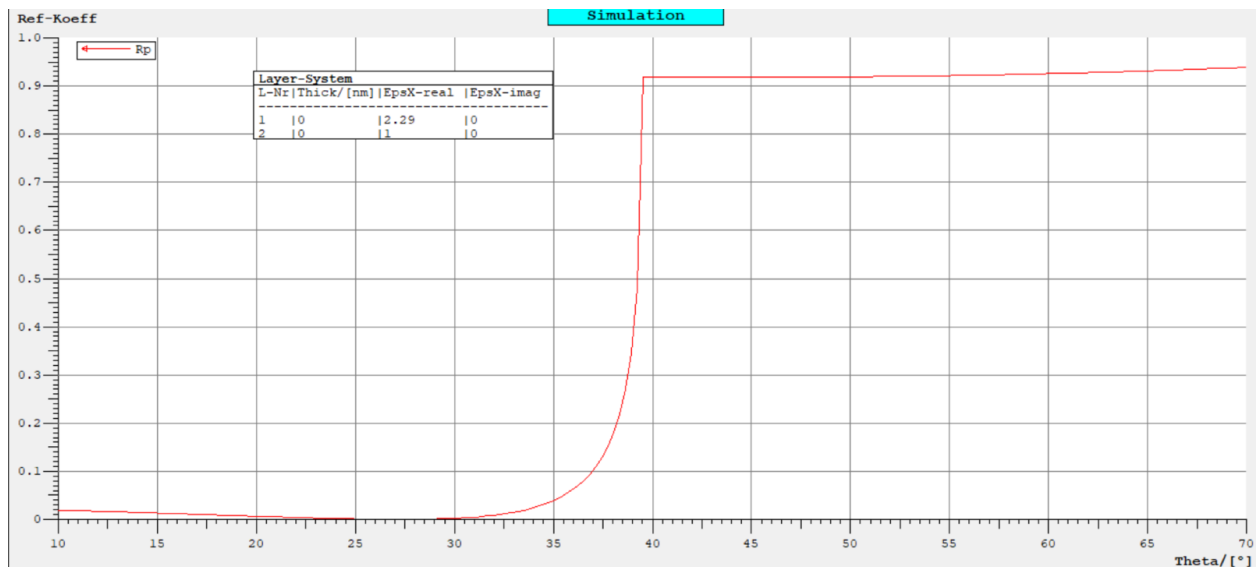


**Figure 18.** Simulation of Reflectivity Curve for Total Internal Reflection using WinSpall.

From the simulated reflectivity curve, at angles lower than 30 degrees, all light is transmitted through the prism without any reflection. After 30 degrees, more and more of the light is reflected until at 39.47 degrees where total internal reflection is reached. This simulation, while not able to consider every real-world parameter, gives us a useful estimate of at what angles we should expect to see total internal reflection occurring based on the wavelength of our laser diode and the material chosen for our right-angle prism.

## 7.A.2 Surface Plasmon Dispersion for Different Wavelengths

For our device, we have chosen a laser diode module with a wavelength of 635 nm. The chosen wavelength, as discussed in Section 5.C.2.1, was determined using the dispersion relation of surface plasmons to the dielectric function of the gold film. This section will illustrate the various equations and simulations used to come to the conclusion that longer wavelengths are preferred for our final device.

During our initial determination of which wavelength to use for our laser diode, we decided to compare theoretically the use of a 532 nm laser diode to a 635 nm laser diode. The two wavelengths were chosen due to their large availability when compared to other laser diode modules of different wavelengths and to allow us to easily see how longer wavelengths would affect our final experiment compared to shorter wavelengths. The software Winspall was used to create a simulated resonance curve for both a 532 nm and 635 nm laser diode when directed through a right-angle N-BK7 glass prism and a 50 nm gold film layer, as can be seen in Figure 19 below.

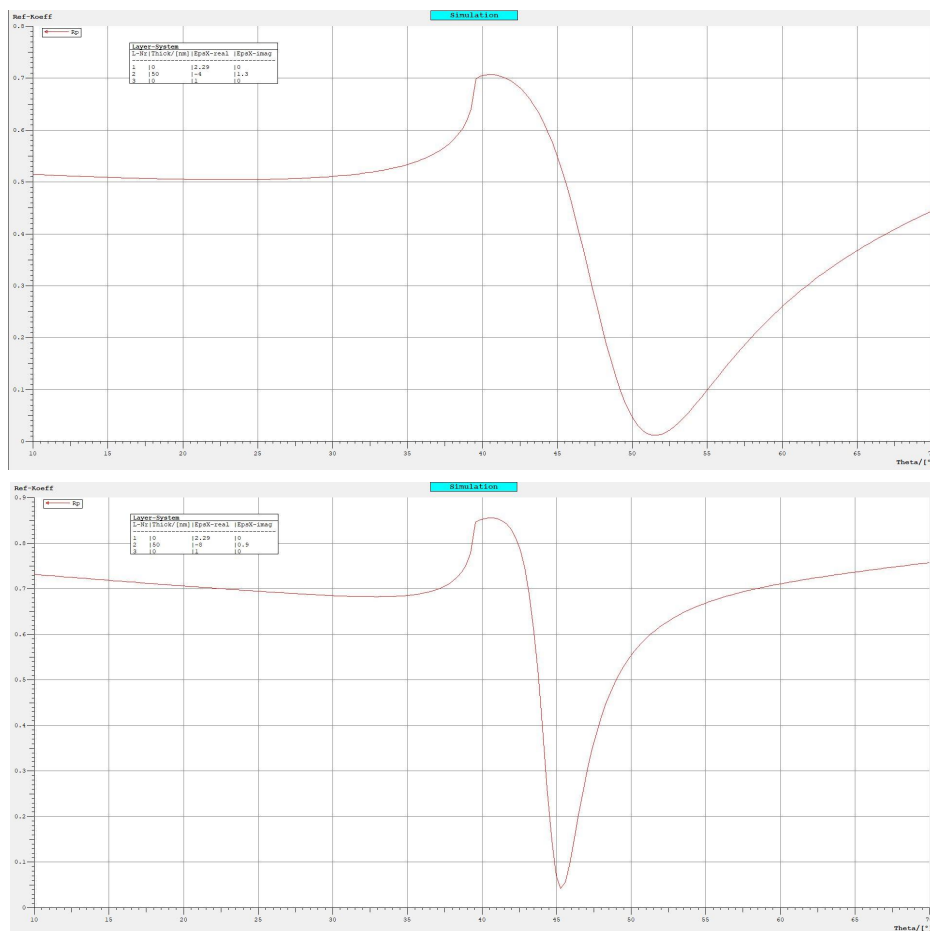


**Figure 19.** Winspall Simulation of Surface Plasmon Resonance Curve: 532 nm laser diode (top) and 635 nm laser diode (bottom).



The real and imaginary parts of the gold film dielectric function used in the simulations are free fitting parameters. They were determined by first using known real and imaginary values for typical 50 nm gold film and were fitted using the simulation to match known resonance curves of similar wavelengths. The given estimations of the dielectric function are also supported by the fact that the absolute value of the real part of the dielectric function increases as the wavelength increases and the absolute value of the imaginary part of the dielectric function decreases as the wavelength increases, as is to be expected due to the relation of wavelength with the dielectric function of metal. As can be seen in the figure above, the 532 nm laser diode creates a broader resonance curve when compared to a 635 nm laser diode. To determine the reason behind this broad curve, we had to investigate parameters such as the propagation length of the surface plasmons along the metal interface, the phase velocity, and the effects of the imaginary part of the dielectric function of the gold film. Finding these values would provide us with crucial insight into how the surface plasmons disperse on the metal surface in relation to the wavelength.

To find these values, we began by using the transverse and longitudinal electromagnetic field of the surface plasmon oscillations. The fluctuations created by the electron charges on a metal boundary are called surface plasmon oscillations. The charge fluctuations contain a transverse and longitudinal electromagnetic field. The field is given by Equation 3 below.

$$E = E_0^{\pm} \exp [ + i(k_x x \pm k_z z - \omega t)]$$

**Equation 3.** Transverse and Longitudinal Electromagnetic Field of Surface Plasmon Oscillations.

In the equation above, the transverse and longitudinal electromagnetic field which disappears as  $|z| \rightarrow \infty$ , with a maximum on the surface at  $z = 0$ , with + for  $z \geq 0$ , - for  $z \leq 0$ , and the imaginary  $k(z)$  leading to an exponential decay of the field  $E(z)$  [11]. Using Maxwell's equations, the retarded dispersion relation for the plane surface of a semi-infinite metal with the dielectric function ( $\epsilon_1 = \epsilon'1 + i\epsilon''1$ ) next to a medium such as air, denoted by  $\epsilon_2$ , is given in Equation 4 below.

$$D_0 = \frac{k_{z1}}{\epsilon_1} + \frac{k_{z2}}{\epsilon_2} = 0$$

**Equation 4.** Retarded Dispersion Relation for the Plane Surface of a Semi-infinite Metal.

The dispersion relation equation above can be used along with Equation 5 below. In the equation below,  $k(z,i)$  relates to the transverse components of the surface plasmon wave vector, while  $\epsilon(i)$  relates to the dielectric function for both metal and air.

$$\epsilon_i \left( \frac{\omega}{c} \right)^2 = k_x^2 + k_{zi}^2 \quad \text{or}$$

$$k_{zi} = \left[ \epsilon_i \left( \frac{\omega}{c} \right)^2 - k_x^2 \right]^{1/2}, \quad i = 1, 2 .$$

**Equation 5.** (1) Dielectric Function of Metal-air Interface; (2) Transverse Components of SP Wave vector.

The dispersion relation in Equation 5 can be rewritten as Equation 6 below, now showing the complex wave vector between the metal and air interface.

$$k_x = \frac{\omega}{c} \left( \frac{\epsilon_1 \epsilon_2}{\epsilon_1 + \epsilon_2} \right)^{1/2}$$

**Equation 6.** Complex Wave vector at Metal-air Interface.

In the above equation,  $\epsilon_1$  relates to the dielectric function of the metal and  $\epsilon_2$  relates to the dielectric function of the medium adjacent to it. Therefore, the real and imaginary parts of the complex wave vector can be found. The real part of the complex wave vector is shown by Equation 7 and the imaginary part of the complex wave vector is shown by Equation 7.

$$k'_x = \frac{\omega}{c} \left( \frac{\epsilon'_1 \epsilon_2}{\epsilon'_1 + \epsilon_2} \right)^{1/2}$$

**Equation 7.** Real part of the Complex Wave Vector.

$$k''_x = \frac{\omega}{c} \left( \frac{\epsilon'_1 \epsilon_2}{\epsilon'_1 + \epsilon_2} \right)^{3/2} \frac{\epsilon''_1}{2(\epsilon'_1)^2}$$

**Equation 8.** Imaginary part of the Complex Wave Vector.

The values of the dielectric function for the metal interface are shown below in Table 6. The dielectric function value of air is a known value of 1, while the values of the dielectric function of the metal were found using typical values of 50 nm gold film and fitting them to a rough estimate using the software Winspall as stated previously.

Wavelength (nm)	Real Part of the Dielectric Function of 50 nm Gold, $\epsilon'1$	Imaginary Part of the Dielectric Function of 50 nm Gold, $\epsilon''1$
532	-4.0	1.3
635	-8.0	0.9

**Table 6.** Real and Imaginary Part of the Dielectric Function of 50 nm Gold as a Function of Wavelength.

The real and imaginary parts of the complex wave vector for each wavelength were then calculated using the values from the table above. The calculated values for the complex wave vector can be seen below in Table 7.

Wavelength (nm)	Real Part of the Complex Wave Vector, $k'(x)$	Imaginary Part of the Complex Wave Vector, $k''(x)$
532	$1.364 \times 10^7$	$7.387 \times 10^5$
635	$1.0578 \times 10^7$	$8.50 \times 10^4$

**Table 7.** Real and Imaginary Parts of the Complex Wave Vector for Different Wavelengths.

At higher frequencies, the mode diameter is smaller [10], which leads to more light on the metal surface. The metal absorbs the light and increased mode overlap is observed, leading to an increase in dissipation. This increase in dissipation leads to a decrease in the amplitude of oscillation, known as damping [10]. From the estimated imaginary parts of our complex dielectric function, it can be observed that shorter wavelengths will have stronger damping in comparison to longer wavelengths.

Surface plasmons decay along the direction of propagation until their energy is lost due to absorption in the metal interface or scattering into free space [11]. The length of this intensity decay can be calculated using Equation 9 below.

$$L = \frac{1}{2k''_x}$$

**Equation 9.** Length of Intensity Decay of Surface Plasmons Along the Direction of Propagation.

As can be seen, the length of decay is inversely related to the imaginary part of the complex wave vector. The imaginary part of the complex wave vector therefore plays a role in the internal absorption of the metal. Equations x and x were used to calculate the real and imaginary parts of the complex wave vector and were subsequently used to calculate their respective length of decay. The computed values for the decay length of each wavelength can be seen in Table 8.

Wavelength (nm)	Length of Intensity Decay Along the Direction of Propagation, L (μm)
532	0.677
635	5.88

**Table 8.** Length of Intensity Decay of Surface Plasmons for Different Wavelengths.

It can be observed that as the imaginary part of the complex wave vector decreases, as can be seen for longer wavelengths, the length of intensity decay increases as well. The phase velocity of the surface plasmons is another parameter to investigate, with can be calculated using Equation 10 below.

$$v_p = \frac{\omega}{k'_x}$$

**Equation 10.** Phase Velocity of Surface Plasmons.

The phase velocity of the surface plasmons is inversely related to the real part of the complex wave vector, again showing the relationship between the phase velocity and the wavelength used to excite the surface plasmons. The calculated phase velocity for both wavelengths can be seen below in Table 9.

Wavelength (nm)	Phase Velocity, v(p)/c
532	0.866
635	0.935

**Table 9.** Phase Velocity of Surface Plasmons for Different Wavelengths.

Comparing the phase velocity of the two wavelengths, it is clear that the velocity increases with longer wavelengths.

As mentioned in Section 5.C.2.1, a longer wavelength light source is preferable for our device. Light slows down when coupled to a plasmon [10], but it can be concluded from our calculations that the phase velocity is slower for shorter wavelengths when compared to longer wavelengths. The decrease in phase velocity, alongside the strong

damping observed by shorter wavelengths, leads to a noticeable broadening of the resonance curve. The broadening informs us how quickly over a distance the modes lose their amplitude [10]. As the plasmon propagates over many wavefronts, the angle of the light source must be exact so phase matching can occur between the phase fronts of the incident beam and those of the plasmons. For longer wavelengths, the precise angle for phase matching to occur is only required over a short distance, as can be seen by the narrower dip of the resonance curve. However, shorter wavelengths require that the angle of the incident beam allow for phase matching to occur over a longer distance of wavefronts. A slight tilt of the angle would lead to the system being out of phase and coupling to the plasmons will not occur [10].

## 7.B Initial Designs and Related Diagrams

Our initial design idea for the surface plasmon resonance sensor began with the document “Divide and Conquer”. The purpose of this document was to lay out a blueprint for our project which could later be built upon as we continued to research and modify our goals and objectives. Figure 20 shows the initial block diagram that was created which later became the portable surface plasmon resonance sensor.

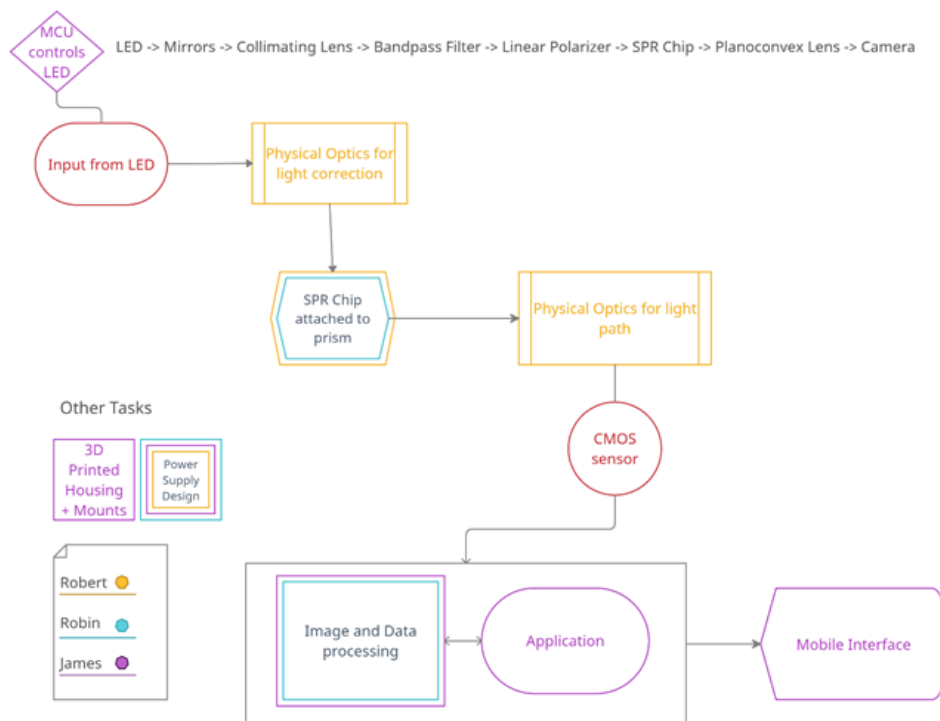


**Figure 20.** Initial Divide and Conquer Block Diagram.

The final design for our project has evolved since we created the initial block diagram above, with many of the technologies illustrated having changed or been discarded

altogether. Nevertheless, this initial diagram provided us with a basic concept of what we wanted to accomplish and how we could go about it. A crucial point in any project is its initial design, which serves as the backbone of the finished product. The research into past technologies, the different optical and electrical components used, and the final design all were based on the original figure above. Although basic in design, it allowed us to begin the plans for our finished product.

The following sections serve as a journal of the evolution of our hardware components for the project. Through research and testing, the final concept for our project was formed to ensure our device was as efficient as possible.

### 7.B.1 Initial Design Idea – Smartphone Based SPR Sensor

When we first decided upon the idea for our senior design project, our initial thought was to utilize a smartphone device to act as the controller and sensor for our surface plasmon resonance sensor. This idea came from past low-cost surface plasmon resonance sensors that would mitigate the overall cost by taking advantage of the high-powered CPUs and high-resolution cameras that come with most smartphone devices today. Our initial idea was to use multimode optical fiber as a way to direct the incident light onto the sensing surface and towards the detector. But after careful consideration, we decided that a prism-coupled SPR sensor would fit better for our purposes. This was due to the simplicity that a prism-based system provides, where surface plasmon excitation is created using the phenomenon of total internal reflection and the evanescent wave created that travels the boundary between the prism and air. Figure 21 below shows our original illustration for the surface plasmon resonance sensor using this design idea.

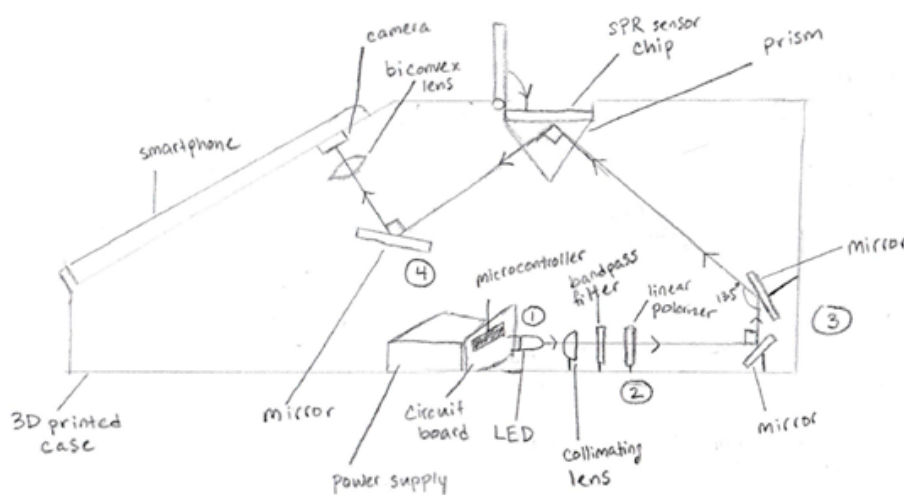


**Figure 21.** First Illustration of SASSPR.

In the illustration above, a green LED would be connected to a microcontroller that would allow the smartphone application to communicate with the system and determine when the light turns on or off. A battery-powered power supply would be used as a power source for the LED and microcontroller. The light from the LED would be manipulated by a 532 nm bandpass filter and linear polarizer, which are used to narrow the range of the LEDs wavelength spectrum and change the incident light into a transverse magnetic wave respectively. This would ensure our incident light was monochromatic and transverse magnetically polarized so that the wave may resonate with the wave created by surface plasmon excitation. Two mirrors would then be used to direct the light onto a right-angle prism. This is where the surface plasmon detection occurs. By angling our incident beam to a 45-degree angle using mirrors, we could create the phenomenon called total internal reflection as the beam hits the right-angle prism. This coupling of the light using the prism creates a perfect situation where surface plasmon excitation can occur as most of the energy from our incident light will be absorbed by the metal/dielectric interface on our SPR chip. This leads to a decrease in intensity of our received light onto the smartphone's CMOS camera. The decrease in intensity of our received light indicates that excitation occurred, and molecular binding took place. The smartphone device would be placed in a mounted area with its screen facing outward. A small hole would allow for the back facing camera of the smartphone device to interact with the optical path of the SPR sensor found inside the casing. The entire structure would be designed using 3D printed components made of thermoplastic polyurethane.

### **7.B.1.1 Light Source Design**

The design described began to change as we continued to research the various technologies we would utilize and the pros and cons of each. The green LED as our light source at the time seemed a cheap solution for us to use in our product while also providing a light source that was separate from the smartphone as opposed to using the LED flashlight on the smartphone which would constrain how much we could manipulate the optical path. However, we discovered that trying to collimate the light from an LED source is very difficult and results in much of the light being lost. This led to us having to reassess what we would use as our light source that was both cost efficient and could be collimated easily. Also, as mentioned in previous sections, through our calculations and simulations it was realized that longer wavelengths would be a preferred choice for our final device. This led to the decision for a 635 nm wavelength light source in our final project. The final decision was to use a 635 nm laser diode module as our light source. Laser diodes are semiconductor devices that provide a beam that is fully collimated. The wavelength 635 nm was chosen due to its steadier output power. These lasers are well suited for applications which require a good beam

quality and high-power stability. For our purposes, the intensity of our light source must remain constant throughout the experiment to avoid any fluctuations being interpreted as surface plasmon excitation occurring. However, using a laser diode as opposed to an LED as our light source brought new challenges. A laser diode is a very efficient light source but also a very powerful one. The light that is directed onto the SPR sensing location and the detector emits a certain wattage of power at a particular spot. Therefore, a low output power laser should be chosen to avoid damaging the detector and sensing location. High output power is not required for surface plasmon excitation to occur. We therefore chose a laser diode module that emits 1.2 mW of output power to avoid damage to our detector and to our sensing location. Another challenge the laser diode brought to our design was the method we would use to ensure the beam intensity remained constant. One of our design goals is to provide a portable SPR sensor which requires us to provide a power source that is battery powered. Thus, it was chosen to keep the laser diode plugged into a wall output to avoid any fluctuations to our emitted power which could lead to incorrect data collection during experimentation.

### **7.B.1.2 SPR Detector Design**

As can be seen in our initial design illustration above, the original design was to have the smartphone's CMOS sensor act as the detector for our SPR sensor. Doing so would mitigate the cost of purchasing a separate camera with a high enough resolution to properly image the intensity changes seen during surface plasmon excitation. But this requires the smartphone device itself to be a part of the optical path, which brought a certain amount of constraints to our product. In order for the SPR sensing device to work, the smartphone used by the consumer would require the back facing camera to be in the same position as the smartphone we will use for designing our project. This is to ensure that the camera is in the correct location for the captured images to properly visualize the transmitted beam from the prism after surface plasmon excitation. Many smartphones vary in the location of their back facing camera, which would therefore limit the type of smartphones that would be compatible with our finished SPR sensor. To ensure our project was more versatile, we discarded the idea of using the smartphone's camera as the detector and chose an external CMOS sensor instead. This removed the smartphone altogether from the optical path, ensuring that we no longer had a hardware compatibility issue for the type of smartphone device used. However, this removed our ability to use the high-resolution CMOS sensor that most smartphone devices provide, forcing us to find a sensor that provided similar specifications at a reasonable price. After careful consideration, the ESP32 microcontroller with the OV2640 camera module was chosen due to its low price, its 1600 x 1200 pixel resolution, its wireless features such as Bluetooth low-energy and Wi-Fi, and onboard JPEG encoder that would offload the processing power to reduce memory on the microcontroller. The sensor also provides fast processing time, which became another factor to consider as the camera must capture and transmit its captured images to the software application in a timely manner. With the CMOS sensor described, we will be able to image the intensity



changes seen during our experimentation to provide an accurate measurement of when surface plasmon excitation takes place.

## **8. Project Testing and Prototype Construction**

After the initial design is created for a project, the next step is to begin testing the functionality of the various hardware and software components. Before any time, money, and resources are spent on the first fully functional prototype, one must ensure that each component is the correct choice for the particular goals and objectives for the project. The following sections describe the hardware as well as software testing done for the completion of our project, as well as the multiple prototypes built for our final product.

### **8.A Hardware Testing**

Testing is a key element of any prototype, ensuring that each component chosen is the most efficient decision for the final output of the product. The following sections will describe the testing done for the electrical and optical components of our hardware that have aided us in deciding the direction our final prototype will take.

#### **8.A.1 Microcontroller and Power Supply Testing**

The chosen microcontroller has two particularly important jobs that both have major influence over the results of our experiment. The first and most taxing responsibility is to capture an image from the CMOS sensor, process and compress the JPG file, then upload it to an asynchronous web server that is hosted by the microcontroller unit itself. This process must be completed in under 500 milliseconds to reach our engineering requirement. The second responsibility is to control the switching behavior of the power source to the laser diode through the use of a MOSFET, acting as an on / off switch.

The ESP32-CAM does not have an onboard USB port and instead uses UART, a universal asynchronous receiver and transmitter. This required the use of a special adaptor that would plug into a USB port of a computer and breakout into 4 pins. Power, ground, transmit, and receive with the latter being the data lines. The decision to not have an onboard USB port was to decrease the size of the device, but at the cost of extra modification in order to use the GPIO pins corresponding with the UART pins to be used for anything but UART. With the limited pins for free use, especially when using the CMOS sensor, this was a must.

Our original power source was a 9v Energizer battery connected to a linear voltage regulator to lower the voltage from 9v to 5v. Two capacitors were installed in parallel with the input and the output power from the regulator to smooth out any fluctuations. Two 9v batteries were used in total to ensure enough current went to our two power consuming devices, in the figure below, the second laser diode is replaced with a blue

LED, so it was unnecessary but still used with two 9v batteries. The original switching circuit for the laser diode, or LED in this case, was using two MOSFET transistors, one P-channel and one N-channel. Figure 22 depicts the microcontroller testing with the L805 voltage regulator and the 9V battery.

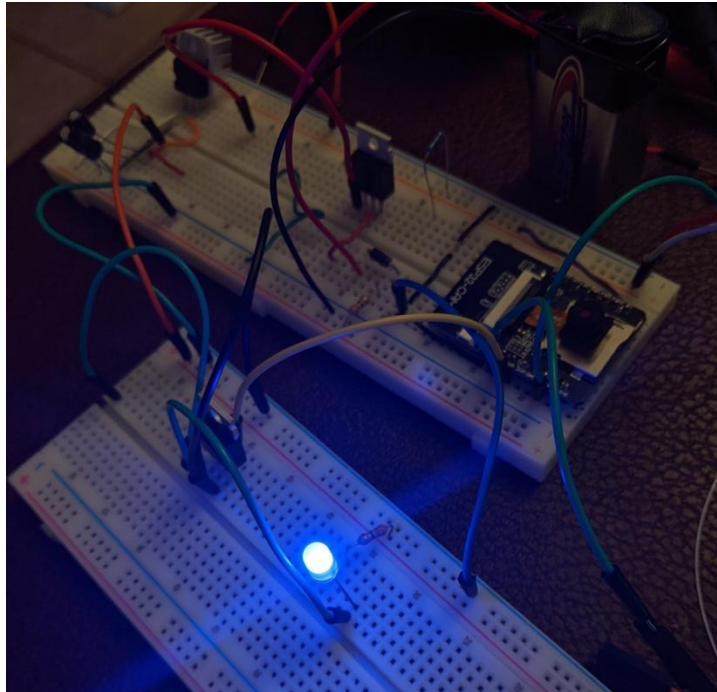


*Figure 22. Microcontroller Testing with L805 Voltage Regulator and 9V Battery.*

Although the 9v battery proved to be appropriate in the initial testing, the rate of voltage drop-off was starting to cause issues and eventually the microcontroller unit ceased to turn on. Although a 9v battery has a capacity rating of 500 mAH, this was when our team learned how the capacity rating was measured and how it changes depending on the current draw. There was no reason to continue using 9v batteries without being extremely wasteful and buying 9v batteries by the bulk.

The power source was changed to a 2-cell 7.4v lithium polymer rechargeable battery rated for 40 Amps with 1600mAh capacity. It was designed for the use of consumer RC cars which most have high potential for large spikes in current consumption. This can be considered ‘overkill’ for our power requirements, but this ensures we have room for expansion and high efficiency for our engineering requirements.

Another discovery that was made just before switching away from 9v batteries was the inefficiency of a linear voltage regulator. Unfortunately, about two thirds of the energy was dissipated as heat through the voltage regulator. With our marketing and engineering requirements, this was a large drag on our power consumption, and we decided to move away from it at the cost of moderately complicating the power supply design. The move was made to a LM2596 switching regulator purchased from TI that

has a potential max efficiency of 96 percent. This required the use of a diode, two electrolytic capacitors for smoothing out spikes in voltage, and an inductor to properly regulate the feedback loop of the switching regulator.

The original switching circuit for the laser diode was simplified to only use a single N-channel MOSFET that can be seen in Figure 23 below.

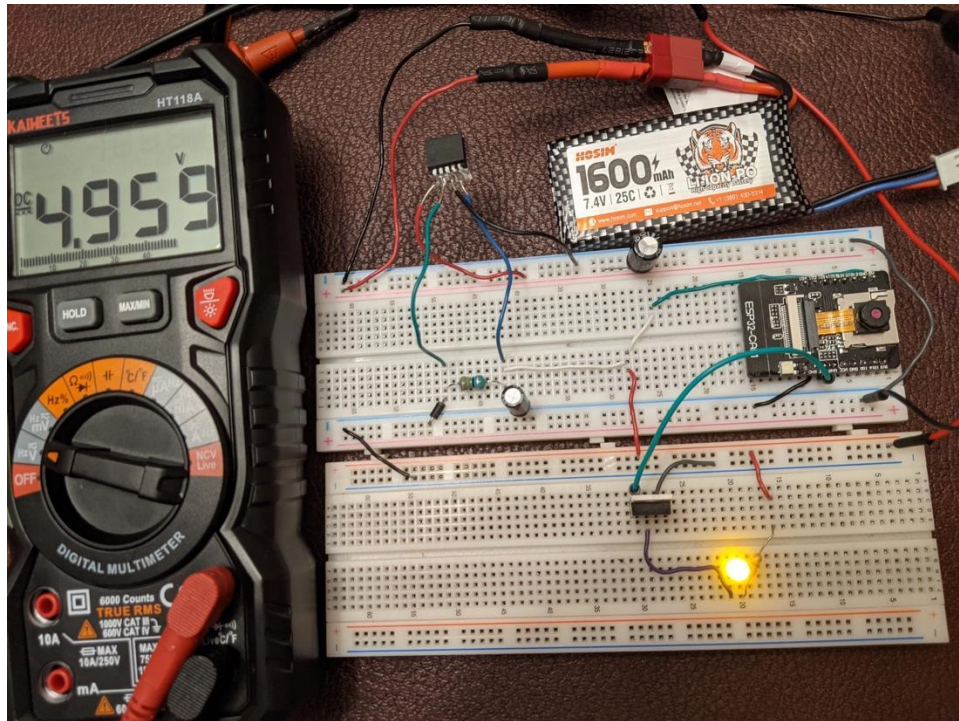


**Figure 23.** Microcontroller Testing with LM2596 Switching Regulator and 7.4v LiPo.

Below in Figure 24 is an example of the ESP32-CAM capturing an image and uploading to the asynchronous web server hosted by the microcontroller. At any point, if the IP address of the device is used for an HTTP GET request with the “/capture” route, the microcontroller will be instructed to both capture and upload the image upon loading the request on the client side. There seems to be inconsistencies with the timing of the capture function, it is unknown if it is a memory or energy complication, but the average is 200ms which is below our 500ms engineering requirement.

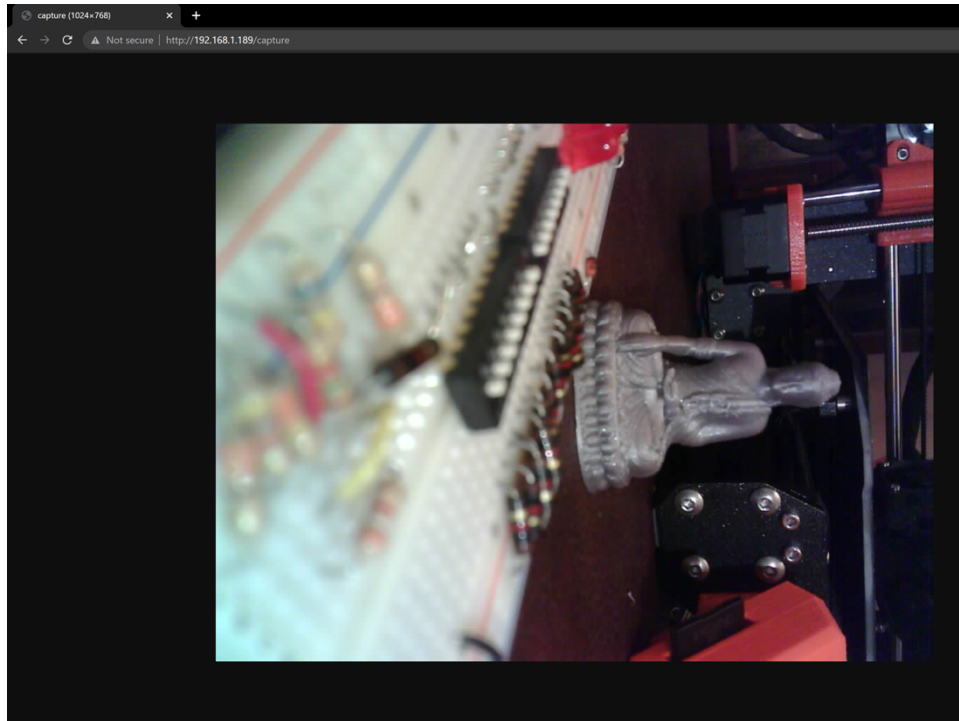


**Figure 24.** Capture Test with Microcontroller.

In Figure 25 below, an asynchronous web server is being used similar to the figure above, but the HTTP route is changed to “/laser” in this scenario. When the GET request is sent to the web server, it will return the current state of the laser.

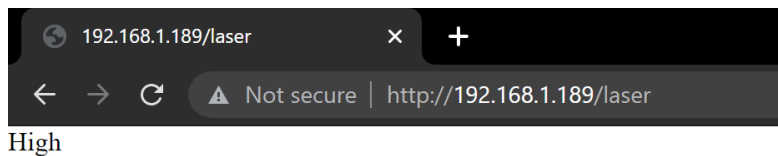


**Figure 25.** Async Webserver Test with Microcontroller.

The original switching circuit design did not account for the current load on the laser diode as the prototype version in the figures above were only powering a single LED. The IRF510 MOSFET had too low of a drain current for the 3.3v from the GPIO of the ESP32CAM for proper saturation. To properly supply the 200 mA to the laser diode, the voltage from the ESP32CAM would have to be boosted or a new MOSFET would be

used for the switching circuit. Figure 26 below shows the correlation of the applied voltage and drain current.

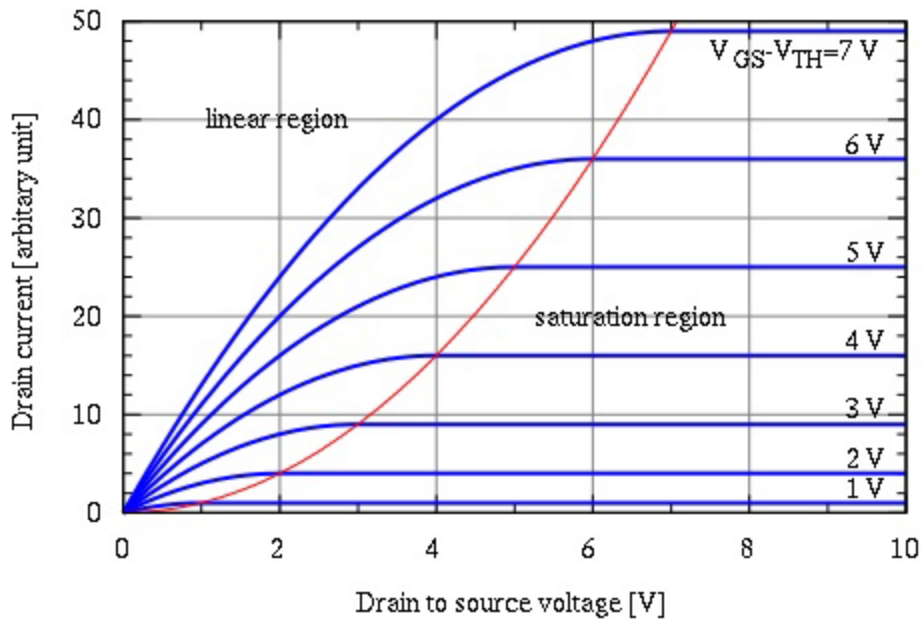


**Figure 26.** Drain Current and Voltage Saturation Graph.

The power supply design needed to be expanded to accommodate an AC-DC wall adaptor through the use of a 3-pin chassis-mounted DC jack. We wanted to be able to unplug the SPR device from the DC jack and have the battery supply instantaneously take over as the power supply of the system as well as plug the device in and switch to the DC jack as the power supply. The battery will be always kept inside the device with a USB cable extending through a hole in the 3D printed housing to be used for charging. We ordered a 7.5v / 800 mA AC-DC wall adapter to be used alongside the battery but what we received was a 10.5v AC-DC wall adapter. To accommodate the extra voltage that needs to be bucked, a second LM2596 was added to the circuit, this one being adjustable. Using the datasheet provided by TI, the feedback resistor values were calculated to buck the 10.5 volts down to 8 volts. This will be fed into the second voltage regulator that will behave the same as if the power was coming from the battery. This will ensure a much higher overall efficiency of the system to further reach our engineering requirement. Figure 27 below is the schematic designed in Altium for easier analysis and an easier time soldering to a perforated board.



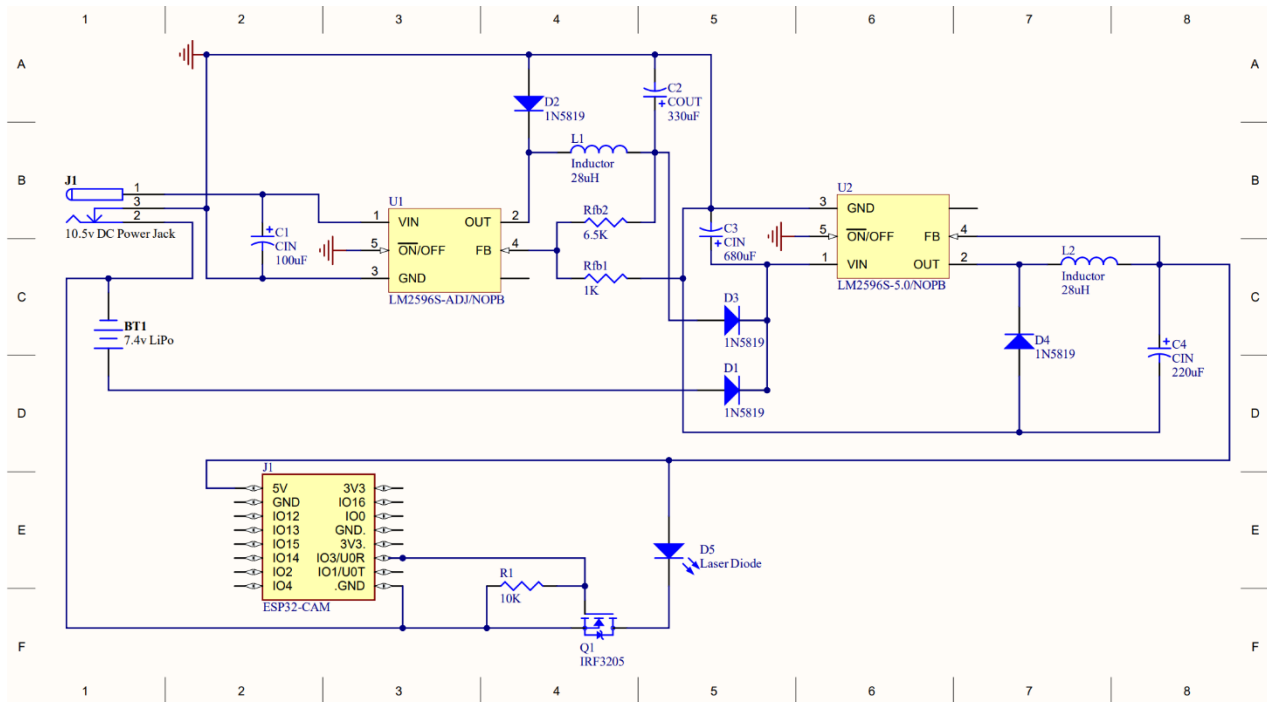


**Figure 27. Final Schematic for Power Design.**

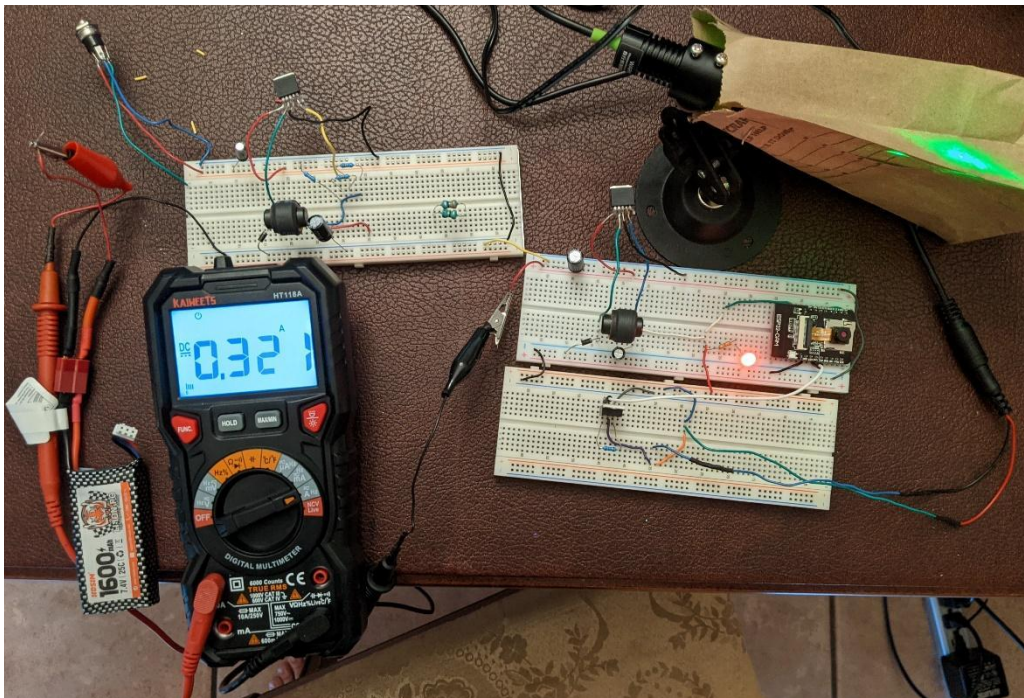


**Figure 28. Battery Powered System Test.**

Figure 28 above and Figure 29 below shows the final power circuit design on a breadboard. The red LED indicates the ESP32, and the laser is powered, the current draw is negligible for the LED. The inductors here are used as a choke and were found

as scrap from Skycraft Surplus, they have been tested to roughly equal the desired inductance and were tested to handle the expected current draw. The DC power jack is also a part that does not have a manufacturing number or any identifying details, but the internals work very similar to the power jack shown in the schematic. For context: the laser is shrouded in a paper bag for safety reasons, it is not strong enough to combust but is strong enough to damage eyes.

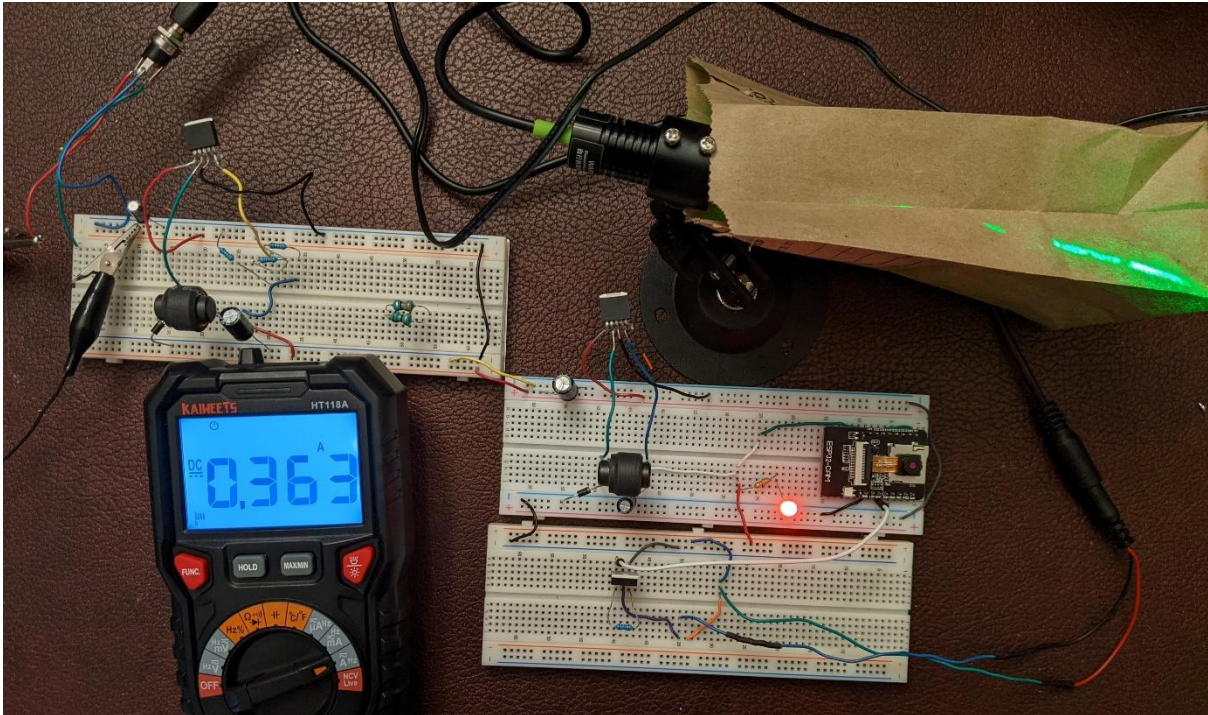


*Figure 29. AC-DC Adaptor Powered System Test*

## 8.A.2 3D Printed Housing / Mounts

To ensure a compact size and decreased cost in materials, we chose to 3D print the housing of the device and as much of the mounts as we can. Our goal is to make the device as portable as possible, which means we must isolate the inside as much as we can from the outside environment. Although not temperature sensitive, all optic components including the camera sensor must be free from any disturbances such as vibration, noise, or unnecessary light. This means we must measure every dimension of every component that will be housed and tolerances of the FDM printer will have to be calculated to allow a proper fit. The design software used is Fusion 360 from AutoDesk.

Figure 30 below showcases the first housing we designed when we expected to use a 9v battery for the power supply. This was used to protect and stabilize the camera during initial testing. Figure 31 further below is a demonstration using an older design of the same housing, this one having the camera held at a different angle.

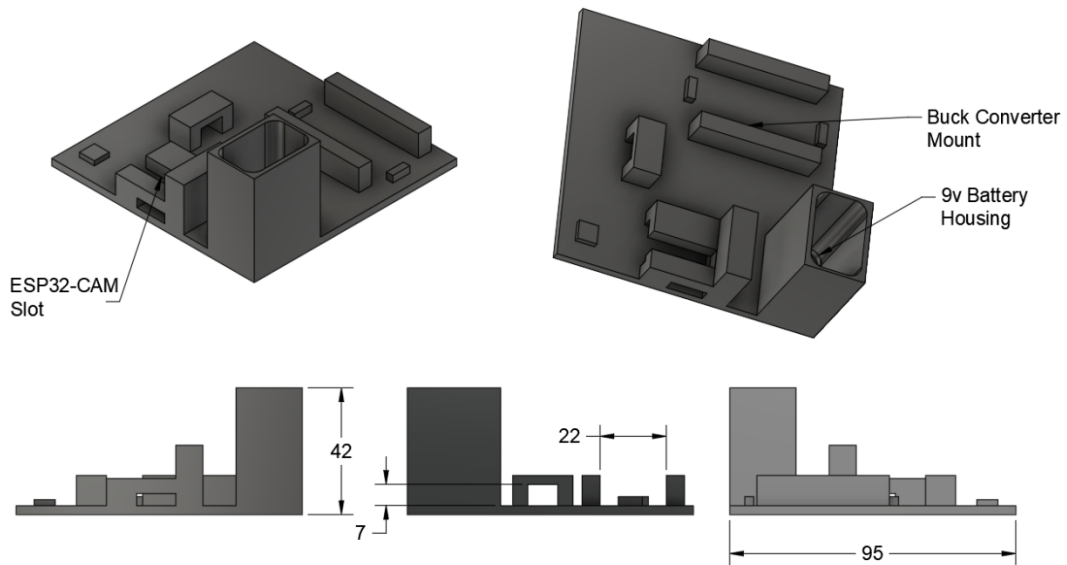


**Figure 30.** First iteration of ESP32-CAM housing using a 9v battery.

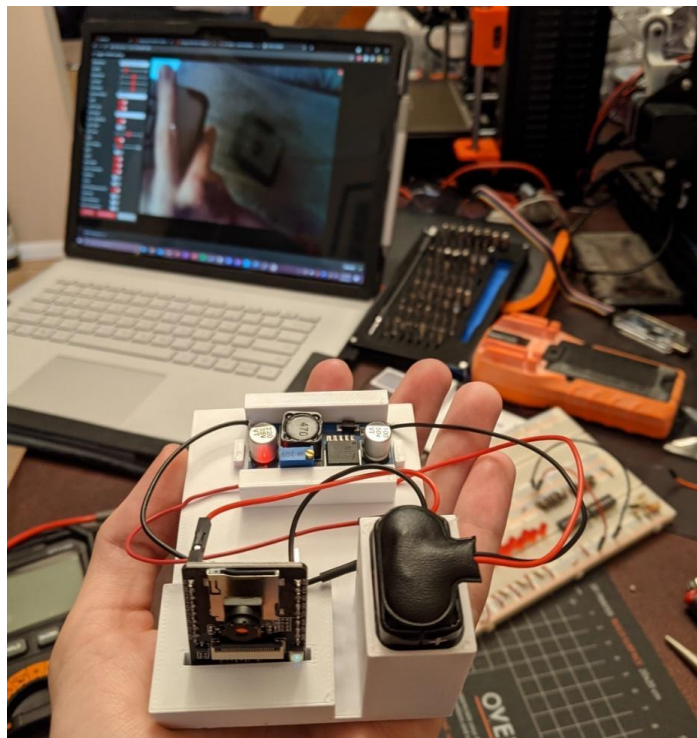


**Figure 31.** First test using housing.

The design process of the ESP32-CAM housing had to be done completely from scratch. Fusion360's community has several extensive catalogs of 3D models to freely download, most of which are popular electrical components such as microcontrollers.



There were several ESP32 models available but due to ESP32-CAM's relatively recent inception, there was none available to download. A housing for this device was especially important to protect the camera from unnecessary stress and to dampen as much vibration as possible to ensure the cleanest data we can. To do the measurements, a caliper was used on the ESP32-CAM for the dimensions of any extrusion or indent. A surrounding shell was made from the model and printed in halves with overlapping sides to give a moderately loose seal. This will later be modified to fit into the permanent housing, most likely using M3 screws. Figure 32 illustrates the semi-final variation of the ESP32-CAM mount.

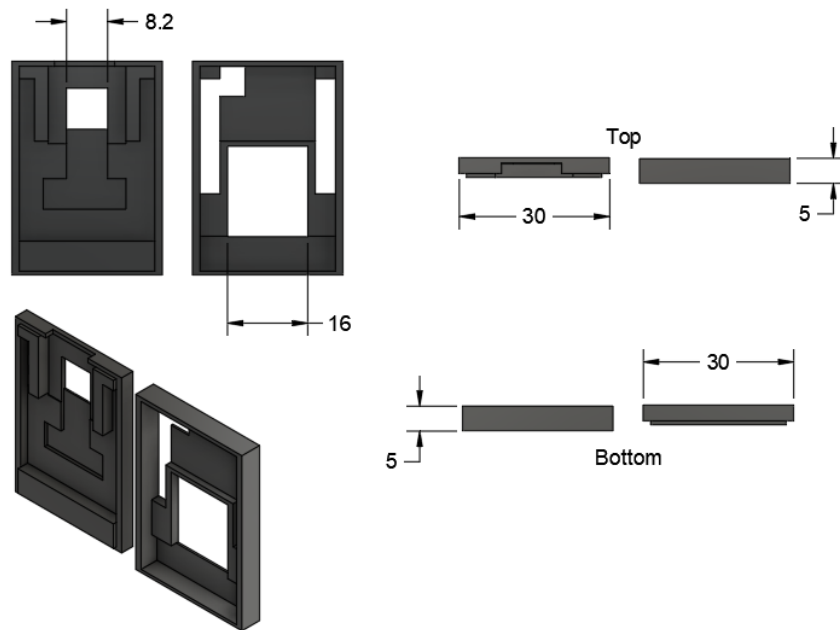


**Figure 32.** Semi-final variation of ESP32-CAM mount.

Figure 33 shows a 3D rendering of the laser diode and a 3D printed mount that will be used to stabilize and dampen the laser. This is a critical aspect of the experiment because we expect perfect control over the angle of the light beam and do not account for any misalignments. This is a prototype design and was only used for an easier experience with handling and to gather tolerances on the dimensions.

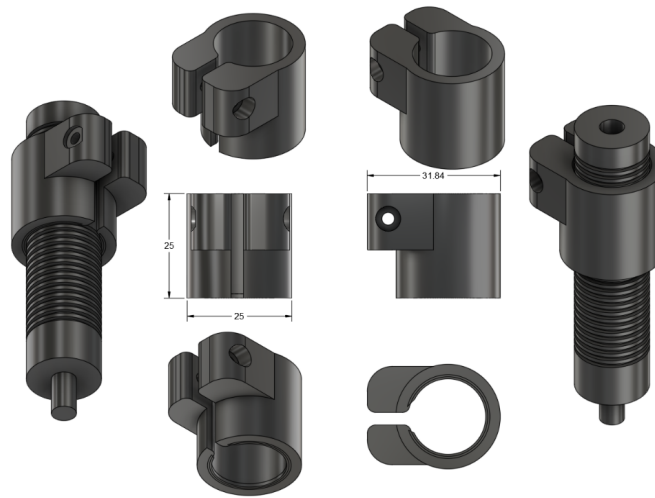


*Figure 33. Prototype mount of laser diode.*

### 8.A.3 Laser Diode Testing

The laser diode plays a crucial role in our SPR sensor, providing the energy that will create the surface plasmon excitation needed for surface plasmon excitation to occur. As described in previous sections, specifications such as the central wavelength, output power, beam divergence, and polarization of our laser diode were all parameters that must be determined based on our particular needs. We concluded that a 635 nm wavelength laser diode module from the company Thorlabs would best serve our purposes, both for its good beam quality and lower cost compared to other laser diodes of similar wavelength on the market. But in the initial testing during Senior Design I, the 532 nm laser diode from the CREOL Undergraduate Lab was tested and used. The beginning of this section will focus on our initial tests using the 532 nm laser and then later changing to the 635 nm laser at the beginning of Senior Design II once simulations, calculations, and discussions with Dr. Kik at the University of Central Florida led us to the conclusion that longer wavelength lasers would better serve our needs.

The first tests were performed with a 532 nm laser borrowed from the CREOL Undergraduate Lab. The laser is capable of emitting an output power of 5 mW and a beam divergence of less than 1 milliradian. Our first test was using an optical power meter to measure the output power the laser diode emitted when plugged in. The measured output power of the laser diode was 5.70 mW which was close to the 5 mW output power expected based on the laser diode specifications from the manufacturer. Figure 34 below shows the optical power meter and the calculated output power of the laser.



**Figure 34.** Output Power of 532 nm Laser Diode Module.

The next test for our laser diode was to determine the polarization of the emitted light. This is important to determine because for surface plasmon excitation, we will need to manipulate the polarization of our incident wave to only allow p-polarized light to interact with the gold film. To determine the polarization of our light, we used a mounted linear polarizer and a power meter to measure the output power as we changed the axis of our polarizer to find the maximum and minimum output power and their specific rotation angles. To begin, we set the rotation angle of the mounted linear polarizer to 0 degrees and began slowly increasing the rotation angle in increments of 5 degrees, monitoring the measured output power from the optical power meter placed after the light exits the linear polarizer, until we found a maximum output power. Once the maximum output power was found, we recorded the measurement and the rotation angle of the linear polarizer. We then rotated the linear polarizer to 90 degrees from the angle where maximum power was found. This was done to find the minimum output power reading for the orthogonal polarization. The measurements were done five times and the results were averaged. The results can be seen below in Table 6.  $P_{\max}$  represents the maximum power found for each rotation angle, while  $P_{\min}$  represents the minimum power found. Ellipticity is the square root of the ratio of  $P_{\min}$  divided by  $P_{\max}$ .

Experiments Performed	$P_{\max}$ (mW)	Polarizer Rotation Angle at $P_{\max}$ (degrees)	$P_{\min}$ (mW)	Polarizer Rotation Angle at $P_{\min}$ (degrees)	Ellipticity
1	3.57	130	1.38	220	0.622
2	3.36	136	1.37	226	0.639
3	3.25	135.5	1.37	225.5	0.649
4	3.26	130	1.36	220	0.646
5	3.13	128	1.34	218	0.654
Average	3.31	131.9	1.36	221.9	0.642

*Table 10. Experimentation to Determine Polarization of the Laser Diode.*

From our results, we could see that the minimum output power never decreased below 1.34 mW. This informs us that our emitted light from the laser diode is elliptically polarized, due to the amplitudes of the maximum and minimum power being of different values but the minimum never reaching an output power of zero. If the light was linearly polarized, the minimum output power detected would be zero or close to zero. If our light was circularly polarized, the amplitudes of both minimum and maximum power measured would be the same. This information is very useful for later experiments to determine the rotation axis of our linear polarizer when we want only p-polarized light entering our system.

As stated previously, the wavelength of our laser was changed from 532 nm to 635 nm at the beginning of Senior Design II. The chosen 635 nm laser was provided by Thorlabs and emitted an output power of 1.2 mW. To determine its true output power, an optical power meter was once again used to measure emitted power when the laser diode was plugged in. The output power was found to be 1.261 mW, which followed the expected value of 1.2 mW. Figure 35 below shows the optical power meter and the calculated output power of the laser.

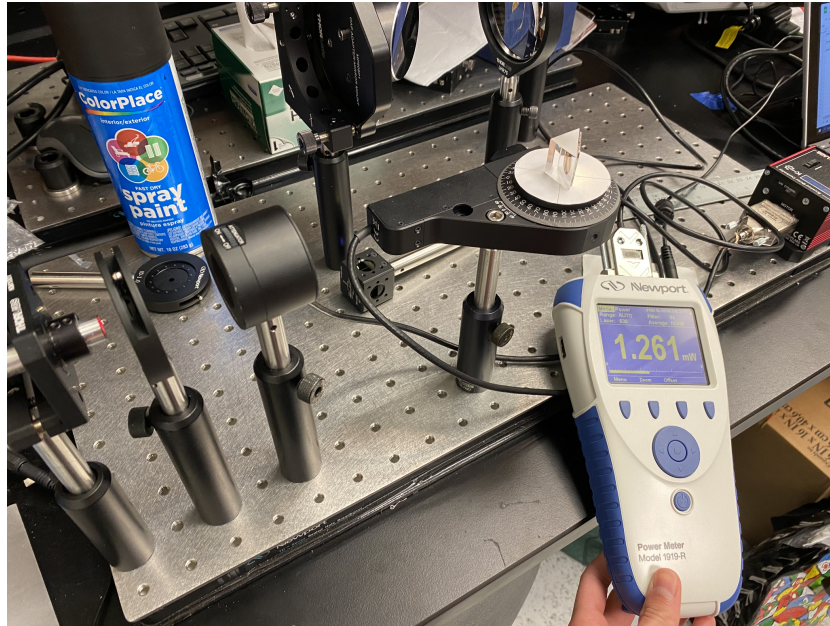


**Figure 35.** *Output Power of 635 nm Laser Diode Module.*

With the laser diode module to be used in our experiments showing an expected output power for our correct wavelength, the experiment could continue to the next step for finding surface plasmon excitation.

#### **8.A.4 Simulating the Surface Plasmon Resonance Curve**

When surface plasmon excitation occurs, a dip in the measured intensity of the reflected beam can be seen. This dip occurs at a certain angle known as the resonance angle or SPR angle. The angle where this dip occurs is related to the changes in the refractive index of the metal being used, as well as other parameters such as the wavelength of the incoming light, the illumination angle, the evaporation process used when depositing the metal, and the refractive index of the prism, metal, and the various layers being tested. The software WinSpall used previously for simulating total internal reflection was now used for simulating surface plasmon resonance curves based on the Fresnel formalism. Using this software, we can calculate a resonance curve specific to our parameters and compare the theoretical results with our experimental results.

Before beginning our experiments, we created a simulation using the software WinSpall to mimic the expected resonance curve based on our specific parameters. In this simulation, the only layers that our light will travel through is the glass prism, the gold film, and air. The real and imaginary dielectric constants for the glass and air layers remain the same as the ones used for simulating total internal reflection. The gold layer will have a thickness of 50 nanometers due to the manufactured SPR chips we purchased having a gold film thickness of 50 nanometers. The real dielectric constant of the gold layer is  $-12.45$  while the imaginary dielectric constant is  $1.3$ . The real and imaginary dielectric constants are typical values for gold film but can vary slightly based

on the evaporation process used by the manufacturers to deposit the gold film onto the chip. Figure 36 below shows the simulation parameters used for simulating the resonance curve with the gold SPR chip.

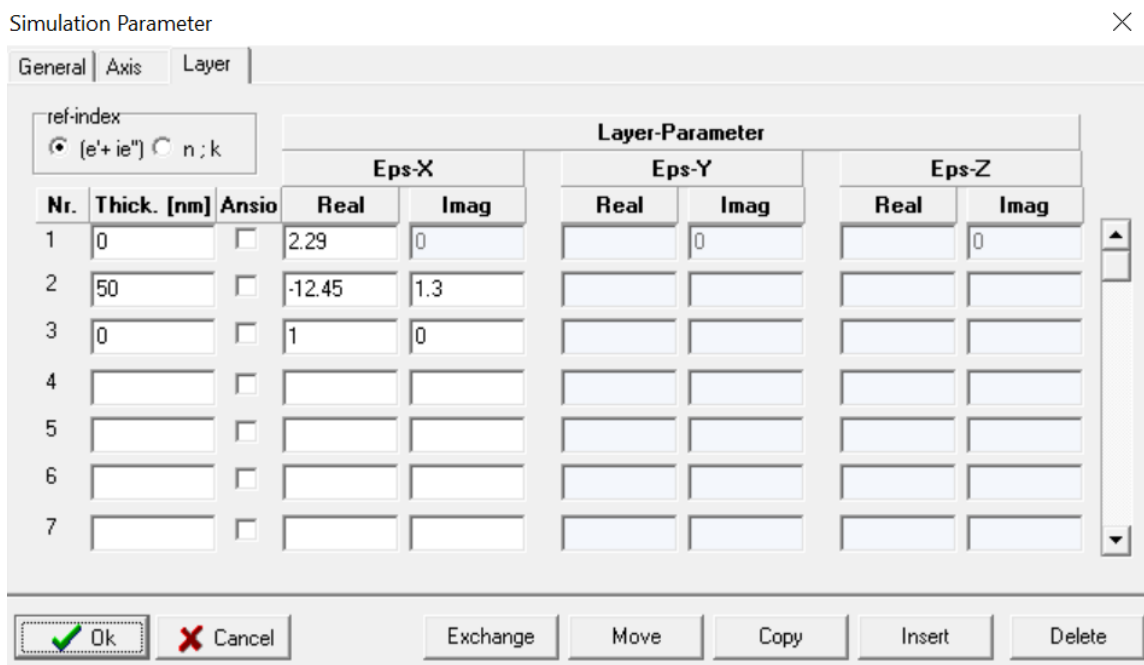


**Figure 36.** Simulation Parameters for the Resonance Curve of Gold Film using WinSpall.

Using the parameters specified, a simulation of the resonance curve for a gold film of 50 nanometers was created. Figure 37 below illustrates the resonance curve that was observed.

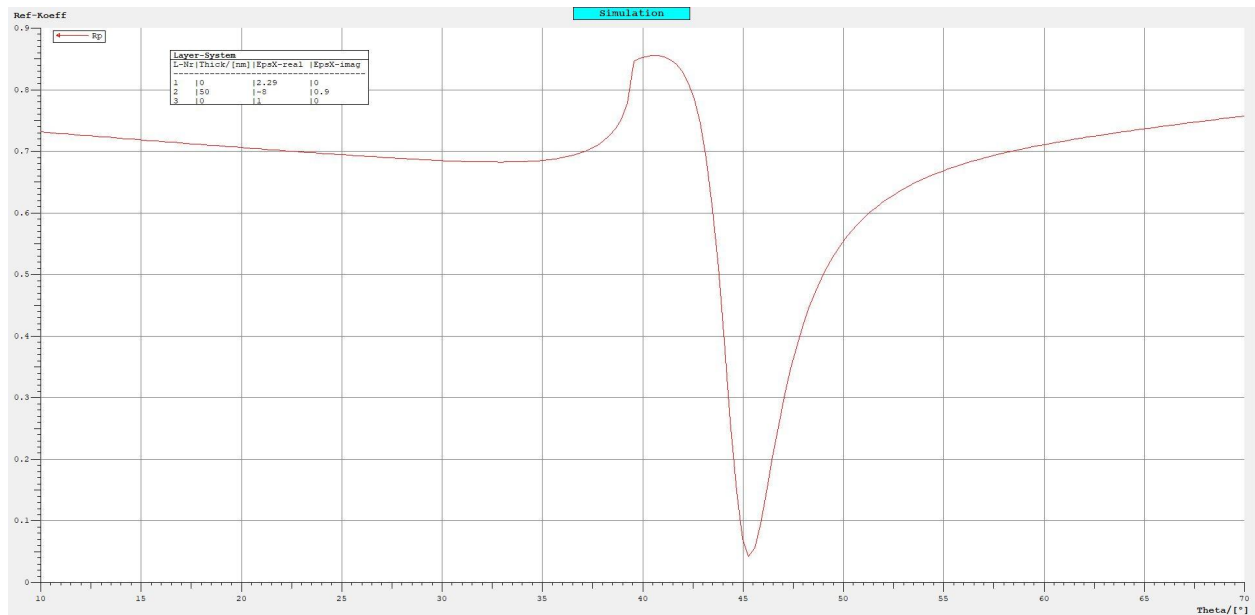


**Figure 37.** Simulation of Resonance Curve of Gold Film using WinSpall.

From the simulation, it can be seen that the increase in reflectivity where total internal reflection occurs at 39 degrees is much shallower compared to the previous simulation for total internal reflection using only a glass prism in air. This shallow increase is due to the reflective properties of the gold film itself. Another key observation from the simulation is that there is a sharp dip in the reflectivity at 45 degrees. This dip is due to the majority of the energy from the photons in our incident light being transferred to the surface plasmons. This simulation informs us that when using a laser diode with a wavelength of 635-nanometers directed at a right-angle prism, we should observe surface plasmon excitation at a resonance angle of 45 degrees. Knowing this theoretical resonance angle will better aid us in finding the resonance angle during experimentations and comparing our results with the simulated ones.

## 8.B Software Testing

Initial software testing was done with a simple Python script running on a desktop, this does not represent the application running on a smartphone, but it creates an easier environment to test out proper scheduling methods to reach our engineering requirement of 2 captures per second. The ESP32-CAM is capable of capturing images much faster than every 0.5 seconds, but this gives diminishing returns to the accuracy of our data and causes unnecessary stress on the system. While the 2 captures per second is an engineering requirement, it may prove to be more often than is needed to reach our accuracy requirement but due to the conceptual nature of our project, this is still in the testing phase.



There are multiple scheduling methods that can be used to reach our engineering requirement of 2 captures per second. Each method comes with its own drawbacks and can influence the power draw of the device. Most methods are reliant on the clock cycles of the microcontroller unit, so if we continue to keep a lowered clock rate then the capture rate could be negatively affected.

Table 11 below shows how the clock rate correlates with the capture rate. There will be no scheduling method used for this testing scenario but instead the C program will poll the CPU as fast as possible and produce an average processing time. This processing time also includes the upload through Wi-Fi which takes a very small and much more consistent amount of time to perform.

Clock Rate	Pixel Resolution	Captures per Second	Average Processing Time	Maximum / Minimum Processing Time
240 MHz	1600 x 1200	12.2	79 ms	209 ms / 73 ms
240 MHz	800 x 600	25.6	40 ms	61 ms / 38 ms
160 MHz	1600 x 1200	11.9	83 ms	162 ms / 74 ms
160 MHz	800 x 600	27.1	39 ms	98 ms / 42 ms
80 MHz	1600 x 1200	8.3	112 ms	185 ms / 67 ms
80 MHz	800 x 600	25.6	39 ms	72 ms / 34 ms

*Table 11. ESP32-CAM Capture vs Clock Frequency*

What the table above does not show is the variation in processing time and capture rates, they seem to get worse as the clock rate is lowered so it seems to be in our best interest to keep the clock rate at the fastest recommended frequency at the cost of a moderately significant power draw increase.

Unrelated to the consistent variation in processing time and capture rates is that the ESP32-CAM has been observed to experience massive capture rate drops, most likely an issue with the pseudo static random-access memory or the frame buffer needing to be reset. What exactly causes these rate drops is unknown and seems to be correlated with higher capture rates as only the 800 x 600-pixel resolution tests experience the issue, albeit inconsistently. These capture rate frequency drops are important to consider when designing the software to call on these captures and must be prepared to accommodate for the improper timing. Not only does the capture rate drop but it can also have rare moments where it's much faster than intended, this is something that might only exist when the processor is being consistently polled so the software should not have this issue.



## 8.C Prototype Construction

The following sections will be dedicated towards the different prototype stages of our project. It will cover the first prototype that was presented at the end of Senior Design I and will finish with the final prototype that is to be presented at the end of Senior Design II.

### 8.C.1 Initial Prototype for Senior Design I

The initial prototype will be an optical set up using a laser, two pinholes, the linear polarizer, a rotation stage that has the prism and a thin gold film glued to one of the faces of the prism, and a screen. The reasoning behind a minimal set up is that most of the optical components are not necessary to display surface plasmon excitation and the resonance of these surface plasmons. To achieve surface plasmon resonance, a technique called total internal reflection must be utilized. When total internal reflection is achieved, a side effect called evanescent waves are created along the surface where the incident light impacts and reflects away. As the incident light reflects, a small amount of light penetrates the second medium at the surface, thus creating a ripple like wave along the boundary of the two mediums. The two mediums being the prism, and the gold film. Surface plasmons can be observed on the screen at an angle greater than the angle of total internal reflection. This optical design will also use the Brewster's Angle to transmit p-polarized light through a linear polarizer while s-polarized light is reflected off of the linear polarizer surface and separated from the transmitted light.

The initial testing was done using a 632 nanometer Helium Neon (HeNe) laser. The purpose of using this laser is that it is easier to align as there are places to adjust the X and the Y axis of the laser diode, and that the dip in intensity is wider than a 532-nanometer diode as can be seen in Figure 38 below. This wider dip in intensity relates to surface plasmon excitation occurring at a particular angle, but unlike the simulated resonance angle for a 532 nm wavelength laser, the 632.8 nm wavelength laser would have excitation occurring for a slightly longer duration. Therefore, it would be easier for us to find where the resonance angle is during our experiments using the HeNe laser at first. It is also important to note that red light is easier to observe than green light, making this diode more visually appealing when attempting to confirm surface plasmon excitation for the first time. A simulation was ran using the software WinSpall using the wavelength of the helium neon laser diode to describe the dip in intensity where surface plasmon excitation occurs and following images will display the light before and after exceeding the critical angle of the prism where power loss occurs. It is uncertain whether surface plasmon excitation occurred or not due to the lack of clarity in the transmission of light. The following power loss could be glue induced or a result of internal scattering within the prism against the glue. This will be investigated further during the second half of the senior design capstone course.

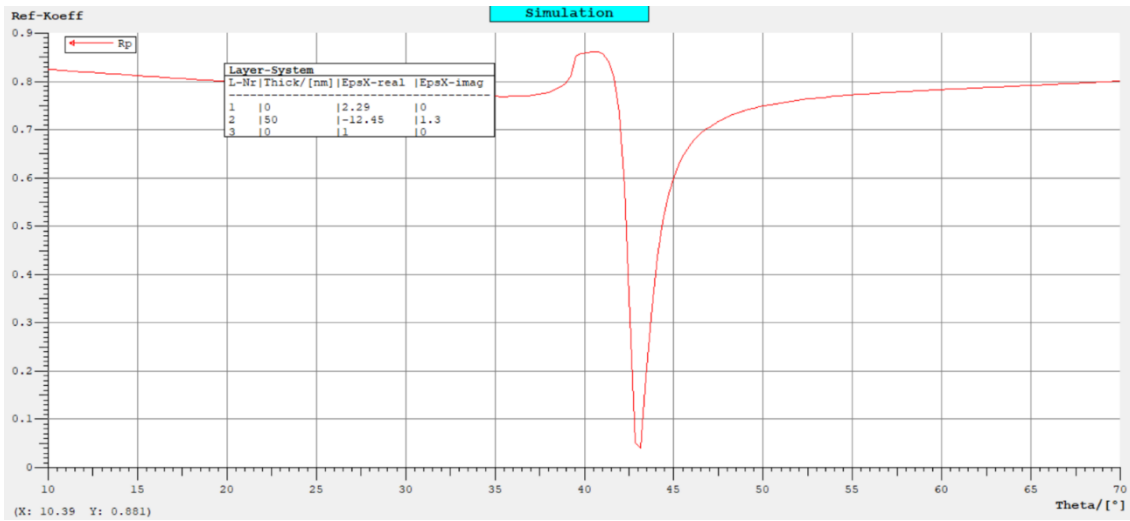


**Figure 38.** Simulation of Resonance Curve of Gold Film with 632.8 nm Wavelength using WinSpall.

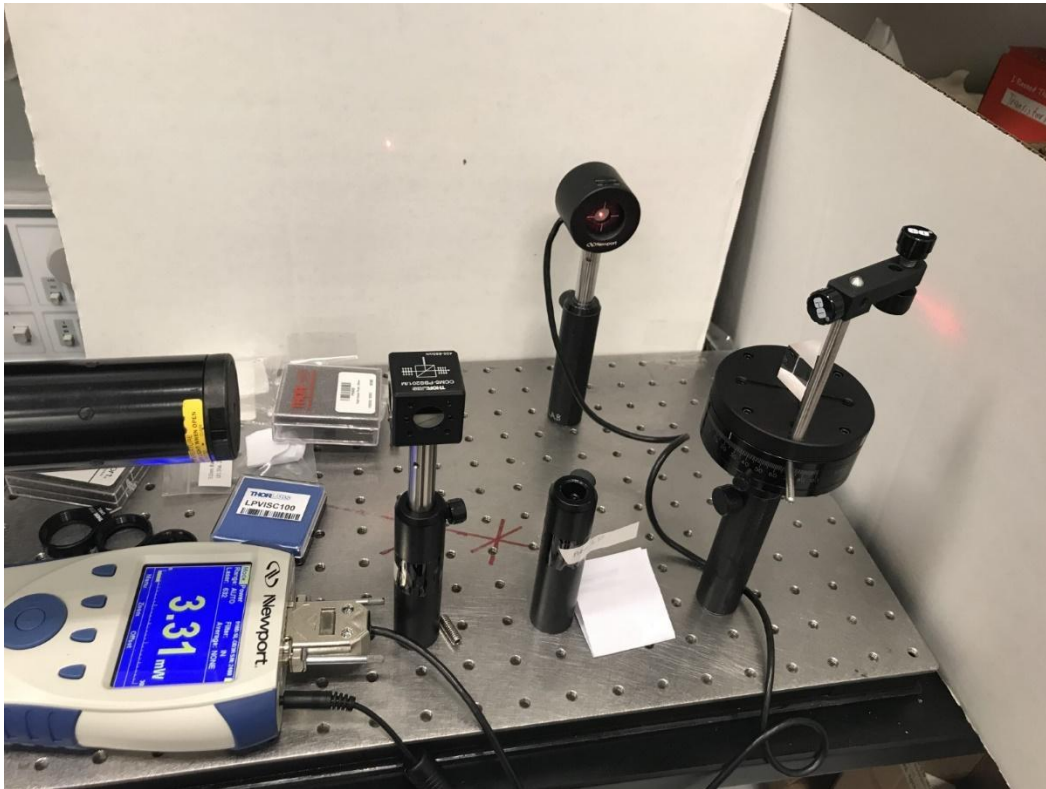


**Figure 39.** Experimental set up that displays an angle smaller than the critical angle.

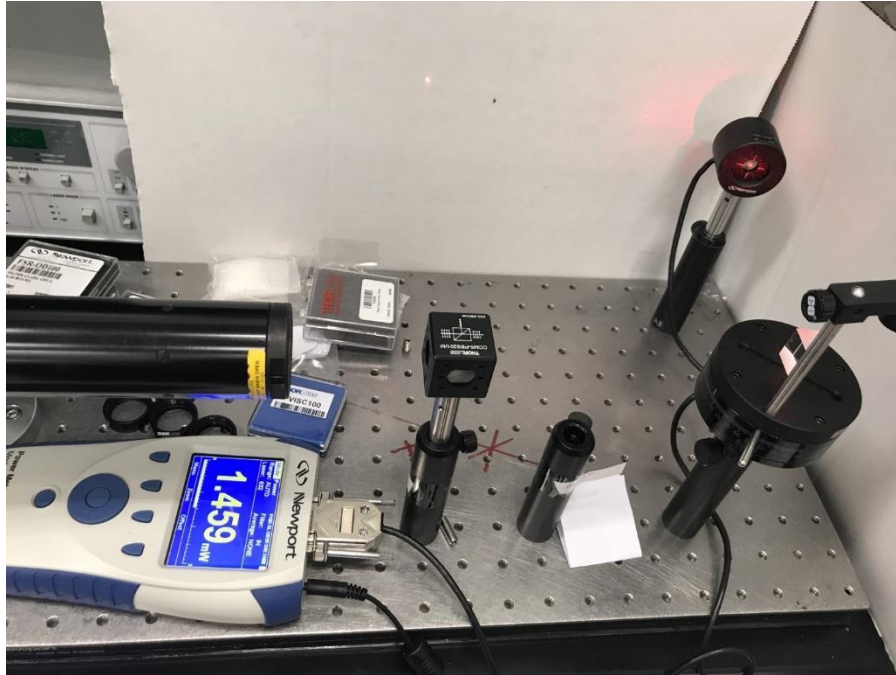


**Figure 40.** 532 nm Experiment Displaying Angle at TIR.

Figure 39 displays the prism set at an angle smaller than the calculated value of the critical angle. When we increased the angle of our prism, total internal reflection was seen and a drop in the output power was observed which can be seen in Figure 40. There is a 55% loss in power at this angle. It is hard to note what the angle of the laser is hitting the prism because the prism had to be moved around to make sure there is contact between the light source and the gold film, but the prism did not move from this exact spot between photos. The final results were deemed inconclusive due to us having to move the prism to acquire the correct contact with the gold film and the loss in power is not a large enough drop to be considered surface plasmon excitation. At this point, we switched to the 532 nm laser diode module to begin designing our first prototype demo.

The prototype demo will utilize a 5-milliwatt laser with similar specifications as the diode from Edmund Optics listed above in section 3.2.B. The reason this laser is chosen for the demonstration is because it was borrowed from the CREOL undergraduate learning laboratory and was readily available for use as well as having an attached mount and holder, allowing ease of alignment along the optical surface. The laser purchased for the device has a smaller diameter and is unmounted so with consideration of the time constraints upon the team members, this prevented the creation or purchase of an adequately sized laser diode mount. To begin the prototype, the laser was aligned using the two pinholes to locate the beam in the near field and far field of the optical system to ensure that the beam travel path will lead directly into the area of the prism necessary for total internal reflection. The laser diode has limited movement in the x-z plane because the mount is attached to the diode, so the direction of the beam can only be manipulated through changes in the angle of the diode with respect to the optical axis.

The prism is placed upon a rotation stage to allow angular changes so the beam can transmit through the prism at different angles to find the appropriate angle for total internal reflection. Figure 41 is a photograph taken of the bare optical system with the laser turned on to show the occurrence of total internal reflection.

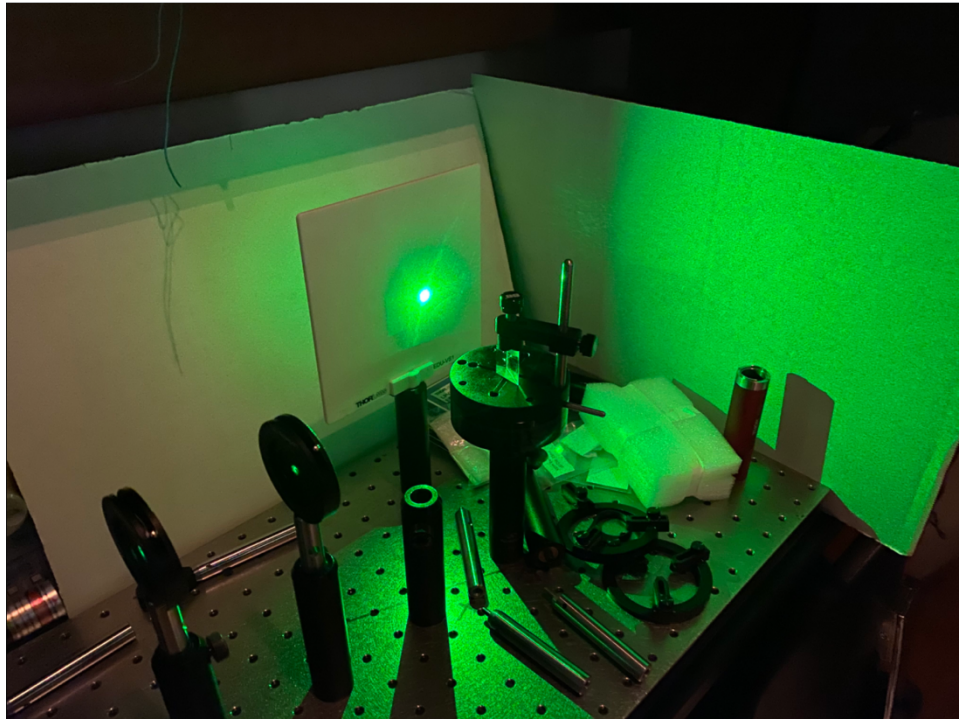


**Figure 41.** Initial Prototype of Optical Setup.

Next, the optical filters were placed into the system to confirm that the optical components are operating properly within the environmental conditions. The pinhole irises were removed from the optical setup as the beam was now properly aligned and their use was no longer necessary. The linear polarizer was placed directly after the laser diode to provide the p-polarized light to the system. After the linear polarizer, the beam is directed onto the right-angle prism on the rotation stage. For the first part of our experiment, the SPR chip is not placed on the prism so that we can establish the correct angle where total internal reflection occurs before excitation. The prism was placed onto the rotation stage so that the beam of our laser diode is incident at 0 degrees to the side of the prism. Moving our rotation stage until only reflected light was emitted from the prism and no light was transmitted, we measured our rotation angle where total internal reflection occurs at 42 degrees. This was very close to the calculated angle that total internal reflection should occur based on the material of the glass prism and the calculated critical angle.

As mentioned prior, for angles of our incident light greater than our critical angle, the glass boundary of our prism will act as a mirror and the incident light is totally reflected.



This matches the measured angle where total internal reflection was found, as 42 degrees is a greater angle than 41.81 degrees.

Once total internal reflection was established without the SPR chip, it was time to add the SPR chip to the prism to determine the resonance angle for surface plasmon excitation to occur. To attach the SPR chip to the prism, clear silicone glue was used. This was chosen based on the SPR chip manufacturers recommendations for use with biological samples and because silicone glue can be removed safely from glass surfaces. Figure 42 illustrates the process of attaching the SPR chip to the right-angle prism.

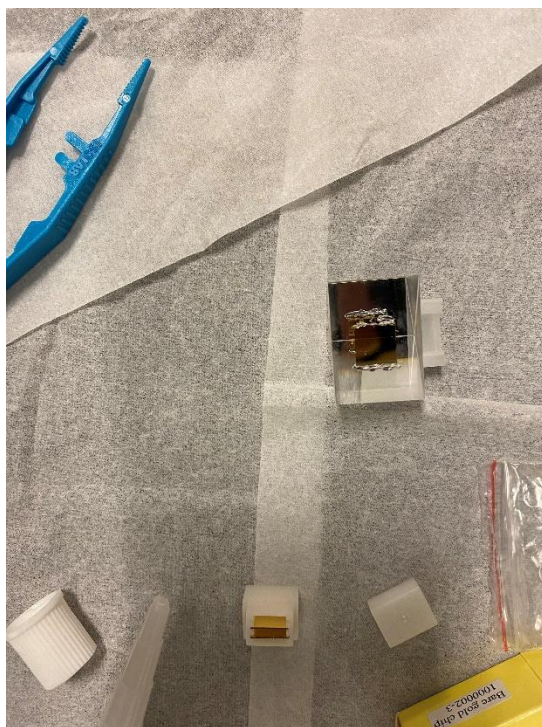


**Figure 42.** Attaching the SPR chip to the Right-Angle Prism.

The glue was allowed to set for one hour to ensure the chip remained fixed to the glass surface. After the glue was set, we placed the prism back onto the rotation stage and aligned it so the beam is incident at 0 degrees to the prism side. We moved our rotation stage until we observed total internal reflection occurring. Total internal reflection began to occur when the prism was at an angle of 46 degrees. Unfortunately, the intensity of the emitted beam on our screen did not seem to decrease when observing with the naked eye. Therefore, we could not be certain if surface plasmon excitation was occurring when the incoming light interacts with the anti-phase light back-scattering from the gold metal film.

To determine if the intensity was decreasing at any point, an optical power meter replaced the location of the screen to allow us to monitor the changes in optical power measured after the incident light interacts with the gold surface. However, we realized

that the SPR chip needed to be removed from the right-angle prism in order for us to measure the difference in output power when the chip was on or off the prism to properly determine when surface plasmon excitation is occurring. A 40 mm right-angle prism from the undergraduate lab was borrowed to replace our prism that had one of the SPR chips attached to its surface with glue. This 40 mm prism would be used instead for the remainder of our optical demo experiments.

To begin our experiments in determining why we were not experiencing surface plasmon excitation, we removed our 20 mm right-angle prism that has the SPR chip and placed the 40 mm right-angle prism onto the rotation stage. The prism was aligned so the laser beam is incident at 0 degrees relative to the prism side. Our issues could be with multiple components in our design: the polarization axis of our linear polarizer or the SPR chip purchased. Various experiments would be done to determine which of these is causing our transmitted light not to create surface plasmon excitation.

### 8.C.1.1 Determining the Polarization of our Incident Light

One possible reason for our incident light not to be destructively interfering with the back-scattered light from the gold metal film is the polarization of the incident light is not polarized correctly. For the light to interfere with the evanescent wave created beyond the boundary of the prism, the light must be p-polarized meaning that the light must have an electric field polarized parallel to the plane of incidence. Reflective linear polarizers, such as the one we used for this experiment, will transmit the desired polarization while reflecting the others. The linear polarizer used in our experiments is mounted with a rotation axis which allows us to easily see which angle the polarizer is rotated to. The mounted linear polarizer used can be seen in Figure 43.

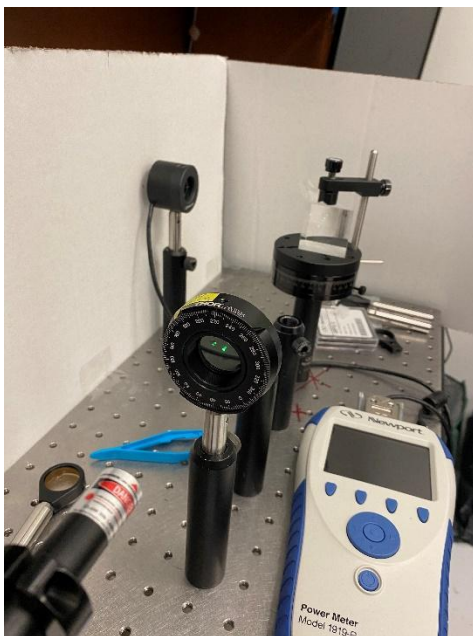


**Figure 43.** Mounted Linear Polarizer for Optical Demonstration.

To determine which angle is appropriate for us to only allow p-polarized light into our system, we began by testing the measured output power of the beam after passing through the right-angle prism without the SPR chip attached while changing the rotation angle of the linear polarizer and then once again measuring the output power of the beam at the same angles with the SPR chip attached. This would provide us with a reference measurement of output power with and without the SPR chip included in the optical setup.

The first experiment was with the right-angle prism without the SPR chip included. The prism's rotation stage was moved until total internal reflection was established, which was at an angle of 42 degrees. We then set the rotation angle of the mounted linear polarizer to 0 degrees and began slowly increasing the rotation angle in increments of 5 degrees, monitoring the measured output power from the optical power meter placed where the reflected light from the prism was emitted, until we found a maximum output power. Once the maximum output power was found, we recorded the measurement and the rotation angle of the linear polarizer. We then rotated the linear polarizer to 90 degrees from the angle where maximum power was found. This was done to find the minimum output power reading for the orthogonal polarization. The measurements were done five times and the results were averaged. It was determined that at a rotation angle of 133.2 degrees, the maximum output power of our laser was 2.99 mW. The minimum output power of our laser was 1.23 mW at a rotation angle of 223.2 degrees.

The next experiment to perform was to attach the SPR chip to the prism and measure the output power at the rotation angles found in the previous experiment to compare any changes to the power readings. For these experiments, we used clear packing tape to attach the SPR chip to the prism in a way that allows us to easily remove the chip and not have any excess glue on the prism itself. The tape was placed at the top corner of the SPR chip to avoid the tape from interfering with the location of the chip where the beam would interact. An image of our SPR chip attached to our prism with the tape can be seen in Figure 44 below.



**Figure 44.** SPR Chip Attached to 40 mm Right-Angle Prism.

Once the SPR chip was attached, we rotated the rotation stage of our prism until total internal reflection was observed, which was measured to be at a rotation angle of 42 degrees. We then changed the rotation axis of our linear polarizer to the previously found angles and recorded the output power at the various minimum and maximum output locations. The measurements from each experiment mentioned to determine the polarization axis for our experiment can be seen below in Table 12 and Table 13.  $P_{\max}$  represents the maximum power found for each rotation angle, while  $P_{\min}$  represents the minimum power found.

Experiments Performed	$P_{\max}$ (mW)	Polarizer Rotation Angle at $P_{\max}$ (degrees)	$P_{\min}$ (mW)	Polarizer Rotation Angle at $P_{\min}$ (degrees)
1	3.12	134	1.22	224
2	2.98	136	1.24	226
3	3.01	134	1.25	224
4	2.96	130	1.22	220
5	2.87	132	1.23	222
Average	2.99	133.2	1.23	223.2

**Table 12.** Experimentation for Determining Polarization Axis for SPR Effect: Right-Angle Prism without SPR Chip Attached.

Experiments Performed	$P_{\max}$ (mW)	Polarizer Rotation Angle at $P_{\max}$ (degrees)	$P_{\min}$ (mW)	Polarizer Rotation Angle at $P_{\min}$ (degrees)
1	2.98	134	1.24	224
2	2.35	136	1.26	226
3	2.76	134	1.24	224
4	2.81	130	1.21	220
5	2.82	132	1.23	222
Average	2.74	133.2	1.24	223.2

**Table 13.** Experimentation for Determining Polarization Axis for SPR Effect: Right-Angle Prism with SPR Chip Attached.

From our experiments, there was no moment during the changes in rotation of the linear polarizer that we noticed a significant drop in output power intensity. Nevertheless, this experiment did provide us with the rotation angles where the maximum and minimum power transmitted through the linear polarizer occur. In a linear polarizer, the maximum transmission of incident light occurs when the axis of the polarizer is parallel to the plane of polarization while the transmission is minimum when the axis of the polarizer is perpendicular to the plane of polarization. From our previous test, we know that the laser diode is elliptically polarized. We can then conclude that at a rotation angle of around 133.2 degrees the incident light from our laser diode will be parallel to the axis of



the polarizer. With this information we could determine the best possible rotation angle for our polarizer to aid us in creating surface plasmon excitation.

Determining when our incident light is p-polarized using only a mounted linear polarizer became time-consuming and other avenues to ensure we have only p-polarized light in our system were investigated. This led to the discovery of the polarizing beam splitter. A polarizing beam splitter is a device that uses the idea of the Brewster's Angle to create a phenomenon where only the p-polarized light directed at a medium is transmitted through while the s-polarized light is reflected. To do this, two right angle prisms are cemented together to create a cube shape. The cube is coated with a dielectric coating along the diagonal interface between the two right angle prisms which will reflect s-polarized light and transmit p-polarized light. The extinction ratio of the polarizing beam splitter is 1000:1 in favor of p-polarized light, ensuring that the emitted beam has the highest polarization purity possible. This device is perfect for our surface plasmon resonance sensor because it will ensure that the optical components of our experiment are correct since only p-polarized light will be emitted from the beam splitter. This will aid us in eliminating the possible issues that are causing us not to have surface plasmon excitation occur. Figure 45 is an image of the polarizing beam splitter used in our experiment, where a diagram etched onto the device can be seen that shows the s-polarized light will be reflected to the left relative to the plane of incidence while the p-polarized light will be transmitted through.

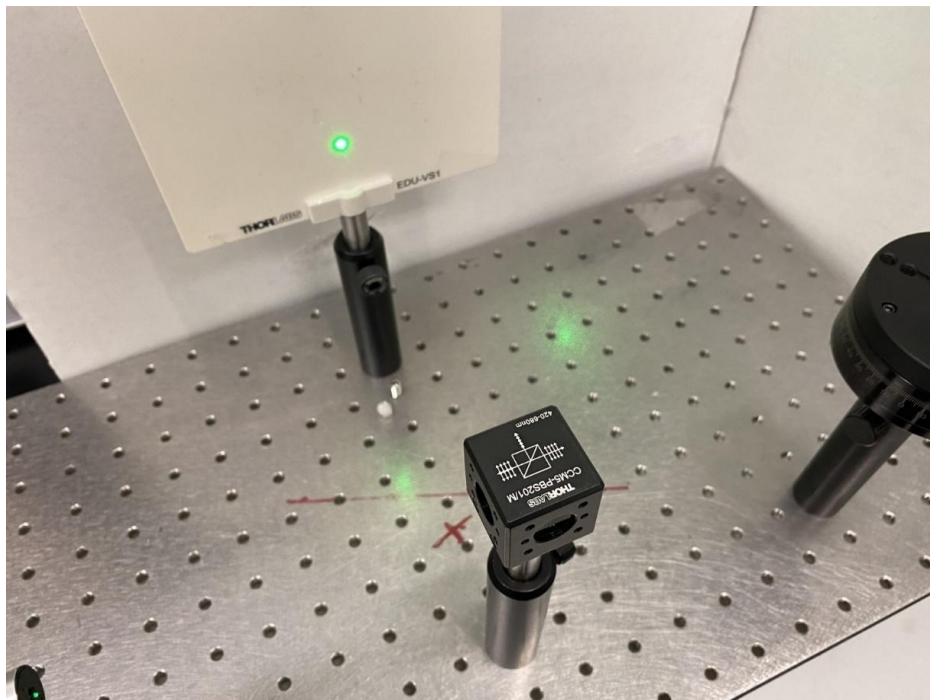


**Figure 45.** Polarizing Beam Splitter for Transmitting P-polarized Light.

The polarizing beamsplitter was placed between the laser diode module and the rotation stage where our prism was placed. A white screen was placed to the left of the

polarizing beam splitter to block the s-polarized light reflected from the dielectric coating inside the beam splitter itself. Before beginning our experiments to determine if surface plasmon excitation is now occurring when the p-polarized light from the beam splitter is directed onto the prism, we first measured the output power of the laser diode before and after the light enters the beam splitter. Using our optical power meter, the output power measured before the light enters the polarizing beam splitter was 6.10 mW. Figure 46 below shows the output power measured on the optical power meter.

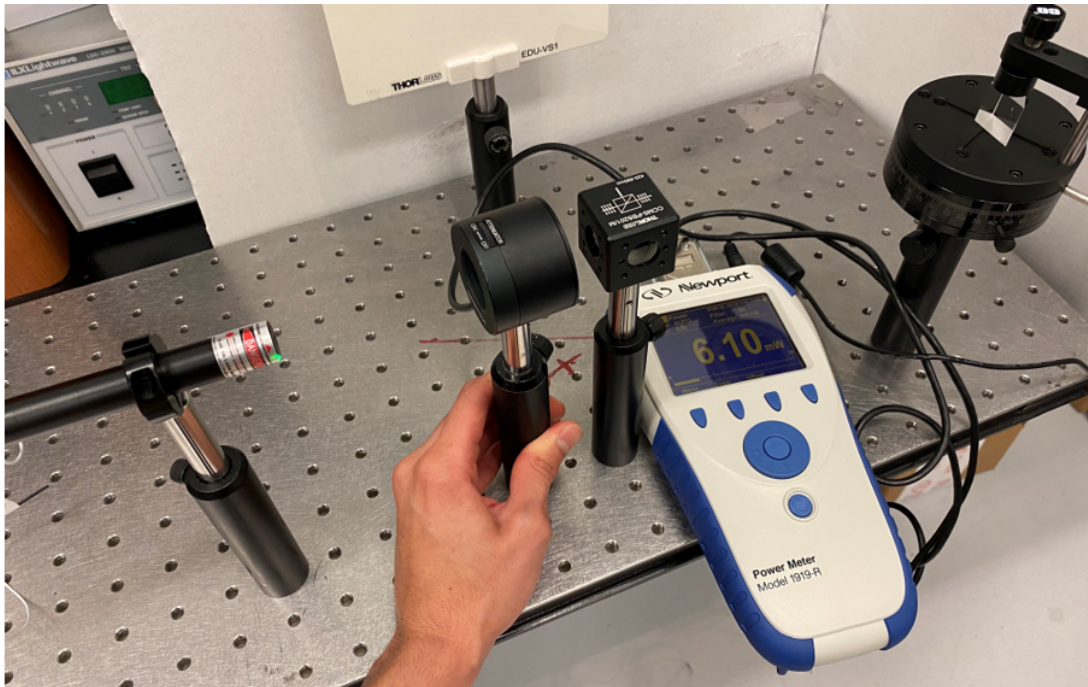


**Figure 46.** Measured Output Power before Polarizing Beam Splitter.

We then measured the output power of our beam after only p-polarized light is allowed to transmit through. Once again using the optical power meter, the output power of our p-polarized light was found to be 4.18 mW. Figure 47 below shows the output power measured on the optical power meter.

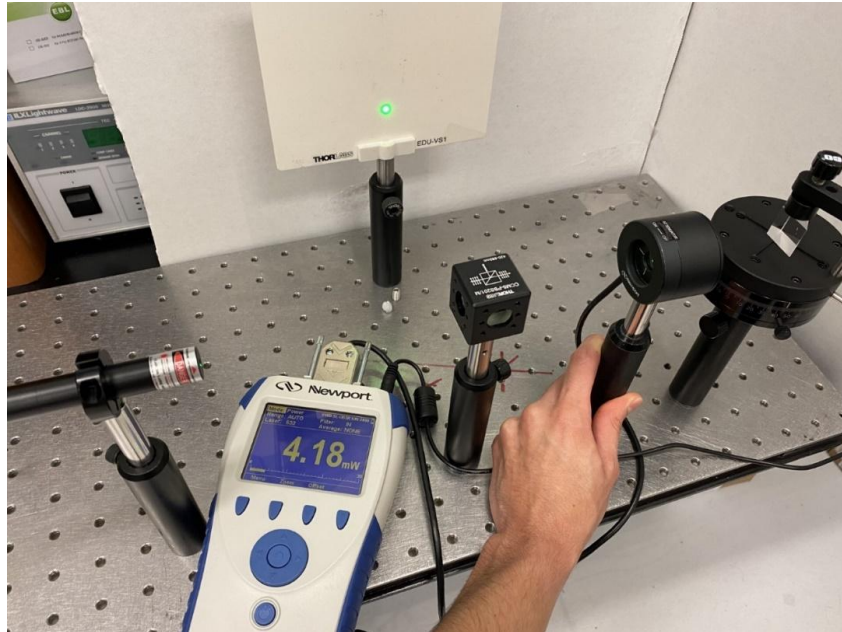


**Figure 47.** Measured Output Power of P-Polarized Light.

We also measured the output power of the s-polarized light to determine how much of our light was being lost due to the s-polarization of our incident light being reflected. Using our optical power meter, the output power of our s-polarized light was found to be 1.524 mW. Figure 48 below shows the output power measured on the optical power meter.



**Figure 48.** Measured Output Power of S-Polarized Light.

From the measured output power, it can be seen that our p-polarized light is about 1.5 mW less than our emitted light from the laser diode module. This also shows that our elliptically polarized light from the laser diode contained a majority of p-polarized light.

Our next experiment was to measure the output power of our beam after interacting with the SPR chip attached to the prism at different angles of rotation to determine if surface plasmon excitation is occurring. The right-angle prism was once again placed so the laser beam is incident at 0 degrees relative to the prism side. We then rotated the rotation stage until total internal reflection was observed, which was found at the rotation angle of 42 degrees. The optical power meter was then placed to capture the emitted light that is reflected off the prism's surface in order to measure the output power as we slowly rotated the prism by 0.5 degrees until total internal reflection was no longer observed. The measured output power for each rotation angle can be seen below in Table 14.

Angle of Rotation Stage, degrees	Output Power (p-polarized light), mW
42	4.18
42.5	4.16
43	4.20
43.5	4.23
44	4.21
44.5	4.21
45	4.22
45.5	4.20
46	4.15
46.5	4.13
47	4.15
47.5	4.12
48	4.13
48.5	4.11
49	4.12
49.5	4.15
50	4.10

**Table 14.** Experimentation to Measure Output Power with Polarizing Beam Splitter.

From our experiment, no significant drop in output power was measured when rotating our right-angle prism. Therefore, as we have now ensured that our beam is polarized correctly and that the angle is allowing for total internal reflection to occur, the reason surface plasmon excitation has not happened must lie with the SPR chip itself.



### 8.C.1.2 Investigating the Properties of our SPR Chip

For surface plasmon excitation to occur, one must consider certain parameters. The SPR chip must be within a nanometer of contact with the prism used. This includes the glue or epoxy used to mount the chip onto the prism. A proposed solution to this crucial parameter is using index matching gel to mount the SPR chip onto the prism. The index matching gel will have the same index as the BK7, also known as crown glass. This will prevent any light deviation from occurring as the beam will interpret the gel as part of the prism. The prevention of deviation is important to this device because the light must hit the surface connecting the prism and the SPR chip at a specific angle, and any refractive index change along the optical path will result in either a greater or lesser change in angle. Using any sort of glue, such as Elmers or a higher-grade silicon glue will result in a randomized angle of incidence on the SPR chip. This was displayed during the prototype demonstration for the College of Optics and Photonics, as surface plasmons could not be displayed on the provided screen due a lack of contact between the chip and prism as well as the silicon glue's index of refraction being unknown. The refractive index could be tested however the testing and calculation of the refractive index is strenuous and time consuming compared to the alternative of purchasing index matching gel, which will be demonstrated during the second half of this capstone course.

Another important property that is necessary for surface plasmon excitation to occur is chip dimensions. During the testing phase to investigate the occurrence of surface plasmon excitation, it was noticed that as the angle of incidence grew as the rotation stage was turned the incident light would exceed the size of the gold chip. This resulted in constant adjustments of our prism to maintain contact between the beam and the chip. The prism dimensions are 20x20x20 mm and the chip dimensions are 10x10x0.3 mm. The chip was glued directly to the center of the hypotenuse of the prism, limiting the amount of angular change in the system. Any time the stage was rotated far enough that the light no longer contacted the chip, the prism had to be moved to retain contact. Any slight change in the prism's orientation affects the generation of surface plasmons as the angle of incidence gets changed during the movement. The chosen solution to surpass this is to purchase another set of gold chips that similarly sized to our prism to maintain contact throughout the angular changes.

Our plans for the Fall semester will be to use the index matching gel purchased from Thorlabs to attach the 20x20x20 mm bare gold SPR chip to the base of our prism. This should ensure that our chip and prism are in close contact to allow surface plasmon excitation to occur. Once we are able to excite the surface plasmons using the index matching gel as an adhesive, we can investigate other methods besides using an adhesive to press the chip firmly against the prism during experimentations. One method we will investigate is by 3D printing a flow cell where our analyte solution will go which will have a spring mechanism on it to mechanically press the SPR chip against the prism during the entire experiment. This way the user does not need to use any

adhesive to create the close contact needed for surface plasmon excitation to occur. Once the angle is found, it will be translated into the device by mounting mirrors onto a fixed platform that allows the light to reflect into the mirror at said angle. With these fixes in place, the design should operate as intended for data collection.

### **8.C.2 Final Prototype for Senior Design II**

At the beginning of Senior Design II, two key components of the device were changed. These changes were due to discussions with experts in the field and various simulations and calculations performed.

The first key change was in the wavelength of the laser diode module. In previous sections, the simulations and calculations performed to come to this conclusion have been discussed. In the end, it was concluded that longer wavelengths were preferable for surface plasmon resonance sensors compared to shorter wavelengths. This led to us purchasing from Thorlabs the 635 nm laser diode module. The laser emits an output power of 1.2 mW, which was confirmed using an optical power meter in the lab. The beam divergence of the laser diode was 0.6 milliradians, an acceptable divergence for our purposes. The laser diode module was mounted into a kinematic mount with two adjuster screws for the X and Y axis. This ensured that the laser is correctly aligned throughout our experiment.

The second key change was the purchase of a motorized rotation stage. During Senior Design I, a manual rotation stage was used to observe surface plasmon excitation. After discussions with Dr. Pieter Kik, an expert in nanophotonics at CREOL and who teaches a course on the fundamentals of surface plasmons, we determined that a motorized rotation stage would ensure that we rotate our prism to the proper angle for phase matching to occur between the wave of our incident light and the wave of our surface plasmons. The motorized rotation stage was purchased from Thorlabs. It has a bidirectional repeatability of  $\pm 0.1^\circ$  and 25 arcseconds of achievable incremental motion. Alongside this, it has a percentage accuracy of 0.1%, making this a highly precise tool to use for our purposes. Another added benefit of the motorized rotation stage is that it allows for an automated portion of our device for the user, allowing the user to easily move the rotation stage to their desired position using the Kinesis software provided by Thorlabs, or with the K-Cube DC Servo Motor Controller that allows for a software-free option to control the direction of the rotation stage.

The new design also included adding a parabolic mirror and a plano-convex lens to direct and focus the reflected light off of the prism onto the CMOS sensor camera. Figure 49 below shows the schematic diagram of the prototype including these new components. This illustration, however, changed from our final prototype which will be discussed later in this section.

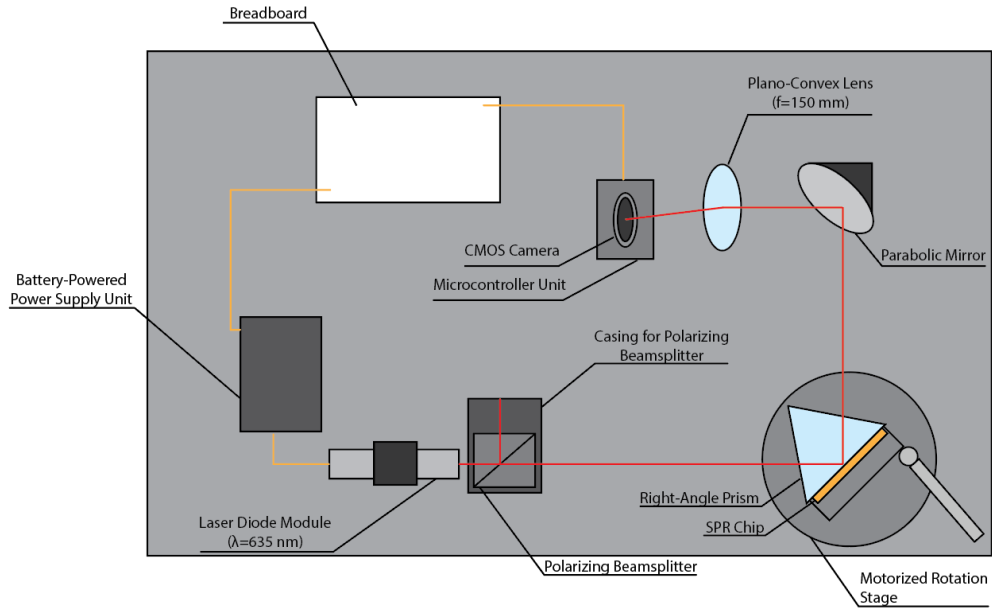


**Figure 49.** Schematic Diagram of SASSPR Version 2.

The first step in designing our new prototype was to first confirm that surface plasmon excitation is occurring with our new optical setup. To do this, an experiment was performed in free space where the power of the light is monitored at different angular increments to see if a significant drop in its intensity is observed, a confirmation that excitation of the surface plasmons had been established. The right-angle prism was carefully placed on top of the motorized rotation stage so that it was positioned at the 0° mark on our rotation stage. Figure 50 below shows our initial setup for the experiment.

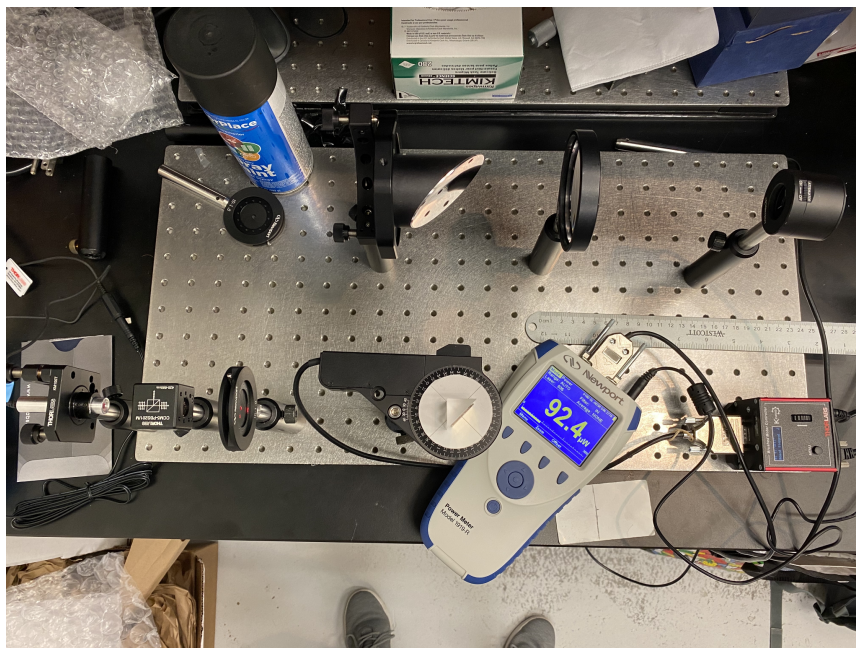


**Figure 50.** Experimental Setup for Final Prototype.

The motorized rotation stage was rotated until the critical angle of the right-angle prism was found, which was found to be  $41^\circ$ . This closely matches the calculated critical angle found previously, confirming the prism was correctly placed onto the rotation stage. With the critical angle found, we slowly increased the angle on our motorized rotation stage until total internal reflection occurred. Total internal reflection was seen at angles greater than  $41^\circ$ . With the critical angle found, we then placed the bare gold SPR chip onto the right-angle prism surface using index matching gel. Figure 51 shows the right-angle prism with the SPR chip attached using the index matching gel.

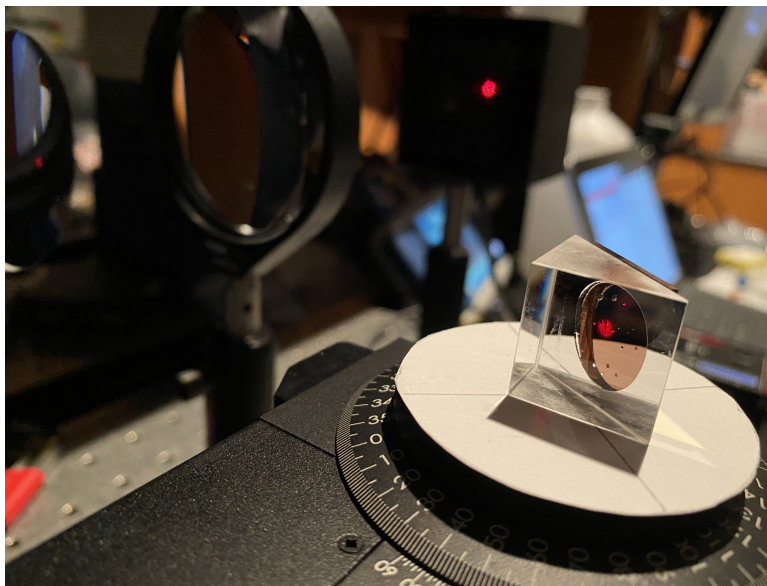


**Figure 51.** SPR Chip Attached to Prism using Index Matching Gel.

With the SPR chip attached to the surface of the prism, and the stage rotated back to  $0^\circ$ , the motorized rotation stage was rotated until the critical angle was found again. The critical angle was seen again at  $41^\circ$ . From our research, we know that surface plasmon excitation can occur at angles greater than the critical angle. Using the optical power meter, we began rotating the prism in  $0.5^\circ$  increments from a starting position of  $38^\circ$  until reaching  $50^\circ$ . The measured power readings for each angle were recorded to determine if a significant drop in intensity was observed. Table 15 below contains the recorded measurements for our experiment.



Angle (°)	Power (μW)
38	420
38.5	426
39	426
39.5	428
40	430
40.5	430
41	440
41.5	450
42	470
42.5	480
43	520
43.5	530
44	470
44.5	152
45	210
45.5	280
46	300
46.5	319
47	331
47.5	339
48	341
48.5	347
49	342
49.5	354
50	315

**Table 15.** Experiment for Surface Plasmon Excitation using 635 nm Laser Diode.

It was observed that a significant drop in intensity was seen at 44.5°, with an increase in intensity seen at angles greater than 45°. This was determined to be the angle where surface plasmon excitation occurred. To compare the experimental results with that of

the simulation using Winspall, the measured power readings were normalized to match the reflectivity range of the light from 0 to 1, with 1 being the maximum output power of the laser after the polarizing beamsplitter and 0 being no power observed. The normalized measurements were graphed alongside that of the simulation for easy comparison, which can be found in Figure 52 below.

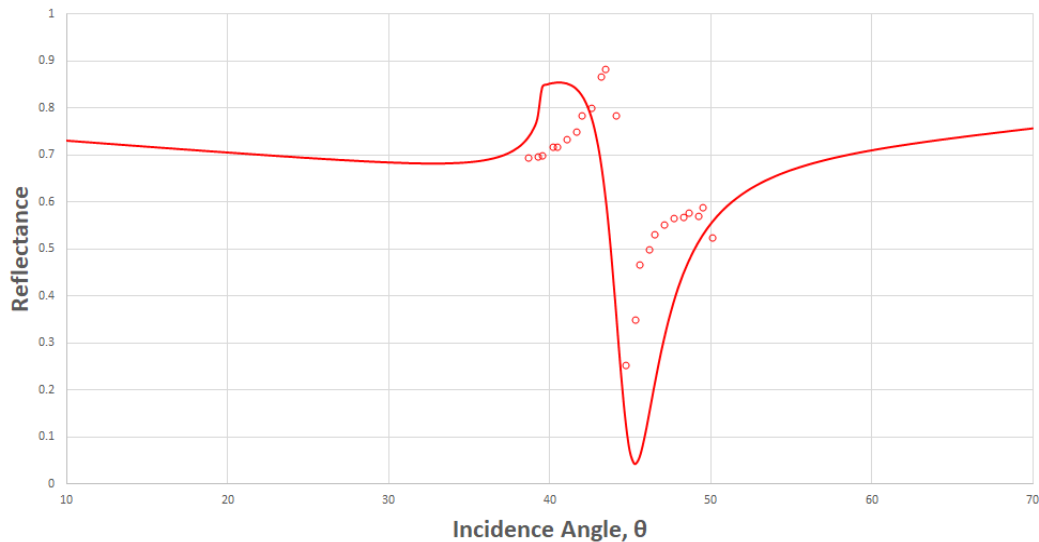


**Figure 52.** Simulation vs. experimental: reflectance as a function of incidence angle measured. Solid line corresponds to simulated data, open circles correspond to experimental data.

Comparing the simulation data with that of the experiment, the angle where SPR occurred for the experiment closely resembled that of the simulation. The simulation observed the critical angle at  $39.5^\circ$  and the experimental critical angle was found at  $41^\circ$ , giving a margin of error of 3.7%. The maximum drop in intensity in the experiment was found at  $44.5^\circ$  while the maximum drop in intensity simulated was found at  $45^\circ$ . This gives us a percentage accuracy of 98.8%. It was noted, however, that our experimental value did not see as significant a decrease in intensity as the simulated curve observed. This could be due to a number of factors: differences in the thickness of the gold film on the entire surface of the SPR chip could affect the final results, or the chip may not have been pressed as firmly to the glass side of the prism which could lead to the photons not able to transfer all their energy to the surface plasmons. Nevertheless, the experimental results proved that SPR had occurred and did not differ significantly from the expected results from the simulation.

It was noted during our experiment that as the prism was rotated, the reflected beam was unable to stay fixed in one position. This became a challenge as our CMOS sensor camera would have to be fixed at a stationary position during the entire experiment. The final conclusion was to remove the parabolic mirror and the plano-convex lens which were unable to keep our beam from moving over a longer range of angles. The final optical setup was therefore simplified, and the CMOS sensor camera was mounted close to the prism surface where the beam would exit. This allowed for the reflected

beam to stay centered on the lens of the CMOS sensor camera as we rotated the prism to create surface plasmon excitation. The final schematic diagram can be seen below in Figure 53. This is the final design for our device and how the final prototype was designed.

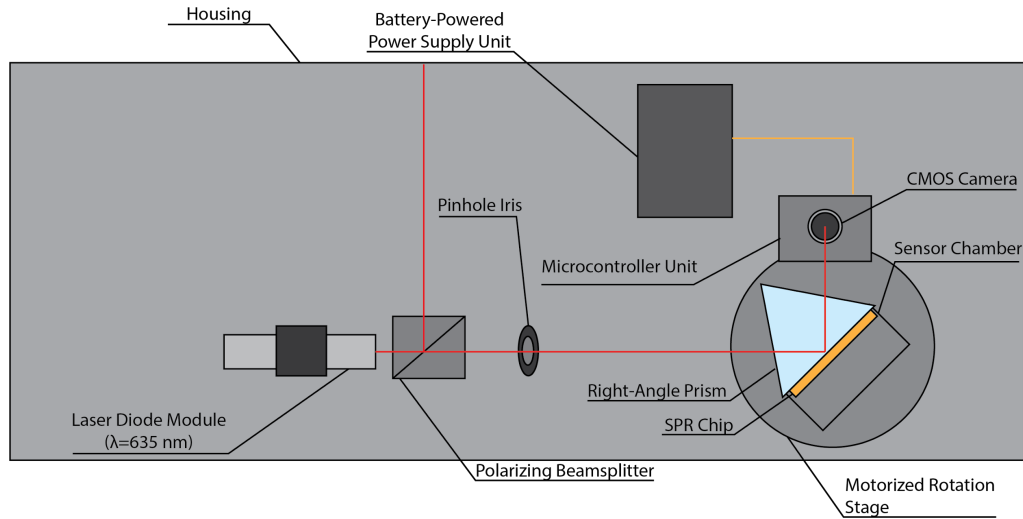


**Figure 53.** Final Schematic Diagram for SASSPR.

The next step was to confirm the experimental results could be detected by our CMOS sensor camera and the designed software. To do this, the rotation stage was set at 44° and rotated at a velocity of 0.5° per second until reaching 48°. In this experiment, surface plasmon excitation was found at 46°. This slight change in the angle was due to a new SPR chip attached to the surface of the prism as well as the prism having to be readjusted from its original place in previous experiments. The intensity of the reflected beam was captured by the camera and the intensity profile of each image processed and displayed graphically using the software application, which can be seen in Figure 54.

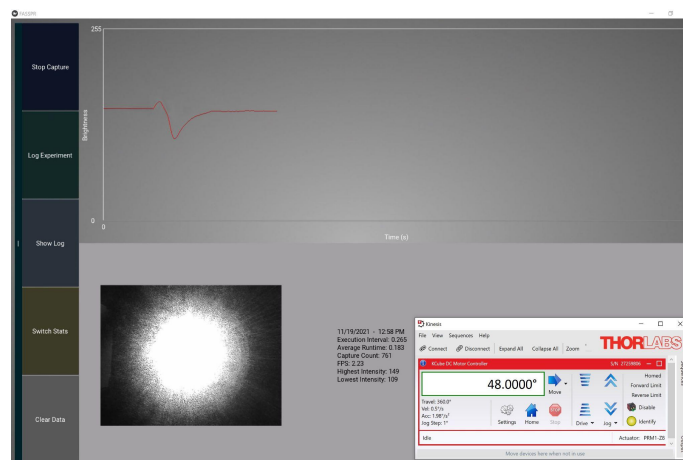


**Figure 54.** SASSPR software displaying graphically the SPR curve in air as Reflectance vs. Time.

The change in intensity displayed on the software follows closely to that observed experimentally using an optical power meter. The experiment using our software was tested multiple times using different gold SPR chips, and the angle and drop in intensity observed remained relatively consistent for each experiment. This showed that our device can easily repeat experiments even with different SPR chips applied to the sensing location.

Next, distilled water was added into the sensor chamber at the SPR angle found in air. Distilled water was chosen for a number of factors. The primary reason was distilled water having a refractive index of 1.324, which is greater than that of air. Choosing a dielectric material with a higher refractive index allows us to demonstrate our device as it detects shifts in the resonance angle when increasing the refractive index of the material in contact with the interface of the gold film. Distilled water was also chosen due to the distillation process removing the electrical charge from atoms and molecules in the water, thus providing more accurate results in laboratory settings. Once the distilled water was added to the sensor chamber, the intensity of the reflected light immediately increased. This indicated that our SPR angle had shifted due to a change in the refractive index observed on the surface of the gold film. This shift stems from the critical angle of the prism being altered as the refractive index on the opposite side of the surface changes. This portion of the experiment proved our device could monitor changes in the resonance angle using intensity modulation. Figure 55 shows the increase in intensity observed graphically using the software application.

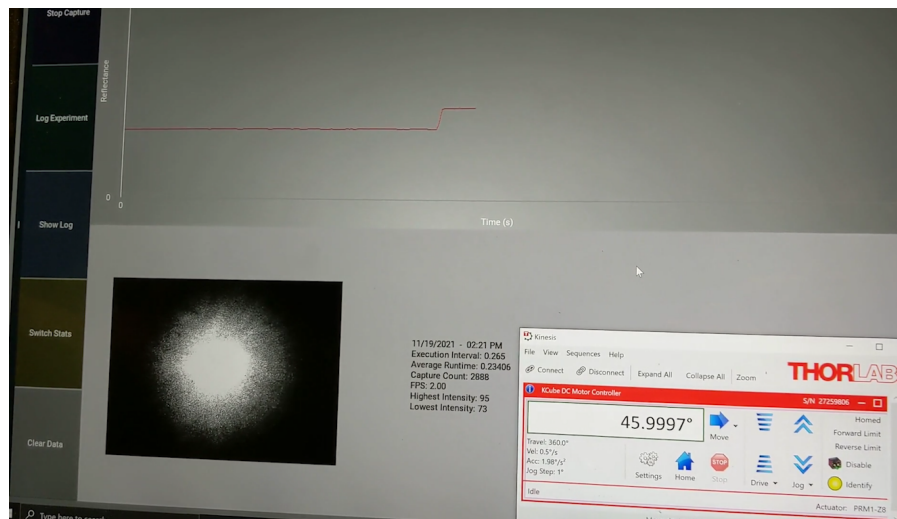


**Figure 55.** SASSPR software displaying graphically the SPR curve in distilled water as Reflectance vs. Time.

## 9. Bill of Materials

This section will provide a table of the various optical, electrical, computer, and biological components used for the completion of our SPR sensor. Table 16 provides information on each component, where it was purchased, how much each component cost, and the total cost of the project. This provides one with a clear representation of the cost of our entire project and how affordable it may be for future replication.

Item	Quantity	Price \$	Out of Pocket	Seller
Right-angle Prism	1	51.68	51.68	Thorlabs <a href="#">Link</a>
Polarizing Beam Splitter	1	282.44	282.44	Thorlabs <a href="#">Link</a>
Laser Diode Module	1	97.37	Covered by CREOL	Thorlabs <a href="#">Link</a>
Laser Diode Module Mounting Kit	1	217.51	Covered by CREOL	Thorlabs <a href="#">Link</a>
Motorized Precision Rotation Stage with 2.56" Platform	1	945.26	Covered by CREOL	Thorlabs <a href="#">Link</a>
K-Cubed Brushed DC Servo Motor Controller	1	677.41	Covered by CREOL	Thorlabs <a href="#">Link</a>
15V Power Supply Unit for One K-Cube	1	35.36	Covered by CREOL	Thorlabs <a href="#">Link</a>
Distilled Water 64 oz	1	23.99	23.99	Chem world <a href="#">Link</a>
MC and CMOS Camera	1	18.00	18	Amazon <a href="#">Link</a>
9V Battery Cable Clips	1	3.99	3.99	Amazon <a href="#">Link</a>
USB to UART Serial Adaptor	1	10.99	10.99	Amazon <a href="#">Link</a>
Bare Gold SPR Chips 3 pack	3	75	75	Sofchip <a href="#">Link</a>
LM2596 – 5 / NOPD	1	5.21	5.21	TI <a href="#">Link</a>
LM2596 – ADJ / NOPD	1	3.66	3.66	TI <a href="#">Link</a>
10V / 1A AC Wall Adaptor	1	8.99	8.99	Skycraft (Local)
7.4V 1600mAh 25C Li-Polymer Rechargeable Battery	1	26.99	26.99	Amazon <a href="#">Link</a>
T Plug Connectors	1	7.99	7.99	Amazon <a href="#">Link</a>
<b>Total Cost</b>		<b>2491.84</b>	<b>518.93</b>	

*Table 16. Project Financing Table.*

## 10. Project Milestones

In this section, the project milestones for our project are shown in Table 17 below. Each week, from the initialization of our project design to the final presentation of our prototype, is represented below alongside the week each task should be completed. This table serves as a clear guide to ensure we remain on track to complete our final prototype by the end of the Fall 2021 semester.

<b>Week</b>	<b>Description</b>
<b>1-12</b>	<b>Senior Design I</b>
1	Project Conception
2 - 3	Research and Role Discussion
4 - 5	Initial Project Documentation Draft
5 - 6	More Research
7 - 8	Initial Project Documentation Final
9 - 10	Order Parts
11 - 12	Build and Present Project Demo
	End Of Summer Session
<b>13-27</b>	<b>Senior Design II</b>
13 - 14	Build Prototype
15 - 16	Testing and Redesign
17 - 18	Finalizing Design
19 - 20	Fine Tuning
20 - 21	Peer Presentation
22 - 26	Finish Report
27	Presentation

*Table 17. Project Milestones Table.*

Over the course of the first senior design course the project milestone timeline changed from our initial plan. Our parts were ordered early because of purchasing through third party vendors and arrived anywhere between week 5 and 8. This time range results from inconsistencies in purchases and incorrect shipping information. The mirrors for our device were never retrieved as the United State Postal Service sent the package with the mirrors back to China within 24 hours of delivery because the address was incorrect and did not contact the group member who purchased the mirrors before doing so, resulting in the mirrors being reordered. The project demo was designed around week 8 and was continuously tested until week 12. The rest of the timetable parallels the progress made over the course of the semester.

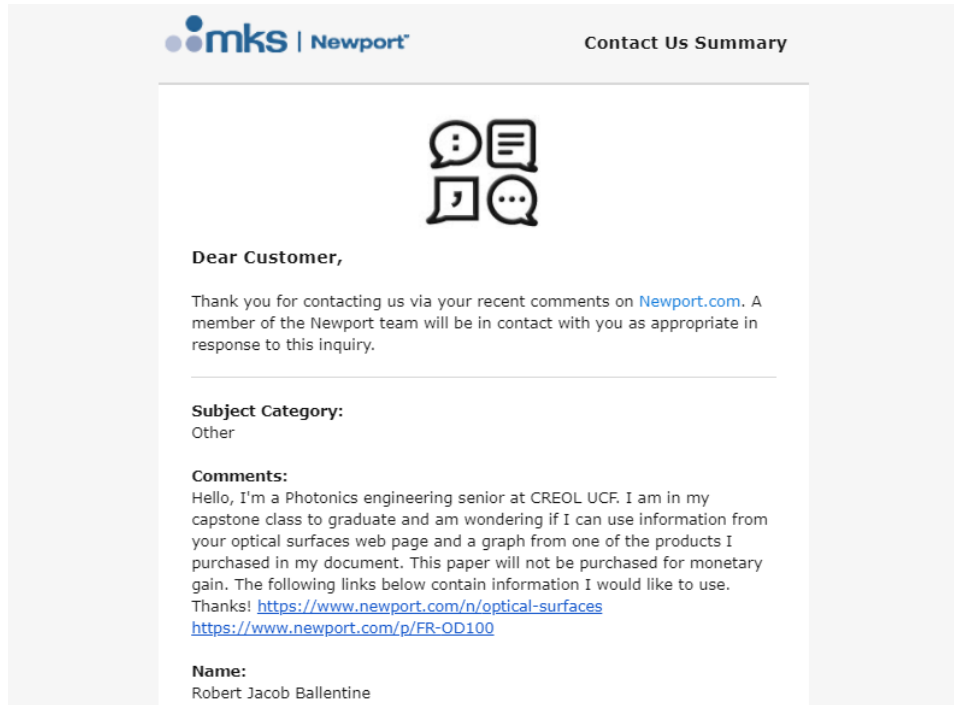
## **11. Conclusion**

We have presented a device that allows for surface plasmon resonance on thin metal films to be observed and recorded. The optical components ensure that the proper polarization, wavelength, and alignment of our laser source is correct for phase matching to occur between the wave of our incident light and the wave of the surface plasmons on the metal film, while the electrical and computer components ensure our detector properly captures the necessary intensity changes observed and represents them in a user-friendly software application. We have also demonstrated that the surface of the metal film is highly sensitive to changes to its refractive index, which was confirmed when distilled water was introduced into the sensing chamber and an increase in intensity was detected at the angle where surface plasmon excitation was previously seen. Our device could be later improved to allow for the software application to fully control the laser source and motorized rotation stage for more precise measurements of the exact angle of surface plasmon resonance to be determined. Nevertheless, we have presented a device that can detect and display surface plasmon excitation and monitor shifts in the resonance angle through intensity modulation.


## Appendix A – Permissions

The following are the various forms of permission and their current status for use of citations and figures in our documentation. Approval status for various sources mentioned below may still be pending.

Permission from Newport Optics.



**mks | Newport** Contact Us Summary



**Dear Customer,**

Thank you for contacting us via your recent comments on [Newport.com](https://www.newport.com). A member of the Newport team will be in contact with you as appropriate in response to this inquiry.

---

**Subject Category:**  
Other

**Comments:**  
Hello, I'm a Photonics engineering senior at CREOL UCF. I am in my capstone class to graduate and am wondering if I can use information from your optical surfaces web page and a graph from one of the products I purchased in my document. This paper will not be purchased for monetary gain. The following links below contain information I would like to use. Thanks! <https://www.newport.com/n/optical-surfaces>  
<https://www.newport.com/p/FR-OD100>

**Name:**  
Robert Jacob Ballentine



## Permission from Ebay Seller.

New message from: [mei-2014](#) (1,167 ★)

Dear friend

The BG9 picture you can use, because it is the picture we drew when measuring our products  
But LB1 picture and JB470 picture are not from us, we use them for reference. you can easily  
get these pictures on the internet.

Best regards

Reply


### Your previous message

Hello,

I'm an undergraduate photonics engineering student at UCF. I am in my capstone class to graduate with my undergraduate and am wondering if I can use some of the graphs on your products in my research paper. The graphs I am requesting permission to use are the BG39 shortpass filter, the LB1 bandpass filter, and the JB470 long pass filter. The filters I have not purchased may be purchased in the future if my capstone project needs a different filter. The following images are the graphs I would like to use. Thank you.

-Robert B

## Permission from author of Optoelectronics and Photonics, 2<sup>nd</sup> Edition.

 **Safa Kasap (Professor)** <sok533@usask.ca>  
Wed 7/7/2021 9:42 PM  
To: Robert Ballentine

Yes, you can.  
I don't think you would need permission for use in an academic report/thesis and it is a very small fraction of the book so it would also go under "fair use"  
SK

---

On 7/7/2021 7:38 PM, Robert Ballentine wrote:

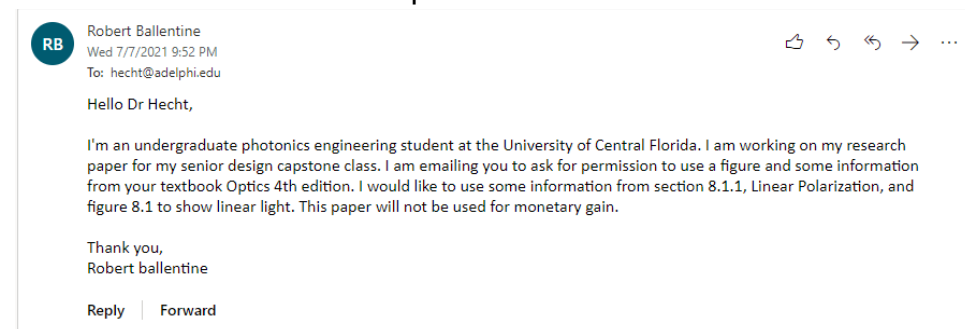
**CAUTION: External to USask. Verify sender and use caution with links and attachments. Forward suspicious emails to [phishing@usask.ca](mailto:phishing@usask.ca)**

...

Hello Dr Kasap,  
I'm an undergraduate photonics engineering student at the University of Central Florida. I am in my capstone class to graduate with my bachelor's degree. I am writing to you today to ask permission to use some figures from your book Optoelectronics and Photonics 2nd edition. The figures I would like to use are figure 3.29 on page 240 and figure 4.1 on page 282. Figure 3.29 is an energy band diagram of a p-n junction before and after an applied bias and figure 4.1 is a figure about absorption, spontaneous emission, and stimulated emission. These figures will not be used for monetary gain.

Thank you,  
Robert Ballentine

## Permission from author of Optics 4<sup>th</sup> Edition.



## Permission from citation [1].

### Rights and permissions

This work is licensed under a Creative Commons Attribution 4.0 International License. The images or other third party material in this article are included in the article's Creative Commons license, unless indicated otherwise in the credit line; if the material is not included under the Creative Commons license, users will need to obtain permission from the license holder to reproduce the material. To view a copy of this license, visit <http://creativecommons.org/licenses/by/4.0/>

## Permission from American Chemistry Society.

Dear Robin:

Thank you very much for contacting ACS. Yes, ACS is granting you a permission to cite Safety in Academic Chemistry Laboratory (SACL) 8/e as a source documentation of your project. Please include the following ACS copyright credit line whenever the SACL as is quoted or excerpts are used:

***Quoted/ used with permission from ACS Safety in Academic Chemistry Laboratory 8<sup>th</sup> edition , Copyright 2017, American Chemical Society. Not to be used for commercial purposes.***

There is no charge for this one time use.

Please let me know if I can be of any help to you.

Marta Gmurczyk

**Marta U. Gmurczyk, Ph.D.**

Senior Safety Programs Manager| Scientific Advancement Division

## Permission from Elsevier Journal.

Dear Robin Howell,

Thank you for placing your order through Copyright Clearance Center's RightsLink® service.

### Order Summary

Licensee: University of Central Florida  
Order Date: Jul 8, 2021  
Order Number: 5104310924117  
Publication: Sensors and Actuators B: Chemical  
Title: A smartphone based surface plasmon resonance imaging (SPRi) platform for on-site biodetection  
Type of Use: reuse in a thesis/dissertation  
Order Total: 0.00 USD

View or print complete [details](#) of your order and the publisher's terms and conditions.

Sincerely,

Copyright Clearance Center

## Permission from Royal Society of Chemistry.

### 1. Analytical methods

0.00 USD

Article: A smartphone-based surface plasmon resonance platform

Order License ID	Pending	Publisher	RSC Publishing
ISSN	1759-9679	Portion	Page
Type of Use	Republish in a thesis/dissertation		

[Hide Details](#)

### LICENSED CONTENT

Publication Title	Analytical methods	Publication Type	e-Journal
Article Title	A smartphone-based surface plasmon resonance platform	Start Page	4732
Author/Editor	Royal Society of Chemistry (Great Britain)	End Page	4740
Date	01/01/2009	Issue	39
Language	English	Volume	10
Country	United Kingdom of Great Britain and Northern Ireland	URL	<a href="http://www.rsc.org/Publishing/Journal...">http://www.rsc.org/Publishing/Journal...</a>
Rightsholder	Royal Society of Chemistry		

Permission from citation [4].

## Copyright

Copyright © 2018 ChenGuang Zhang et al. This is an open access article distributed under the **Creative Commons Attribution License**, which permits unrestricted use, distribution, and reproduction in any medium, provided the original work is properly cited.

Permission from citation [6].



Study on intensity-modulated surface plasmon resonance array sensor based on polarization control

Conference Proceedings: 2010 3rd International Conference on Biomedical Engineering and Informatics

Author: Boshu Sun

Publisher: IEEE

Date: Oct. 2010

Copyright © 2010, IEEE

---

### Thesis / Dissertation Reuse

The IEEE does not require individuals working on a thesis to obtain a formal reuse license, however, you may print out this statement to be used as a permission grant:

*Requirements to be followed when using any portion (e.g., figure, graph, table, or textual material) of an IEEE copyrighted paper in a thesis:*

- 1) In the case of textual material (e.g., using short quotes or referring to the work within these papers) users must give full credit to the original source (author, paper, publication) followed by the IEEE copyright line © 2011 IEEE.
- 2) In the case of illustrations or tabular material, we require that the copyright line © [Year of original publication] IEEE appear prominently with each reprinted figure and/or table.
- 3) If a substantial portion of the original paper is to be used, and if you are not the senior author, also obtain the senior author's approval.

## Permission from citation [5].

License Number 5121060960650

[Printable Details](#)

License date Aug 02, 2021

### Licensed Content

**Licensed Content Publisher** Elsevier  
**Licensed Content Publication** TrAC Trends in Analytical Chemistry  
**Licensed Content Title** Wavelength-modulation surface plasmon resonance sensor  
**Licensed Content Author** Xia Liu, Daqian Song, Qinglin Zhang, Yuan Tian, Lan Ding, Hanqi Zhang  
**Licensed Content Date** Nov 1, 2005  
**Licensed Content Volume** 24  
**Licensed Content Issue** 10  
**Licensed Content Pages** 7

### Order Details

**Type of Use** reuse in a thesis/dissertation  
**Portion** figures/tables/illustrations  
**Number of figures/tables /illustrations** 1  
**Format** both print and electronic  
**Are you the author of this Elsevier article?** No  
**Will you be translating?** No

### About Your Work

**Title** Portable Surface Plasmon Resonance Sensor for Immunoglobulin G Antibody Testing  
**Institution name** University of Central Florida  
**Expected presentation date** Dec 2021

### Additional Data

**Portions** Figure 1

## Permission from citation [10].

**PK** Pieter Kik <kik@creol.ucf.edu>  
Mon 11/29/2021 12:28 PM  
To: Robin Howell

Hi Robin, thanks for asking. Feel free to reference lecture slides. Usually there are references on the slides themselves to the original papers, if that helps. Best, -Pieter

**RH** Robin Howell  
Mon 11/29/2021 12:02 PM  
To: Pieter Kik <kik@creol.ucf.edu>

Hello Dr. Kik,

As you may recall, my Senior Design project is developing a surface plasmon resonance sensor. In our final documentation, I would like to reference some of your lecture slides on surface plasmon excitation. Would I have your permission to reference your lecture notes from the class OSE 6650 in our Senior Design 2 Final Documentation, specifically Lectures 11 and 12 on SP excitation and detection from Spring 2020? Thank you for your help and hope to hear from you soon.

Robin Howell

Permission from citation [11].

Header

## Thank you for your order!

Dear Robin Howell,

Thank you for placing your order through Copyright Clearance Center's RightsLink® service.

### Order Summary

Licensee:	University of Central Florida
Order Date:	Nov 29, 2021
Order Number:	5198290243734
Publication:	Springer eBook
Title:	Surface plasmons on smooth surfaces
Type of Use:	Thesis/Dissertation
Order Total:	0.00 USD

View or print complete [details](#) of your order and the publisher's terms and conditions.

Sincerely,

Copyright Clearance Center

Tel: +1-855-239-3415 / +1-978-646-2777  
[customer@copyright.com](mailto:customer@copyright.com)  
<https://myaccount.copyright.com>

## Appendix B – References

1. Liu, Y., Q. Lui, S. Chen, F. Cheng, H. Wang, and W. Peng, *Surface plasmon resonance biosensor based on smart phone platforms*. Sci. Rep., 2015. **5**.
2. Guner, H., E. Ozgur, G. Kokturk, M. Celik, E. Esen, A.E. Topal, S. Ayas, Y. Uludag, C. Elbuken, and A. Dana, *A smartphone based surface plasmon resonance imaging (SPRi) platform for on-site biodetection*. Elsevier, 2017. **239**: p. 571-577.
3. Lertvachirapaiboon, C., A. Baba, K. Shinbo, and K. Kato, *A smartphone-based surface plasmon resonance platform*. Royal Society of Chemistry, 2018. **10**.
4. Zhang, C.G., C.-J. Chen, K. Settu, and J.-T. Liu, *Angle-scanning surface plasmon resonance system with 3D printed components for biorecognition investigation*. Hindawi, 2018.
5. Liu, X., D. Song, Q. Zhang, Y. Tian, L. Ding, and H. Zhang, *Wavelength-modulation surface plasmon resonance sensor*. Trends in Analytical Chemistry, 2005. **24**(10).
6. Sun, B., X. Wang, and Z. Huang, *Study on intensity-modulated surface plasmon resonance array sensor based on polarization control*. 3rd International Conference on Biomedical Engineering and Informatics, 2010.
7. Optics, M.N. *Neutral Density Filter Overview*. 2021 [cited 2021 8 July]; Available from: <https://www.newport.com/p/FSR-OD100>.
8. Association, I.S. *IEEE 1118.1-1990 - IEEE Standard for Microcontroller System Serial Control Bus*. 2019 [cited 2021 8 July]; Available from: [https://standards.ieee.org/standard/1118\\_1-1990.html](https://standards.ieee.org/standard/1118_1-1990.html).
9. Society, A.C., *Safety in Academic Chemistry Laboratories: Best Practices for First- and Second-Year University Students, 8th Edition*. 8 ed. 2017, 1155 Sixteenth Street, NW, Washington, DC 20036, USA: American Chemical Society.
10. Kik, P., SP excitation and detection, in OSE 6650: Optical Properties of Nanostructured Materials. 2021: University of Central Florida.
11. Raether H. (1988) Surface plasmons on smooth surfaces. In: Surface Plasmons on Smooth and Rough Surfaces and on Gratings. Springer Tracts in Modern Physics, vol 111. Springer, Berlin, Heidelberg. <https://doi.org/10.1007/BFb0048319>